Figure 24. Longitudinal monitoring of plasma EV concentration in GBM patients.
EVs were isolated from 2mL of plasma collected from five GBM patients at follow-up, and their concentration was measured by TRPS. The average value from technical triplicates is reported above each bar. When available, the results of MRI were reported below the corresponding timepoint.

4.9 DNA is associated with plasma EVs

Tumour cells shed nucleic acids in the blood, either cell-free (cf) or associated to proteins and extracellular particles, including EVs[212]. Driver tumor mutations have been retrieved by liquid biopsy, either associated with the plasma EV compartment or with cfDNA[95,213,214]. In brain tumors, the detection of ctDNA in plasma is extremely challenging as its mutant allele fraction is quite low[215,216]. Nevertheless, given the significant increase of EVs concentration in plasma from GBM patients, we ought to address whether GBM-EVs carry tumour DNA, and if this DNA mirrors the genomic alterations of the corresponding primary tumor, and relevant for GBM classification[1]. This would support the use of EV-DNA as a reliable surrogate for tissue DNA, representing a non-invasive tool for tumor profiling that may significantly impact clinical practice.

Optical fluorescence microscopy has proven to be a powerful tool for the study of biological molecules, providing spatial information of the biomolecular structure, organization and protein interactions in many cellular and extracellular networks. However, the spatial resolution of widefield and confocal fluorescence microscopy is limited by diffraction to ~200 nm. Moreover, the identification of EVs in the extracellular environment is affected by significant limitations, such as low EVs fluorescence signal. The nanoscale size of EVs poses a challenge for their detection after deposition on glass surface, where the specific fluorescence signal is reduced to background levels.

These issues do not allow to discriminate single EVs and assess the colocalization of EVs and DNA at the single-EV level. Previous attempts to stain single EVs using DiI and PKH dyes have demonstrated the challenges associated with this approaches. Thus, we exploited a bead-based assay, previously optimized for surface tetraspanins detection by conventional flow cytometry, to capture EVs on 3.8µm beads by peptide affinity. Briefly, bead-bound EVs are stained with a pan-tetraspanins (PAN-TS), APC conjugated antibody to allow their detection, and deposited on a glass surface before DNA staining using Hoechst dye.

We conducted a pilot experiment on EVs isolated from a representative primary GBM cell line (GBM#7) to test the efficiency of coupling bead-based EV staining and DNA staining. Next, we optimized high-resolution imaging parameters to capture EVs and DNA colocalization. We stained 5 x 10^8 GBM primary cell-derived EVs, as we previously

determined that this number of EVs allows robust detection of tetraspanins in flow cytometry. A blank control (beads without EVs) was included to evaluate the aspecific fluorescence signals.

Samples were acquired by 3D widefield microscopy by a 1.4 NA 60× oil-immersion objective to guarantee the maximal resolution and sensitivity. Single beads were identified based on their FITC mean autofluorescence intensity. The different levels of FITC/PE signals are intrinsic to distinct beads populations coated with different antibodies. While this feature is useful for multiplex surface protein analysis, it was not relevant for this experiment. After beads detection by FITC fluorescence, the APC and Hoechst staining was evaluated for each bead.

The detection of the blank sample revealed a negligible non-specific signal from APC staining, while Hoechst background was higher, showing an aspecific affinity of the dye with the bead surface (**Figure 25a, b**). This evidence paved the way to correctly assess EVs and DNA co-staining experiments, avoiding possible artifacts.

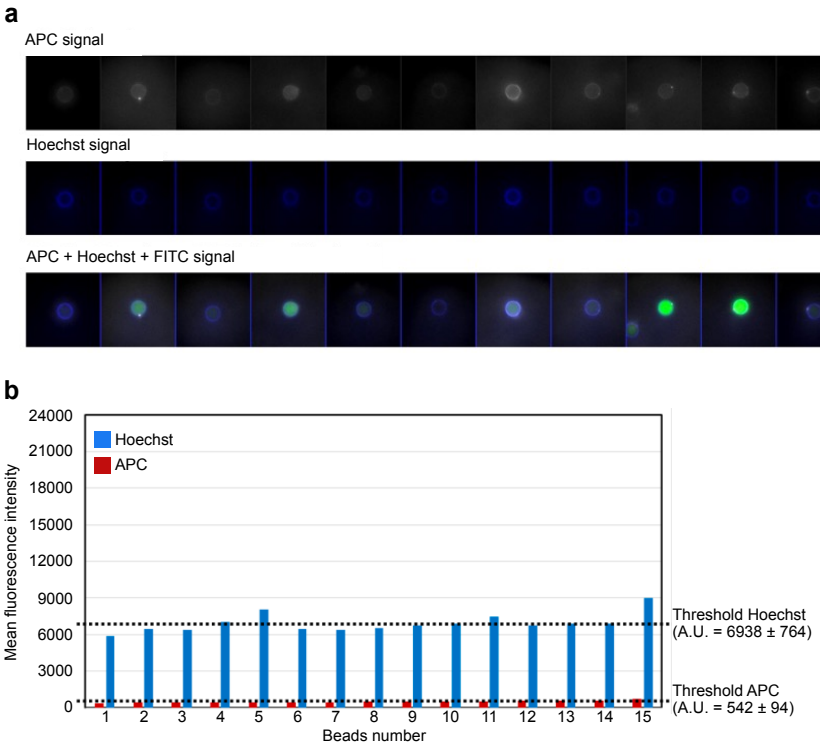

Figure 25. Evaluation of APC and Hoechst background signals.

3D widefield acquisition (a) and fluorescence quantification (b) of blank beads stained with PAN-TS antibodies targeting EVs and Hoechst DNA dye. APC signal corresponds to EVs bound to microbeads. FITC signal corresponds to microbeads.

Moving to GBM primary cell-derived EVs, we first defined APC-positive (APC^{pos}) and APC-negative (APC^{neg}) beads based on the reference threshold set in the blank sample. The

mean intensity value calculated for APC^{neg} beads was used to define the negative beads subpopulation, showing a total or semi-total absence of EVs on the surface. Thus, we set the Hoechst threshold based on the aspecific Hoechst signal of APC^{neg} beads.

Interestingly, we identified several APC^{pos}/Hoechst^{pos} beads (**Figure 26a**): in these samples, the intensity of both Hoechst and APC signals increased proportionally (**Figure 26b, c**), indicating not only that DNA is associated with cell-derived EVs, but also that the amount of DNA correlates with the abundance of detected EVs.

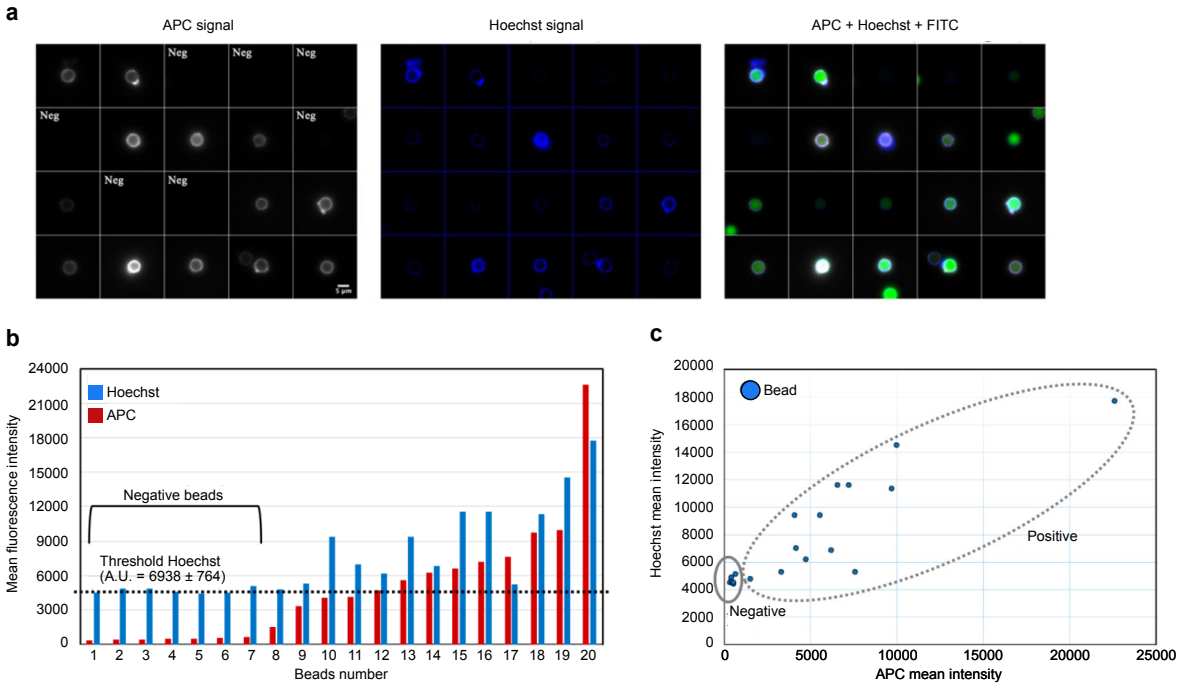

Figure 26. Measurement of EVs and DNA colocalization in primary GBM cell-derived EVs.

3D widefield images (MaxIP) (a) and fluorescence quantification (b) of 5 x 10^8 GBM#7-derived EVs stained with PAN-TS antibodies targeting EVs (APC signal) and Hoechst DNA dye. FITC signal was used to select individual microbeads. (c) Correlation of fluorescence intensity of APC and Hoechst in GBM#7-derived EVs.

Next, we investigated EVs isolated from healthy plasma. Using the same bead-based assay, we determined by flow cytometry the optimal number of plasma-EVs required to achieve good tetraspanins detection (1 x 10^{10} EVs). At saturation, despite a 15 folds increase in the input of EVs, tetraspanins abundance in plasma EVs remained lower with respect to GBM#7-derived EVs, especially for CD63 and CD81 (**Figure 27**), suggesting variations in the characteristics of the EV populations between these two samples. Accordingly, we might expect a lower APC signal intensity detectable in widefield microscopy.

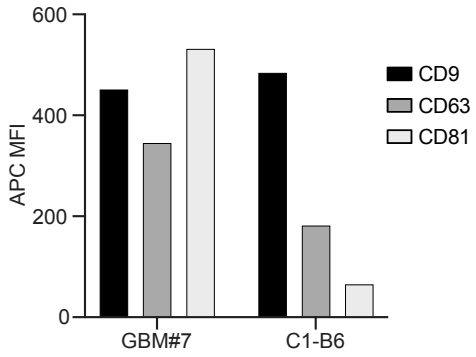

Figure 27. Assessment of optimal input of EVs for pan- tetraspanins detection.

Analysis of pan-tetraspanins expression on 5 x 10^8 GBM#7-derived EVs and 1e10 plasma-EVs isolated from healthy plasma (C1-B6) by bead-based multiplex flow cytometry.

We could detect APC^{pos}/$Hoechst^{pos}$ beads confirming that DNA is also associated with EVs circulating in plasma (**Figure 28a**). As expected, based on the flow cytometry data, the APC^{pos} subpopulation showed lower APC signal intensity in the plasma sample than observed in the GBM primary cell-derived EV sample (**Figure 28b**). Also the Hoechst threshold defined on APC^{neg} beads was higher than that measured in the GBM primary cell-derived EVs (**Figure 28b**). The intensity variations between different experiments were mainly due to the experimental conditions (number of beads, Hoechst dye and APC antibody concentration per bead, labelling saturation), which affected the intensity threshold in each sample.

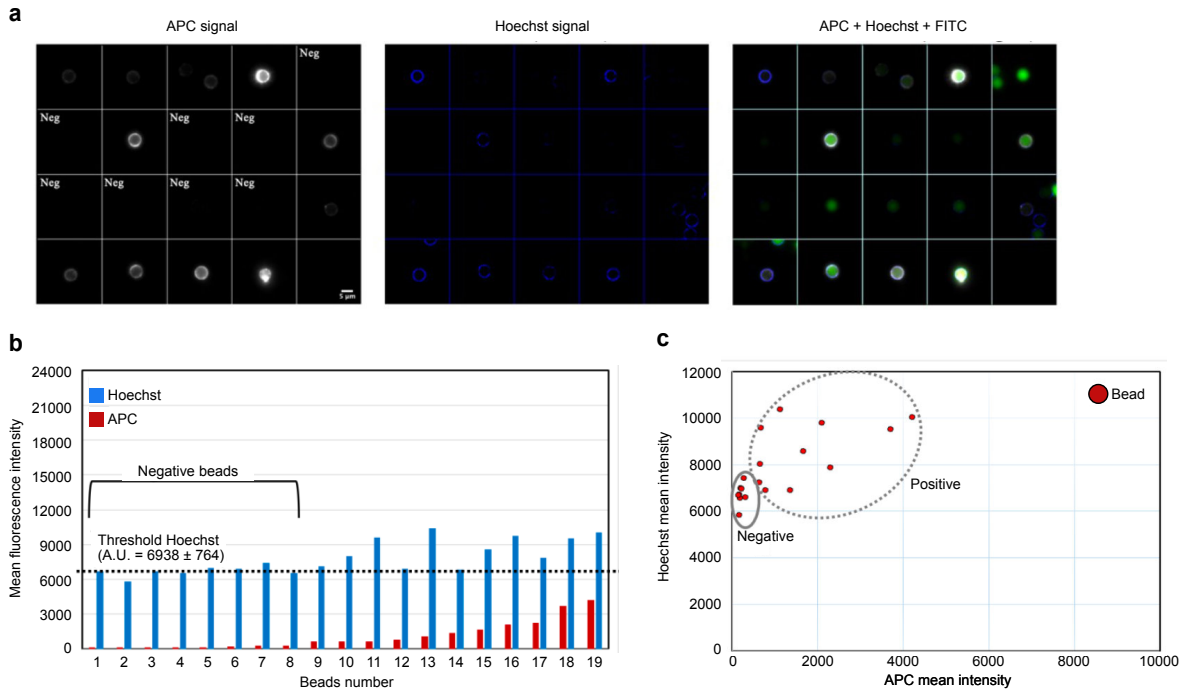

Figure 28. Measurement of EVs and DNA colocalization in healthy plasma EVs.

3D widefield images (MaxIP) (a) and fluorescence quantification (b) of 1e10 EVs isolated from healthy plasma (C1-B6) stained with PAN-TS antibodies targeting EVs (APC signal) and Hoechst DNA dye. FITC signal was used to select individual microbeads. (c) Correlation of fluorescence intensity of APC and Hoechst in C1-B6 plasma-derived EVs.

Having assessed the feasibility and the optimal settings to measure the colocalization of EVs and DNA by high-resolution imaging exploiting peptide affinity capture beads, we conducted a more comprehensive experiment including EVs isolated from two GBM cell lines, and plasma-EVs from two healthy (C1-B21, C1-H19) and two GBM subjects (GBM-H24, GBM-H32). We employed an automated fluoresce microscopy workflow[189], following an analysis-driven protocol (3.10.5 A.M.I.CO. (Automated Microscopy for Image Cytometry) analysis) that allows the automated acquisition of multi-channel images with high-resolution, and their processing to identify single events (i.e. beads).

This pipeline allowed to obtain a high statistical sampling able to collect and analyze hundreds of beads, and a classification of the subpopulation of beads obtained by quantitative measurements of the fluorescence signals on several fluorescence channels with high sensitivity. With the integrated retrieval algorithm, every event (i.e. bead) can be visualized and physically re-positioned on the microscope stage, allowing the execution of a second image-collection phase for a deeper investigation with confocal imaging. Beads position was estimated according to the transmitted light (TL) profile and their identification was based on the mean intensity of FITC and PE signals and morphological parameters (i.e., size (area) and shape (circularity)) (**Figure 29a, b**). EVs bound to bead surface were detected and quantified by APC mean intensity signal, DNA content quantification was estimated by Hoechst dye mean intensity per bead (**Figure 29a, b**).

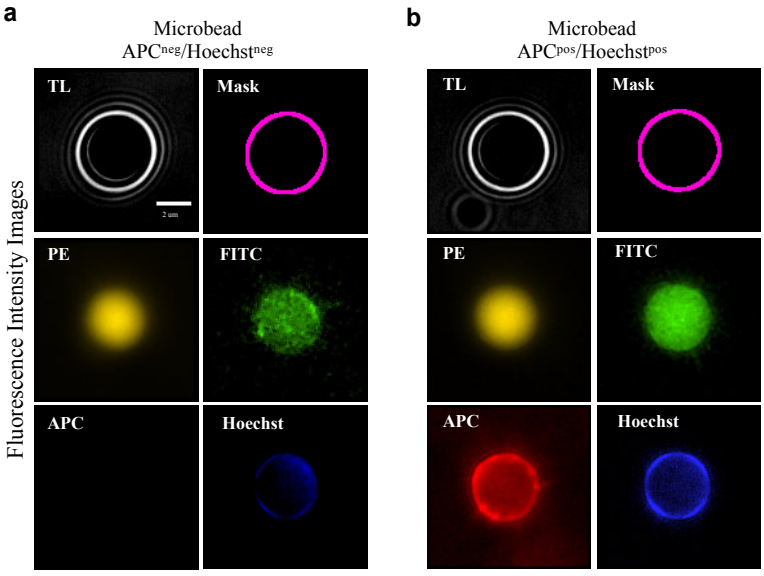

Figure 29. Identification of microbeads and bead-associated EVs and DNA.

(a, b) 2D widefield imaging of microbeads via their transmittet light (TL) profile, and acquisition of bead-associated fluorescence. PE and FITC autofluorescence of microbeads was used to confirm beads position. Blank (a) and EV-bound (b) beads were identified based on APC signal intensity. DNA content of bead-bound EVs was estimated by Hoechst signal intensity.

Widefield images were then analyzed by the A.M.I.C.O. software[189–192] developed by the IEO Imaging Development Unit, that first pre-processes the images to subtract the background and homogenize illumination to allows proper single bead identification. Then, it generates single-bead data that include geometrical parameters and mean fluorescence intensities per each channel. The software allows to further refine the single-beads selection by gating events per circularity and area, and their FITC/PE autofluorescence (**Figure 30a**). Lastly, it enables to set gates on fluorescence intensities (i.e. APC and Hoechst to identify EVs and estimate DNA content, respectively) exploiting a flow-cytometry like interface with 2D plots (**Figure 30b, c**). Thanks to the fully automated acquisition workflow coupled to the image analysis software, we were able to identify APC^{neg}/Hoechst^{pos} beads to set a threshold for the quantification of APC^{pos}/Hoechst^{pos} beads (**Figure 30b, c**).

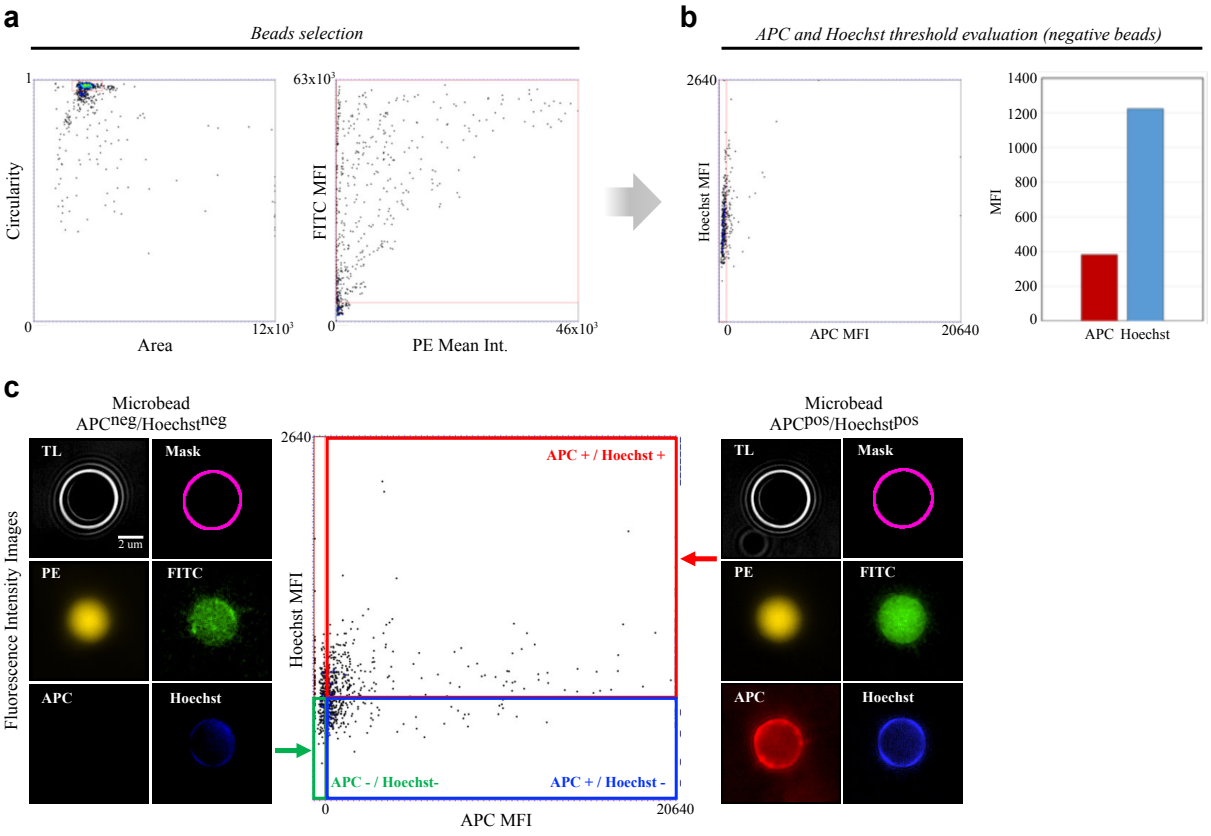

Figure 30. Analysis of widefield images by the A.M.I.C.O. software.

(a) 2D plot representation of single-bead data generated by A.M.I.C.O, including microbeads area, circularity and mean fluorescence intensity (MFI). (b) APC and Hoechst signal intensities of negative beads are quantified to set a threshold for

the identification of EVs and estimation of DNA content. (c) Representative detection of double-negative and double-positive beads by automated widefield imaging, and conversion of imaging data into flow cytometry-like plots by the A.M.I.C.O. software.

The developed image-cytometry tools provided a precise classification of beads-related subpopulations based on APC and Hoechst signals, generating statistics of the corresponding number of events, global (total beads), or relative (restricted to a gated subpopulation), percentage representation, and the average value per bead for every measured parameter in the selected population. We isolated and quantified a relevant population of beads APC^{pos}/Hoechst^{pos} in all samples (**Figure 31a**), ranging across samples from 10% to 50% of the total beads identified (**Figure 31b, c**). We also identified APC^{pos}/Hoechst^{neg} beads (**Figure 31a)**, representing 8% to 36% of total beads in different samples (**Figure 31b, c**), likely indicating that EVs bound to bead surface carry a negligible amount of DNA.

The intensity of the APC signal in APC^{pos} beads was higher in GBM#7 and T98G cell-derived EVs than in plasma EVs (**Figure 31d**), as expected from previous flow-cytometry experiments (**Figure 27**). Conversely, the Hoechst signal intensity of Hoechst^{pos} beads was comparable across all samples (**Figure 31e**).

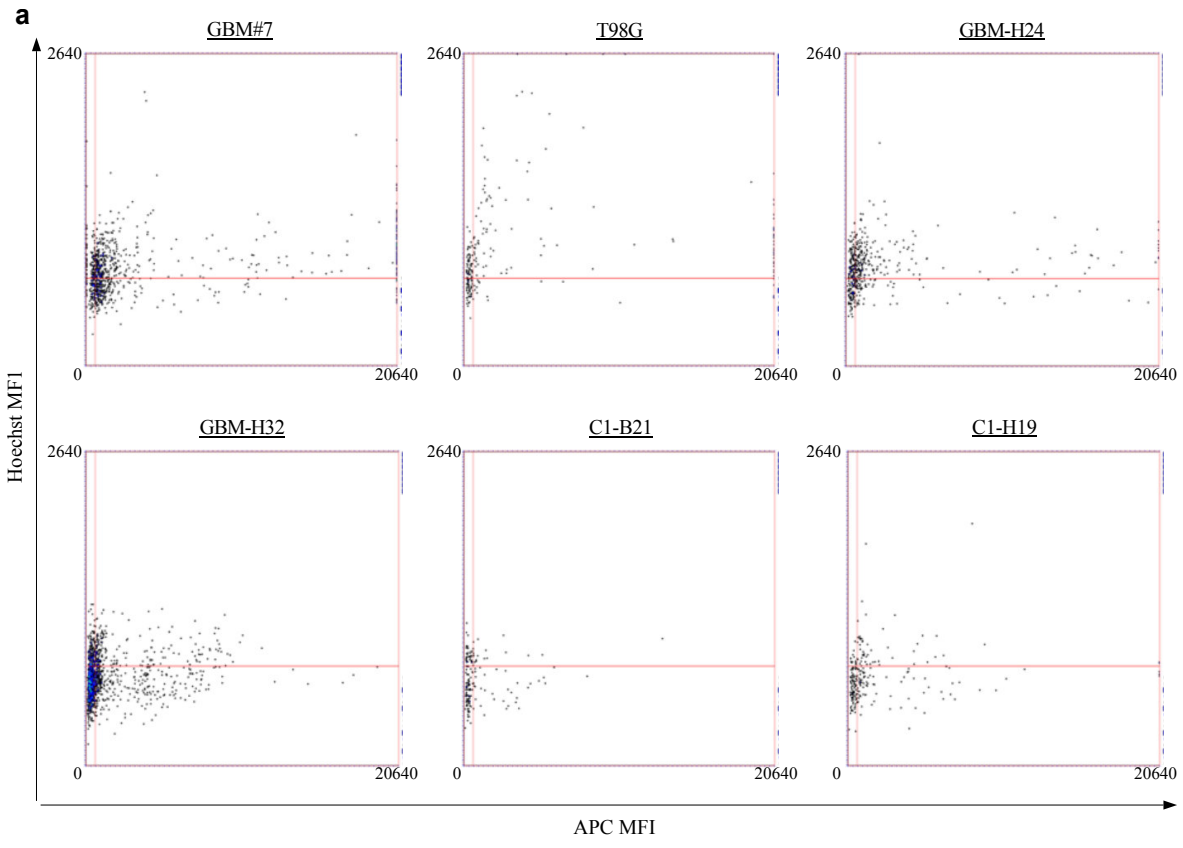

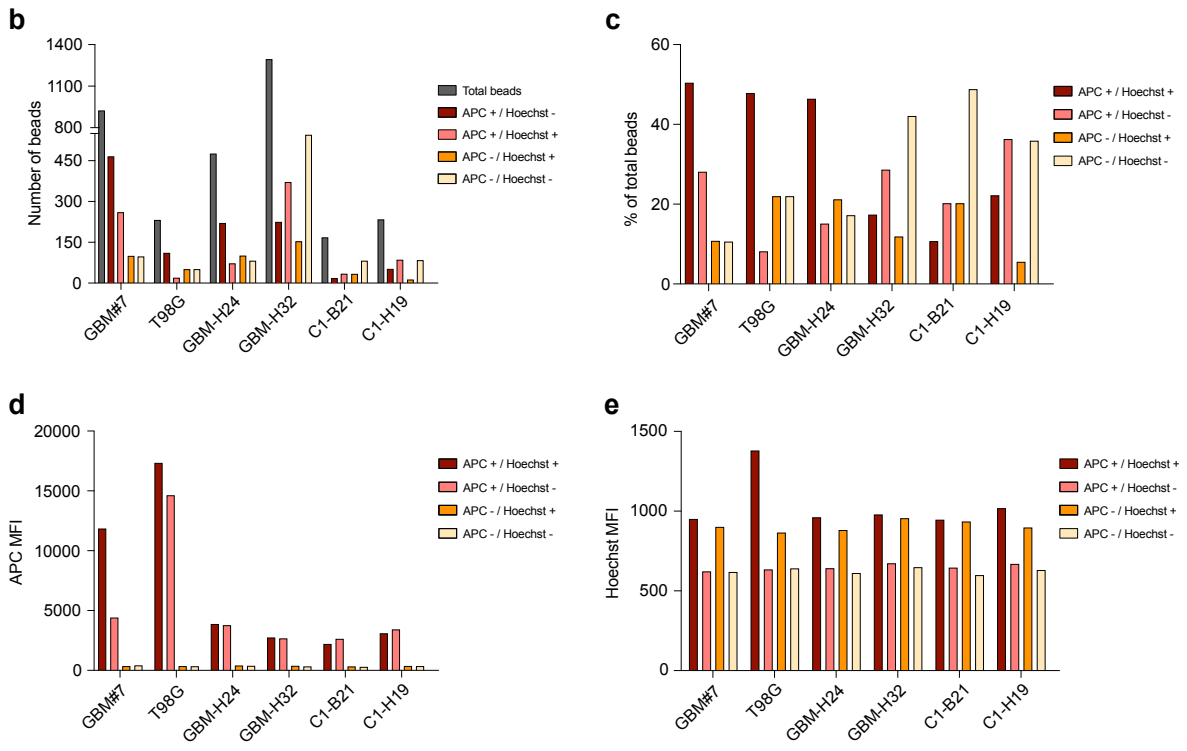

Figure 31. Quantification of beads, EVs and DNA.

(a) Identification of bead-bound EVs and estimation of their DNA content by APC and Hoechst mean fluorescence intensities (MFI). (b, c) Quantification of total, APC$^{pos/neg}$ and Hoechst$^{pos/neg}$ beads (b) and the fraction of APC$^{pos/neg}$ and/or Hoechst$^{pos/neg}$ beads over the total number of beads quantified in each sample (c). (d, e) Mean fluorescence intensity (MFI) of APC (d) and Hoechst (e) in APC$^{pos/neg}$ and/or Hoechst$^{pos/neg}$ beads.

Thanks to the possibility to identify all beads populations and to physically reposition target events on the microscope stage, we acquired confocal images of selected beads per each group (EVs derived from GBM primary cells, GBM plasma and healthy plasma), to observe the 3D distribution of EVs and DNA around the microbeads. Indeed, 3D analysis showed overlapping staining patterns for APC and Hoechst, confirming that DNA is associated to EVs from different sources (**Figure 32**).

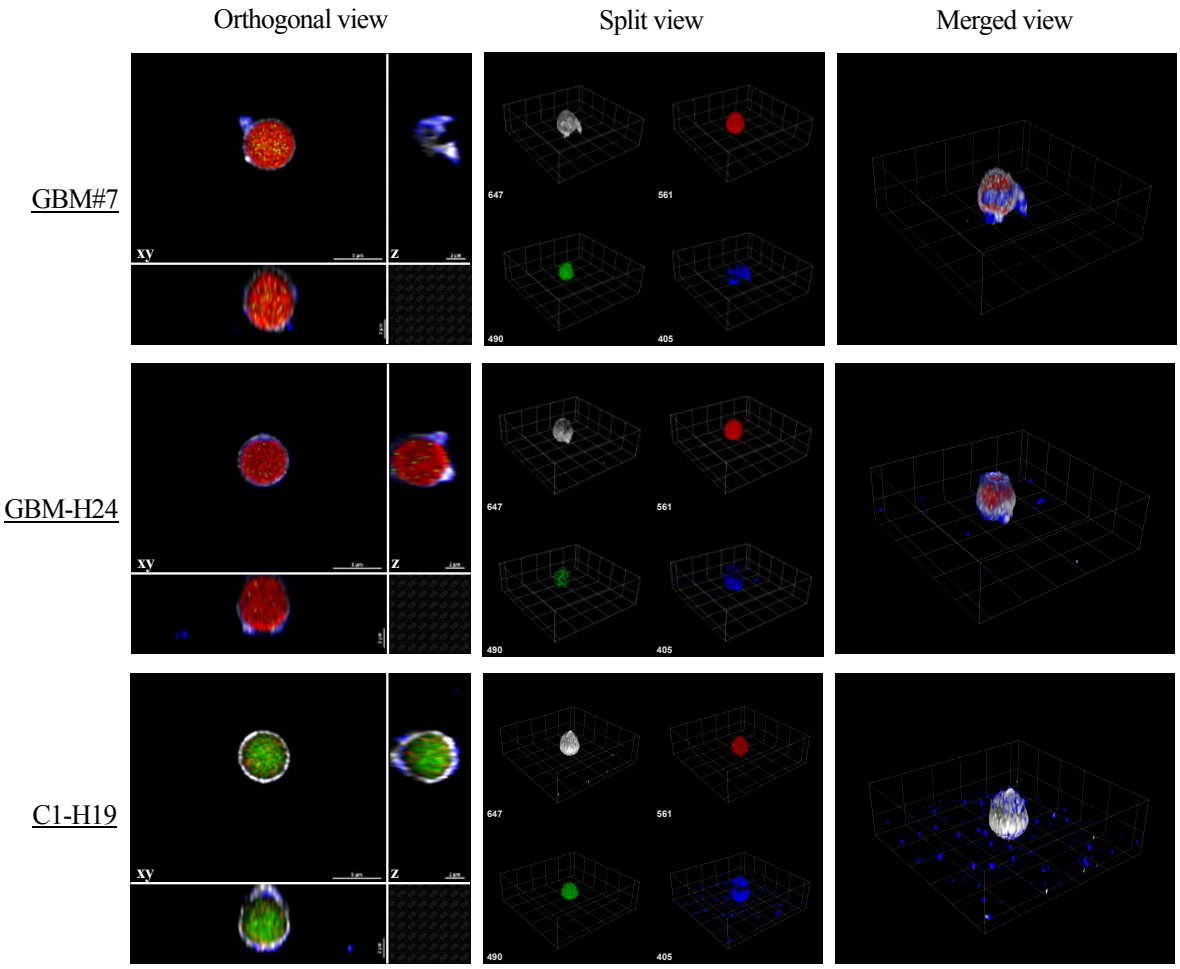

Figure 32. Confocal imaging of EV-associated DNA.

Orthogonal, split and merged view of DNA associated with EVs derived from GBM#7, GBM (GBM-H24) and healthy (C1-H19) plasma. Beads, EVs and DNA are identified by FITC (490nm)/PE (561nm), APC (647nm) and Hoechst (405nm) signals, respectively.

4.10 DNA in EV-rich SEC fractions is scarce and not informative regarding parental genetic alterations

Having stated the presence of DNA in association with plasma EVs, we extracted DNA from EV-rich SEC fractions using the SeleCTEV kit. DNA from SEC F1-4 was barely quantifiable, with detectable levels found in only 3 out of 12 samples (**Figure 33a**). The low yield limited the evaluation of DNA size and quality. When quantifiable, the DNA mainly comprised short fragments, averaging approximately 170 base pairs (bp) (**Figure 33b**).

a

Sample ID	DNA concentration (ng/ml of input plasma)
GBM#13	0
GBM#16	0
GBM#22	0,364
GBM#28	0
GBM#30	0
GBM#31	0
GBM#33	0
GBM#34	0
GBM#37	0,432
GBM#38	0
GBM#40	0,405
GBM#41	0

b

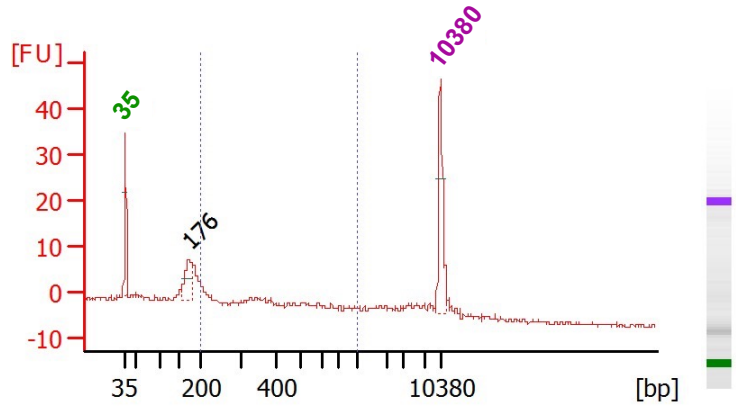

Figure 33. Analysis of the concentration and size of DNA extracted from EV-rich SEC fractions.

(a) Quantification at Qubit of DNA extracted from SEC F1-4 eluted from 2mL of GBM plasma. When quantifiable, DNA concentration was normalized for the input mL of plasma. Values of 0ng/mL indicates that the sample's concentration was below the Qubit detection limit. (b) Size profile at bioanalyzer representative of one of the three samples that were quantifiable with Qubit.

We analysed the DNA samples by droplet digital PCR (ddPCR) which has higher sensitivity and allows the detection of genetic alterations with low input of DNA. Indeed, ddPCR targeting adaptor related protein complex 3 subunit beta 1 (AP3B1) - a consensus reference gene – or EGFR – a gene often mutated or amplified in GBM - revealed the presence of DNA in all samples (**Figure 34a**), despite the relatively low number of copies/µL of both targeted genes confirms the scarcity of EV-DNA. This poses a major challenge to retrieve genetic alterations having a relatively low variant allele frequency (VAF), which is the case for most GBM mutations[217]. In fact, in a pilot experiment on a cohort of glioma patients, we could not detect any genetic alteration (i.e. IDH1 mutation and EGFR amplification) in DNA extracted from SEC F1-4 (**Figure 34b**).

a

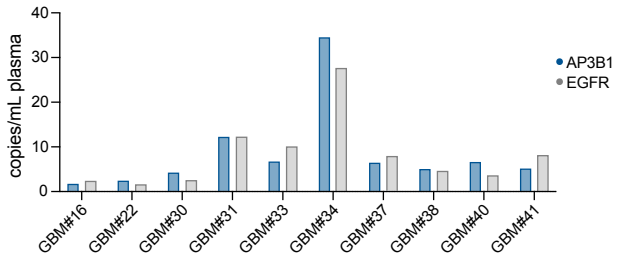

b

Genomic alteration	Sample ID	GBM tumor tissue	F1-4 DNA
IDH1 mutation	Glio#3	✓	-
	Glio#14	✓	-
	Glio#21	✓	-
	Glio#18	✓	-
	Glio#23	✓	-
EGFR amplification	Glio#413050	✓	-
	Glio#6	✓	-
	Glio#16	✓	-

Figure 34. Analysis of DNA in SEC F1-4 by ddPCR.

(a) ddPCR targeting AP3B1 and EGFR in DNA extracted from SEC F1-4 eluted from 2mL of plasma from GBM patients. (b) ddPCR targeting IDH1 mutation and EGFR amplification in DNA SEC F1-4 DNA from 2mL of plasma from glioma (Glio) patients. Genetic alterations were previously identified in tumor tissue via IHC (EGFR amplification), microsatellite analysis (CDKN2A deletion), and Sanger sequencing (TERT mutation).

4.11 The dilution of mutant DNA affects the sensitivity of mutation detection by ddPCR

Plasma EVs originate from very heterogeneous sources, and presumably all cell types secrete EVs as mediators of intercellular communication. In pathological conditions (i.e. cancer), EVs derived from disease cells constitute a minority of all EVs in circulation[218,219]. The enumeration of tumor-derived EVs in GBM is challenged by the lack of molecular GBM-biomarkers, but it's expected that they are less than 10% of total EVs, and in some patients this fraction could fall below 1%.

The dilution of tumor-derived EVs, poses significant limitations for the retrieval of tumor genetic mutations in plasma. We addressed the impact of EVs dilution on the efficiency of detecting genetic mutations by ddPCR. To do so, we isolated EVs from the TP53-mutant GBM cells line T98G (c.711G>A)[220] and verified that the mutation could be retrieved in T98G-derived EV-DNA via ddPCR, even with low DNA input (**Figure 35**).

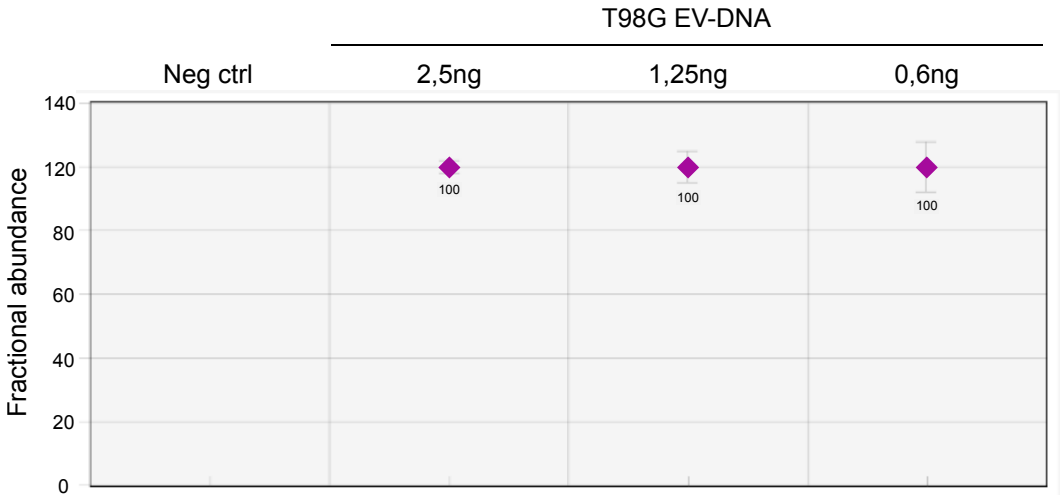

Figure 35. Analysis of TP53 mutation in T98G GBM cells.
Fractional abundance of TP53 mutation in DNA isolated from T98G-derived EVs. TP53-wild type (wt) tissue DNA was used as negative control.

Then, we spiked in serial dilutions of T98G-EVs (from 100µL to 0,01µL) in 2mL of healthy plasma, and then isolated EVs and DNA from SEC F1-4 as before. The detection of TP53 mutation was optimal up to 10µL of spiked-in EVs, then the fractional abundance of TP53-mutant droplets decreased and the mutation could not be detected at 1µL of spiked-in EVs and below (**Figure 36**).

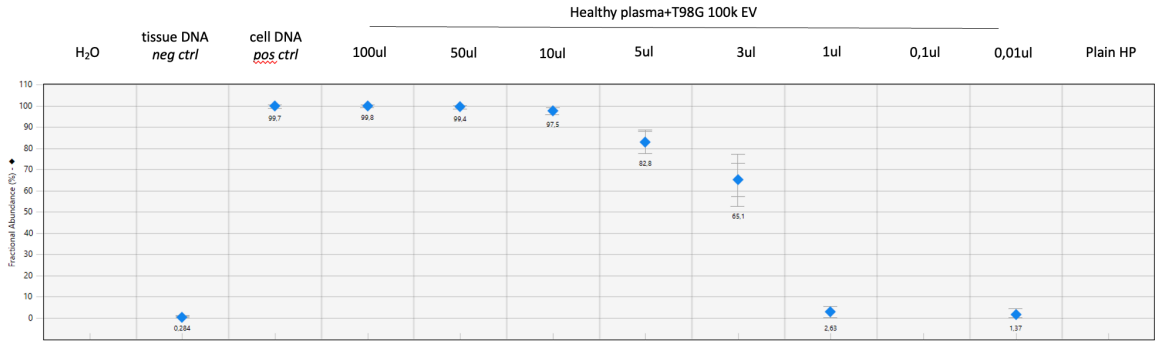

Figure 36. Assessment of the impact of dilution on targeted detection of genetic mutations.

ddPCR analysis of TP53 mutation in healthy plasma spiked with serial dilution of TP53-mutant EVs isolate from T98G GBM cells. TP53-wt tissue DNA and TP53-mut T98G cell DNA were used as negative and positive controls, respectively. DNA extracted from 2mL of plain healthy plasma (plain HP) was analysed to confirm the absence of TP53 mutation.

4.12 Analysis of total extracellular DNA from GBM plasma does not recapitulate the tumor genetic alterations

The analysis of DNA in EV-rich SEC fractions showed that EVs purification by SEC does not correspond to an enrichment of EV-associated tumor DNA. Actually, the content of DNA of EV-poor SEC fractions F5-13 was comparable to or higher than F1-4, both in AP3B1- and EGFR-targeting assays (**Figure 37**). This suggests that EV isolation does not provide an advantage for the identification of parental alterations by liquid biopsy.

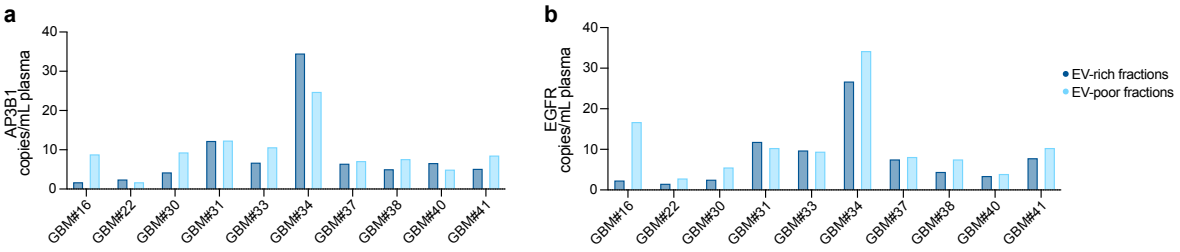

Figure 37. Analysis of DNA in EV-poor SEC fractions.

(a, b) ddPCR targeting AP3B1 (a) and EGFR (b) in DNA extracted from EV-rich and EV-poor SEC fractions from 2mL of GBM plasma.

In agreement with these results, a recent study also showed that the enrichment of EVs upon SEC is not mirrored by an enrichment in DNA[221]. The loss of genetic material due to plasma processing was even more evident when comparing the DNA content in SEC fractions and matched unprocessed plasma.

Given these evidences, we extracted DNA from unprocessed plasma, to increase the likelihood of capturing tumor-derived information in plasma extracellular DNA (exDNA), whether associated with EVs or not. We identified both short and medium-to-high molecular weight fragments in plasma exDNA from GBM patients, and its concentration was significantly higher with respect to DNA from SEC fractions (**Figure 38**).

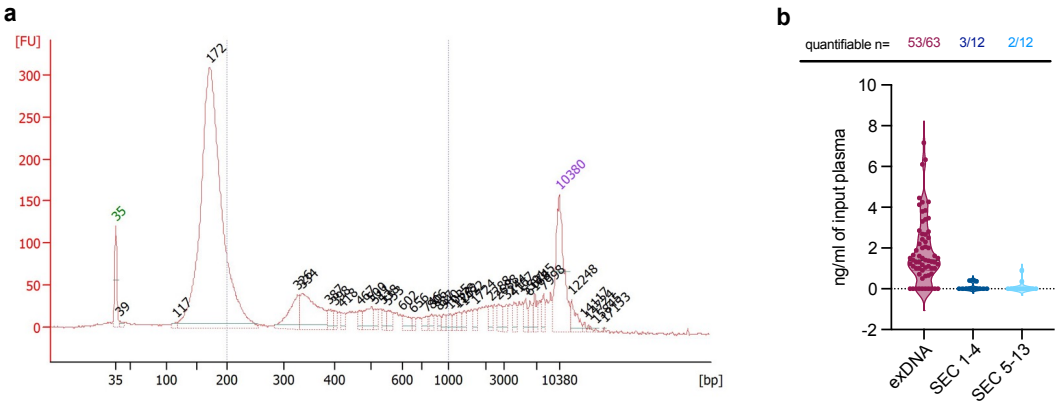

Figure 38. Analysis of the size and concentration of exDNA extracted from plasma.
(a, b) Size profile at bioanalyzer (a) and quantification at Qubit (b) of exDNA extracted from 2mL of GBM plasma.

We assessed the presence of EGFR amplification, CDKN2A deletion and TERT mutation (124C→T) in matched samples of exDNA and tumor DNA. ddPCR confirmed the presence of genetic alterations in tissue DNA, but not in exDNA (**Figure 39**). Also in this case, we suppose that the dilution of tumor-derived material in plasma impedes the detection of parental genetic alterations via liquid biopsy.

	EGFR amplification		CDKN2A deletion		TERT mutation (124C-->T)	
Sample ID	**Tumor tissue**	**ExDNA**	**Tumor tissue**	**ExDNA**	**Tumor tissue**	**ExDNA**
GBM-E02			del	wt	mut (8,2% FA)	wt
GBM-E04			del	wt	mut (45,5% FA)	wt
GBM-E05	amp (73,1)	not amp	del	wt	mut (33,4% FA)	wt
GBM-E06	amp (45,1)	not amp	homo del	wt	mut (44,4% FA)	wt
GBM-E08	amp (34,8)	not amp	del	wt	mut (42,9% FA)	wt
GBM-E09			del	wt	mut (25,9% FA)	wt
GBM-E11			del	wt	mut (42,9% FA)	wt
GBM-E12	amp (36,9)	not amp	del	wt		
GBM-E13			del	wt	mut (20,4% FA)	wt
GBM-E14	amp (47,6)	not amp	del	wt	mut (24,3% FA)	wt
GBM-E15			del	wt	mut (43,7% FA)	wt
GBM-E17			del	wt	mut (18,6% FA)	wt
GBM-E18			del	wt		
GBM-E19			del	wt		
GBM-E21			del	wt		
GBM-E22			del	wt	mut (24,1% FA)	wt
GBM-E23			del	wt	mut (19,8% FA)	wt
GBM-E24	amp (85,9)	not amp	del	wt	mut (43,1% FA)	wt
GBM-E27	amp (53,2)	not amp	del	wt		

Figure 39. ddPCR analysis of matched tumor tissue and extracellular DNA.

ddPCR analysis of matched tumor tissue and exDNA targeting EGFR amplification, CDKN2A deletions and TERT mutation. Genetic alterations were previously identified in tumor tissue via IHC (EGFR amplification), microsatellite analysis (CDKN2A deletion), and Sanger sequencing (TERT mutation).ExDNA was extracted from 2mL of plasma from GBM patients.

4.13 exDNA fragment size, rather than concentration, provides clinical value in liquid biopsy

Several studies demonstrated the utility of assessing cfDNA abundance and size in plasma from GBM patients with respect to healthy controls[222–225]. In our cohort, we did not observe significant differences in exDNA concentration between GBM and healthy samples (**Figure 40a**), while exDNA fragment size was smaller in GBM plasma (**Figure 40b**).

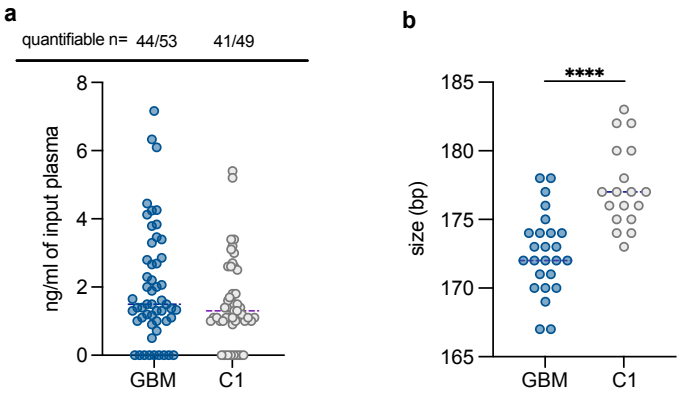

Figure 40. Analysis of exDNA abundance and size in GBM and healthy plasma.

(a) exDNA was isolated from 2mL of GBM (n=53) and healthy (n=49) plasma and quantified at Qubit. (b) Size analysis at bioanalyzer of plasma exDNA from GBM patients (n=25) and healthy controls (n=18). (Mann-Whitney test. P-value < 0,0001).

4.14 Shallow Whole-Genome Sequencing analysis identifies tumor-matched and private alterations in plasma exDNA

Whole-genome sequencing (WGS) provides a comprehensive strategy for the identification of a wide range of genomic alterations, such as single nucleotide variants (SNVs), insertions and deletions (INDELs), copy number variations (CNVs), and structural variants (SVs)[226]. Notably, low-coverage sequencing approaches have demonstrated both specificity and sensitivity in the analysis of CNVs from cancer plasma samples[227,228]. In this regard, large chromosomal aberrations are frequent in GBMs (e.g. chr7 gain/chr10 loss[229], EGFR amplification[230], CDKN2A/B homozygous deletion[231]) and currently used for GBM diagnosis[1]. These features, coupled to their higher frequency with respect to gene mutations in GBM, make them interesting targets in our liquid biopsy approach.

We exploited shallow WGS to determine whether exDNA in plasma could reliably reflect the genomic alterations of the tumor. We analyzed matched plasma exDNA, tissue DNA and germline DNA from six GBM patients at the baseline. For some samples, whole-exome sequencing (WES) data and the copy number aberration (CNA)-profile by multiple ligation probe amplification (MLPA) approach were also available (**Table 3**).

	Shallow WGS			WES		MLPA CNAs
Patient ID	**Tumor**	**Plasma**	**Germline**	**Tumor**	**Germline**	**Tumor**
GBM-E6	✓	✓	✓	✓	✓	✓ (1p, 9p, 10q, 17p, 19q)
GBM-E23	✓	✓	✓	✓	✓	✓ (9p, 10q)
GBM-E27	✓	✓	✓	✓	✓	✓ (9p, 10q, 19q)
GBM-H7	✓	✓	✓			✓ (10q, 17p)
GBM-H30	✓	✓	✓			

Table 3. Resume of DNA samples included in the analysis.
Matched plasma, tumor and germline DNA from six GBM patients was analyzed by sequencing (shallow WGS, WES). When available, MLPA CNA features are outlined.

Sequencing coverage was similar among samples (**Figure 41**). The total number of reads averaged at 47M, and >70% of reads were sequenced at >1X coverage in all samples (**Table 4**).

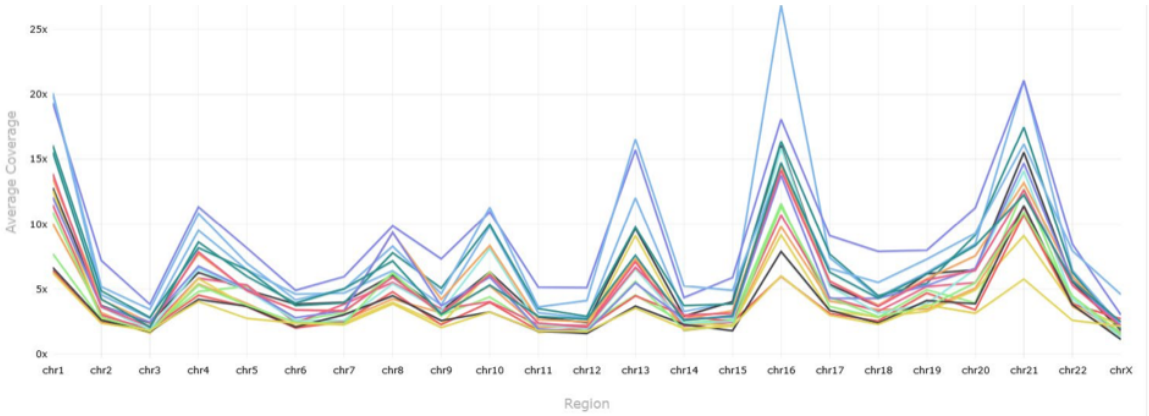

Figure 41. Assessment of the quality of shallow WGS.
(a) Coverage distribution on high quality regions for CNA analysis.

Patient ID	Sample type	Total reads [M]	Mean read length (bp)	Reads coverage (%)				
				≥1X	≥5X	≥10X	≥30X	≥50X
GBM-E6	Germline	35.1	134-125	74	23	11	2	1
	Plasma	73.4	135-130	89	48	24	6	3
	Tumor	43.1	135-127	75	25	12	3	1
GBM-E23	Germline	34.5	135-122	72	23	11	3	1
	Plasma	54.3	135-127	82	35	17	4	2
	Tumor	41.3	134-128	74	21	8	1	1
GBM-E27	Germline	39.3	134-127	75	25	12	3	2
	Plasma	64	135-129	85	41	21	6	3
	Tumor	39.3	134-127	71	20	8	1	1
GBM-H7	Germline	35.6	135-127	73	23	11	2	1
	Plasma	49.3	134-130	75	31	16	4	2
	Tumor	50.5	134-128	81	28	13	3	1
GBM-H30	Germline	58.6	134-126	85	35	18	5	2
	Plasma	45.1	136-127	76	31	15	3	2
	Tumor	44.5	135-125	76	23	9	2	1

Table 4. Assessment of the quality of shallow WGS.

Number of reads, reads length and percentage of reads coverage in germline, tumor and plasma extracellular DNA from five GBM patients.

We performed CNV analysis. In patients for which WES data were available, we observed that CNVs detected by shallow WGS in tissue DNA overlapped with the matched WES profiles (**Table 5**). In detail, copy gains (CN =3) and hemizygous deletions (CN=1) were the most frequent variants identified in GBM tissues, while amplifications (CN=4) and high-level amplifications (CN≥5) were detected to a lower extent (**Figure 42**).

Shallow WGS allowed also variants detection in exDNA. Most CNVs identified in exDNA mapped to intronic and intergenic regions, thus they didn't match with WES data (**Table 5**). CNVs in exDNA were either copy gains or hemizygous deletions (**Figure 42**).

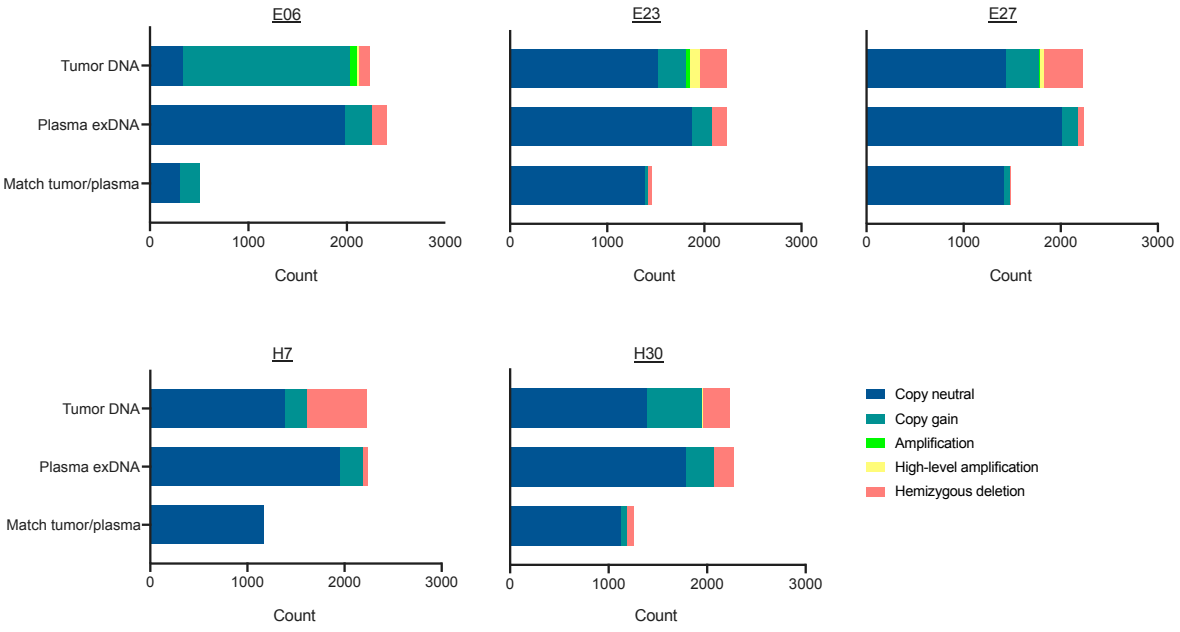

Figure 42. Analysis of the type of CNVs identified in matched GBM tissue and plasma DNA.
Bar plots representing the number of copy neutral (CN=2), copy gain (CN=3), amplifications (CN=4), high-level amplifications (CN≥50) and hemizygous deletion (CN=1) regions identified in matched GBM tissue and plasma extracellular DNA.

Patient ID	CNA matched WES/WGS tissue	CNA matched WES/WGS plasma
GBM-E6	46 (72%)	1 (1,5%)
GBM-E23	13(100%)	0
GBM-E27	47 (96%)	0

Table 5. Comparison of WES and WGS CNV profile of GBM tumor tissue and plasma DNA.
Comparison of whole exome sequencing (WES) profiling of GBM tumor tissue with the CNVs identified in matched GBM tumor tissue and plasma extracellular DNA by shallow whole genome sequencing (WGS) from three GBM patients.

The tumor fraction was consistently higher in tissue DNA than in matched plasma exDNA (**Table 6**). Matched tissue and plasma DNA shared a small part of CNAs, while most CNAs were private to the tissue or plasma DNA sample (**Figure 42, Table 6**).

	Tumor fraction				
Patient ID	Tissue	Plasma	CNV WGS tissue	CNV WGS plasma	CNA matched WGS tissue/plasma
GBM-E6	60,28%	5,56%	1901 (85%)	257 (11%)	99 (5%T, 38%P)
GBM-E23	12,13%	1,91%	716 (32%)	359 (16%)	69 (9%T, 19%P)
GBM-E27	65,30%	5,41%	801 (35%)	217 (9%)	71 (8%T, 32%P)
GBM-H7	46,59%	5,59%	843(37%)	282 (12%)	0
GBM-H30	55,50%	3,23%	846 (37%)	484 (21%)	133 (15%T, 27%P)

Table 6. Comparison of WGS CNA profile of matched GBM tumor tissue and plasma DNA.
Comparison of the tumor fraction and the CNV profiles of matched tissue and plasma DNA identified by shallow whole genome sequencing (WGS). Columns 2-3 indicate the tumor fraction of matched tissue and plasma exDNA. Columns 4-5 indicate the total number of CNVs identified in tissue and plasma DNA, and the percentage of CNV regions (in brackets) versus all sliding windows analyzed along the reference genome (2232 regions of 1Mb for each sample). Column 6 indicates the number of shared CNVs between tissue and plasma exDNA, and its fraction (in brackets) with respect to the total number of CNVs identified in tissue (T) and plasma (P) DNA respectively.

CNVs in tissue and plasma DNA had different amplitudes (**Figure 43**), in agreement with the lower tumor fraction in exDNA with respect to the matching tissue (**Table 6**).

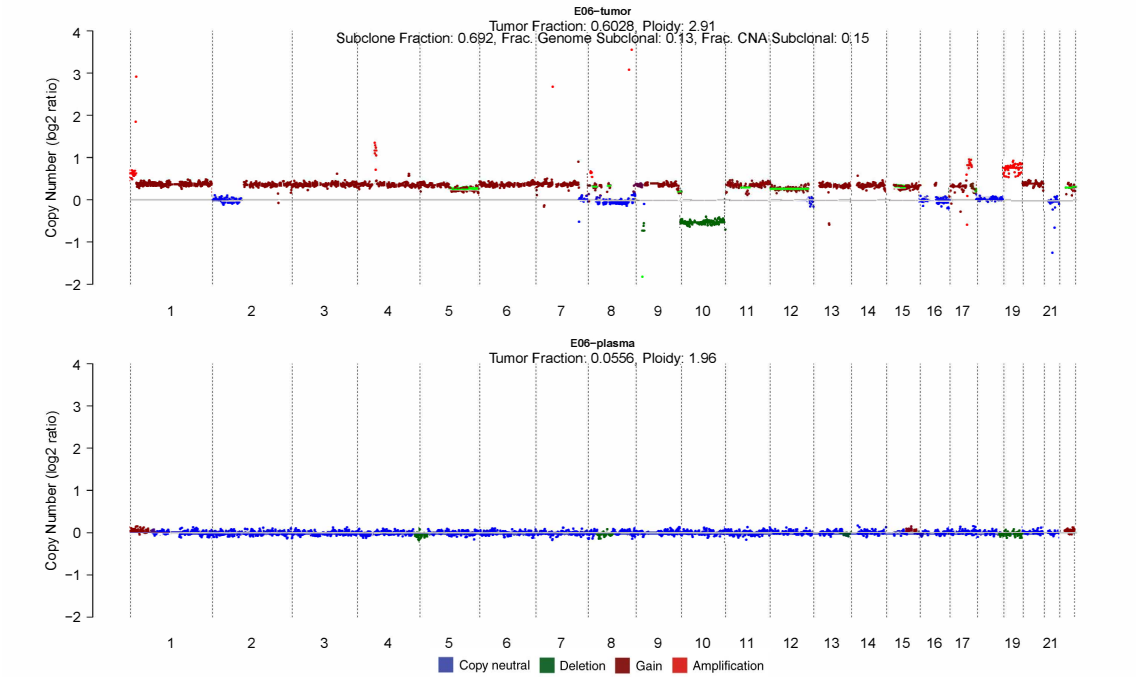
E06−tumor
Tumor Fraction: 0.6028, Ploidy: 2.91
Subclone Fraction: 0.692, Frac. Genome Subclonal: 0.13, Frac. CNA Subclonal: 0.15
Copy Number (log2 ratio)
E06−plasma
Tumor Fraction: 0.0556, Ploidy: 1.96
Copy Number (log2 ratio)
Copy neutral
Deletion
Gain
Amplification

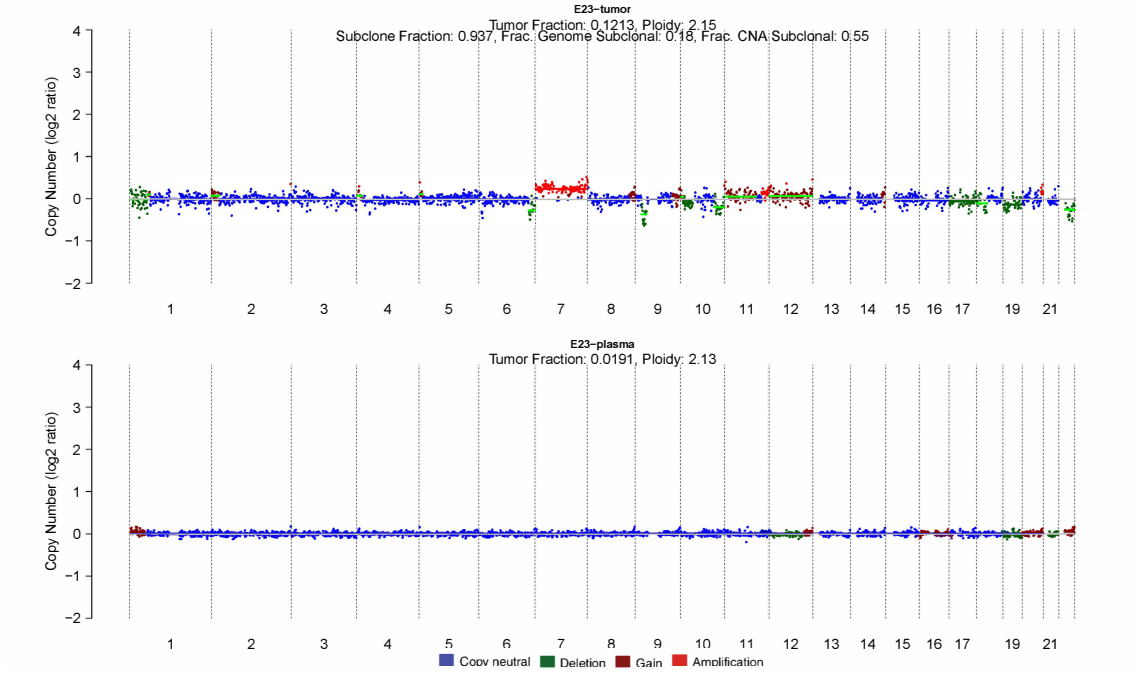
E23−tumor
Tumor Fraction: 0.1213, Ploidy: 2.15
Subclone Fraction: 0.937, Frac. Genome Subclonal: 0.18, Frac. CNA Subclonal: 0.55
Copy Number (log2 ratio)
E23−plasma
Tumor Fraction: 0.0191, Ploidy: 2.13
Copy Number (log2 ratio)
Copy neutral
Deletion
Gain
Amplification

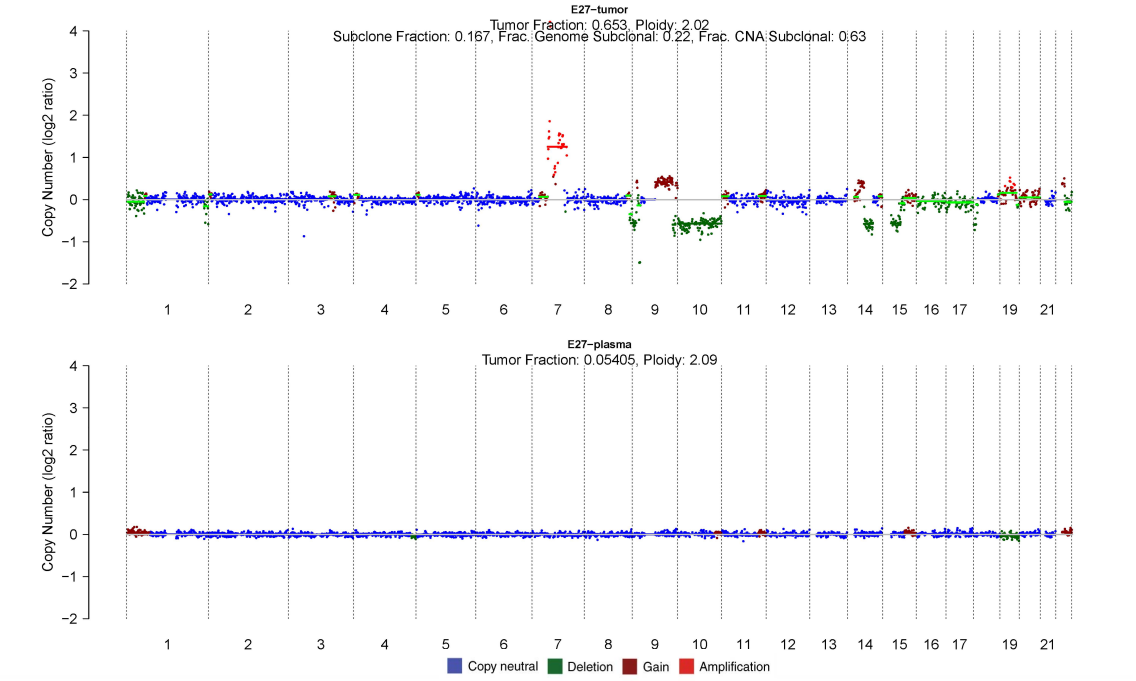
E27−tumor
Tumor Fraction: 0.653, Ploidy: 2.02
Subclone Fraction: 0.167, Frac. Genome Subclonal: 0.22, Frac. CNA Subclonal: 0.63
Copy Number (log2 ratio)
E27−plasma
Tumor Fraction: 0.05405, Ploidy: 2.09
Copy Number (log2 ratio)
Copy neutral
Deletion
Gain
Amplification

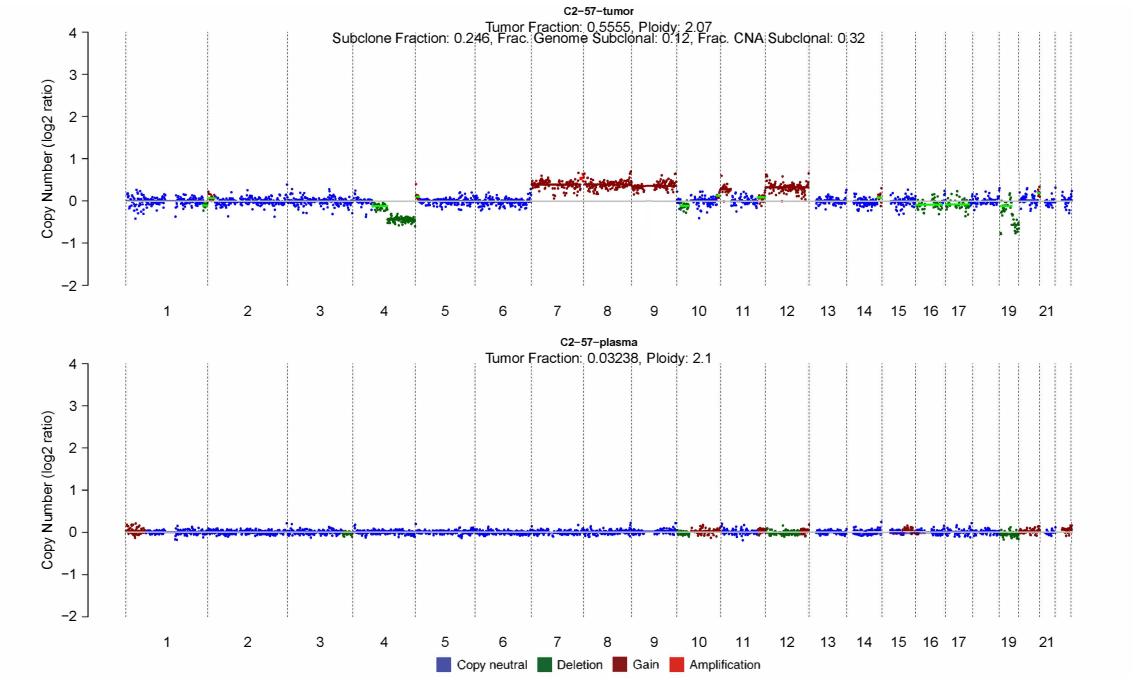
C2−57−tumor
Tumor Fraction: 0.5555, Ploidy: 2.07
Subclone Fraction: 0.246, Frac. Genome Subclonal: 0.12, Frac. CNA Subclonal: 0.32
Copy Number (log2 ratio)
C2−57−plasma
Tumor Fraction: 0.03238, Ploidy: 2.1
Copy Number (log2 ratio)
Copy neutral
Deletion
Gain
Amplification

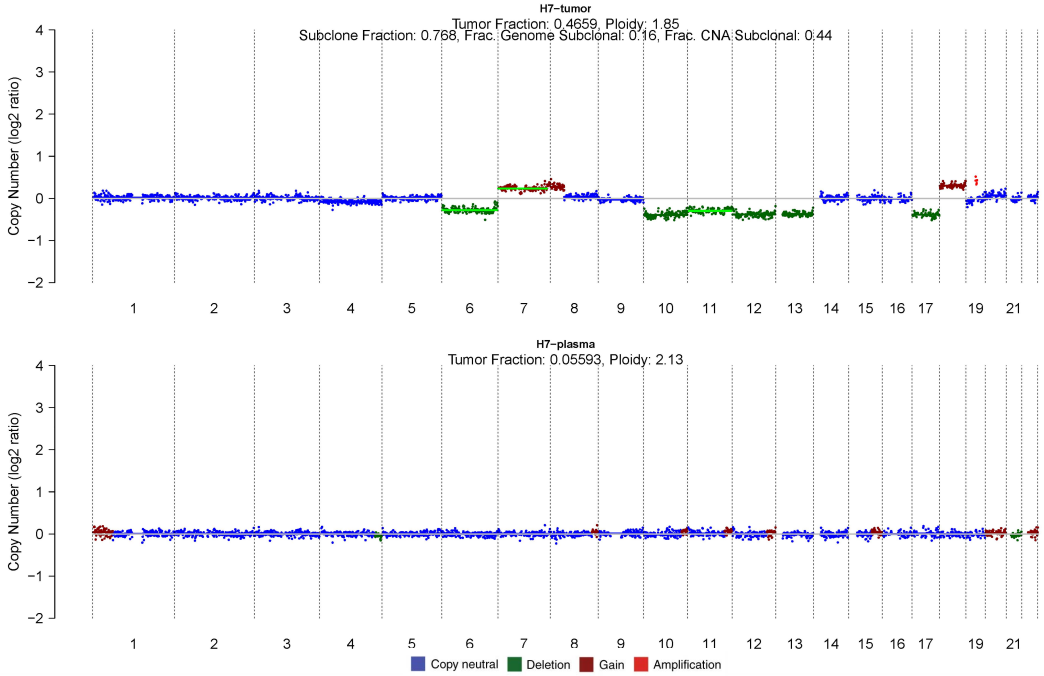

Figure 43. CNV profiles in matched tissue DNA and plasma exDNA.

Representation of the average whole genome CNV profile in matched GBM tissue DNA (upper panel) and plasma exDNA (lower panel) in five GBM patients. The x-axis represents chromosome positions, and the y-axis shows the copy number as a log2 ratio. Dots represent bins, and horizontal fluorescent green lines represent regions of predicted subclonal copy number events.

4.15 LC-MS/MS analysis of plasma EVs is feasible and can capture differences in GBM and healthy plasma EV cargo

Plasma EVs carry a consistent protein cargo that determines their fate and function[232]. EV proteins are a rich source of biomarkers of pathologic conditions[233–237], thus we characterized the proteomic landscape of GBM plasma EVs to identify a distinctive GBM-EV protein signature, with clinical utility at diagnosis and to monitor the tumor's molecular evolution. We performed a pilot mass spectrometry experiment including five GBM patients and five healthy controls to assess the feasibility of the proteomic analysis of plasma EVs. In total, we identified 2232 unique proteins with high confidence (FDR<0,01), and at least 1750 unique proteins per sample (**Table 7**).

Sample ID	Total yield (µg)	Total quantified proteins
GBM-H7	21,6	2055
GBM-H8	19,05	2109
GBM-H9	13,54	1757
GBM-H10	16,02	1826
GBM-H12	19,81	1794
C1-HC8	17,49	2128
C1-HC9	17,54	1932
C1-HC10	19,08	1896
C1-HC11	23,89	2255
C1-HC12	20,06	2165

Table 7. Protein yield and number of proteins identified by mass spectrometry analysis.

To verify the presence of EV-associated proteins, we compared our dataset with a reference list of 388 EV markers (here as 'reference EV-markers') obtained by merging three consensus EV protein repositories most commonly used in EV studies, namely MISEV2023[177] (n=214), EVpedia[238] (n=200) and Exocarta[239] (n=100) (**Table 8**). Only 22 proteins were in common to all three repositories, which supports our choice of merging multiple databases to obtain a comprehensive list of reference EV-markers.

Common (n=22)	CLTC	RAN	ITGAM	ITGA9	IL18	ITGA2	ANXA9	PAICS	ACTBL2
ACTN4	PKM	EEF1A1	TUBE1	VSP4B	ARRDC1	ATG9A	CD14	RACK1	RALA
ANXA2	UBA1	RAB5C	TUBD1	ITGA3	IL1F5	IL1F9	ITGA10	CAPZA1	CLU
ANXA6	FASN	MVP	ITGA5	HLA-A	IL15	TFR2	ITGA4	CALR	ARF4
ANXA1	GNAI2	GDI2	IL16	SHH	IL2	GOLGA2	**Expedia (n=103)**	VIM	PPP2R1A
ITGB1	LDHA	HSP90AA1	TUBG2	CANX	IL9	CAV1	RAB2A	ARHGDIA	RAB35
LGALS3BP	A2M	ATP1A1	VPS4A	CYC1	IL11	TUBA3C	CD44	PRDX6	ATP5B
FLOT1	RAP1B	RAB7A	IL19	IL10	GYPA	Acta2	PSMA2	PSMA3	NPM1
MFGE8	CCT5	PRDX2	IL26	ANXA10	ERBB2	TUBG1	ACTR3	PSMA1	CTSD
SDCBP	RAB1A	YWHAB	CHMP6	H2-K	ITGA7	APOB	VCL	CAND1	GPI
ITGA6	PFN1	RAB8A	CD37	TUBB7P	IL1F6	A4	RPS2	KRT1	VAT1
ALB	CDC42	YWHAZ	TGFB2	ANXA3	CHMP3	TXLNA	HSPB1	PHGDH	CCT8
CD9	GNB1	PGK1	CHMP4A	IL17B	IFNG	ITGA1	CCT4	RUVBL1	CPNE3
GAPDH	TPI1	**Expedia & MISEV (n=11)**	TOMM20	IL22	HLA-DP	IL5	PDCD6	PDIA3	RPS4X
ANXA4	PDCD6IP	TUBA4A	CD3	CD47	IL17F	IL13	RPS18	KRT10	RPS3
HSP90AB1	YWHAE	ARF6	IL17D	IL34	IL4	TUBA3FP	RAB1B	B2M	ATIC
CD81	ACLY	CD59	IL28B	CD55	CD82	FGF1	RDX	CAP1	PSMA7
RHOA	HSPA5	ITGAV	IL33	APOA2	CHMP1B	IL25	TLN1	CNP	RPLP2
HSPA8	CFL1	LAMP1	ITGA11	ITGAD	TUBB6	CD53	KRT9	TAGLN2	PGD
ANXA5	YWHAQ	TUBB4B	PECAM1	AHSG	IL1F10	IL12A	JUP	ATP6V1A	DYNC1H1
ANXA11	PPIA	TUBB	IL23A	BHSPA5	H2-Q	IL28A	RPL7	MDH1	RPS16
TUBA1B	KPNB1	ACTN1	EGF	CD5L	TSPAN8	IL1F8	GANAB	VTN	RPL18
BSG	CCT2	ANXA7	UMOD	IL31	IL21	KRT18	RPLP0	EIF4A1	HSPG2
Exocarta & MISEV (n=6)	MYH9	HSP90B1	IL1A	CHMP5	COL	ITGA8	PGAM1	P4HB	PEBP1
LAMP2	EHD4	FN1	ALIX	ADAM10	TUBB8B	IMMT	GSN	CYFIP1	GNA13
TUBA1A	RAB14	**Exocarta (n=8)**	TUBB2A	ANXA13	LMNA	ITGB5	GNAI3	PSMA5	KRT2
HSPA1A	TFRC	HIST1H4B	IL20	H2-D	ITGB8	CD73	EHD1	CCT6A	
CD63	HIST1H4A	PTGFRN	HLA-DR	TUBA8	APOA1	TUBB4A	FLNB	SLC1A5	
TSG101	THBS1	RAB5A	IL32	ITGB4	HLA-C	CHMP4B	APOE	S100A11	
TUBA1C	LDHB	GNAS	Actg1	ABCC1	FGF2	IST1	PSMD2	ARPC4	
Expedia & Exocarta (n=64)	GNB2	HIST2H4A	ITGB6	IL29	IL24	MAPT	MYO1C	RAP2B	
ACTB	PRDX1	RAB5B	HLA-B	CAV2	ITGB2	IL6	WDR1	MYL6	
ENO1	EZR	ACTG1	CD90	TUBB8	ITGAE	ITGAL	C3	RPSA	
TKT	ARF1	SLC16A1	CHMP2A	TUBA3D	IL27A	TUBB1	PSMB3	GSTP1	
RAC1	VCP	**MISEV (n=174)**	TUBB2B	ITGB3	VEGFA	TUBA3E	RAB10	SLC2A1	
YWHAH	CCT3	IL17A	ANXA8	TUBA3GP	APOB100	CHMP4C	HSPD1	EEF1G	
EEF2	SLC3A2	FLOT2	HLA-DQ	TUBA4B	IL7	EPCAM	PSMB1	RPS8	
STOM	ALDOA	ITGA2B	GP9	TUBB3	CHMP1A	Actc1	TXN	ACTR2	
YWHAG	FLNA	IL8	IL1B	IL3	CHMP7	ITGAX	RPL12	IGSF8	
TCP1	CLIC1	CHMP2B	ANXA8L1	TGFB1	APP	IL17C	IQGAP1	CCT7	
MSN	AHCY	Acta1	ITGB7	Actb	IL1F7	IL1RN	PPIB	HBA1	

Table 8. Reference EV-markers list.

A list of reference EV-markers was generated by merging three consensus EV protein databases. Only 22 proteins were in common among the three repositories, while the remaining 366 proteins were either common to two datasets or unique to one of them.

We confirmed the presence of over 60% of the reference EV-markers were present in our dataset (**Figure 44**).

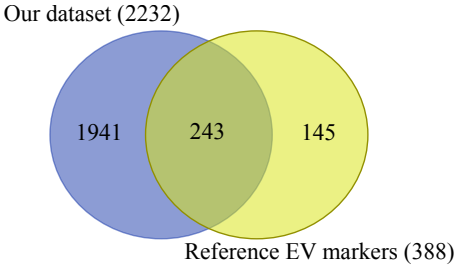

Figure 44. Assessment of the presence of reference EV-markers in our proteomic dataset.
Venn diagram showing the intersection of the list of reference EV-markers and the 2232 proteins we identified in plasma EVs by mass spectrometry.

The gene ontology (GO) analysis of the 2232 identified proteins revealed the enrichment of biological processes (BP) related to secretion, exocytosis and vesicle-mediated transport, alongside the enrichment of cellular components (CC) of extracellular vesicles and exosomes (**Figure 45**).

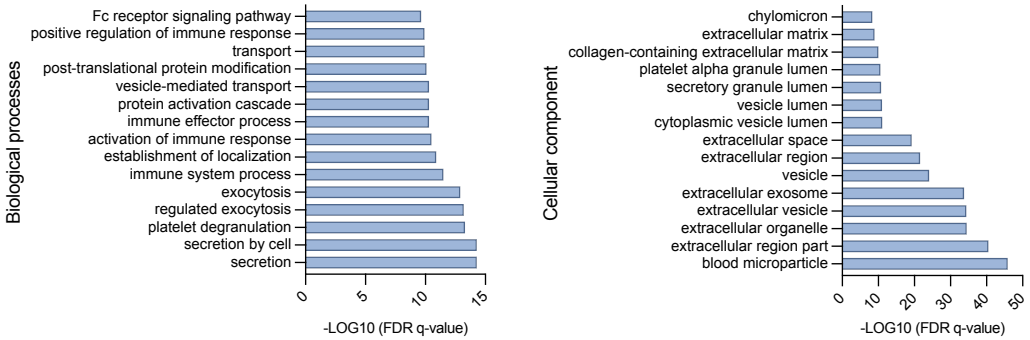

Figure 45. Gene ontology (GO) analysis of the 2232 identified proteins.
Bar plots showing the top 15 biological processes and cellular components enriched by GO analysis in the 2232 proteins identified in plasma-EVs.

Differential expression analysis (DEA) between GBM and healthy samples identified 529 differentially expressed proteins (DEP), of which 115 and 414 were upregulated in GBM and healthy samples, respectively (**Figure 46**).

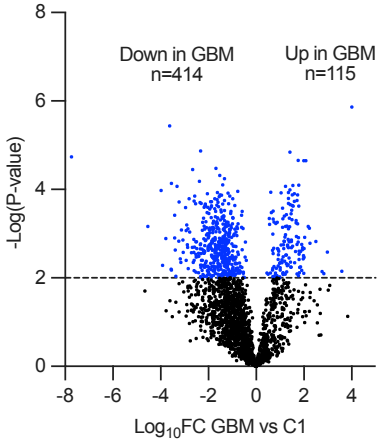

Figure 46. Differential expression analysis of the GBM and healthy EV proteomes.
Volcano plot showing the differentially expressed proteins in GBM vs healthy EVs.

4.16 LC-MS/MS analysis of plasma EVs allows the identification of a GBM-associated protein signature

To identify candidate GBM biomarkers, we extended the proteomic analysis of plasma EVs to a larger cohort of 23 preOp GBM patients and 31 healthy controls. We also assessed the changes in EV protein expression upon tumor resection including 21 plasma samples from GBM postOp patients, of which 17 matched with preOp samples.

A total of 1937 proteins were quantified, with an average of 1668, 1690 and 1740 proteins in GBM preOp, GBM postOp and healthy samples respectively. We observed a broad dynamic range of protein expression in all three cohorts (**Figure 47a**), indicating that the composition and abundance of the identified proteins varied widely within each experimental group. We observed that around 65% of the reference EV-markers defined previously (**Table 8**) were present in the dataset (**Figure 47b**). Additionally, consensus EV markers including the tetraspanins CD9, CD63 and CD81, as well as SYNTENIN-1 (SCDBP), ALIX, FLOT1/2, and TSG101 were among the top 50% of all identified proteins (**Figure 47c**).

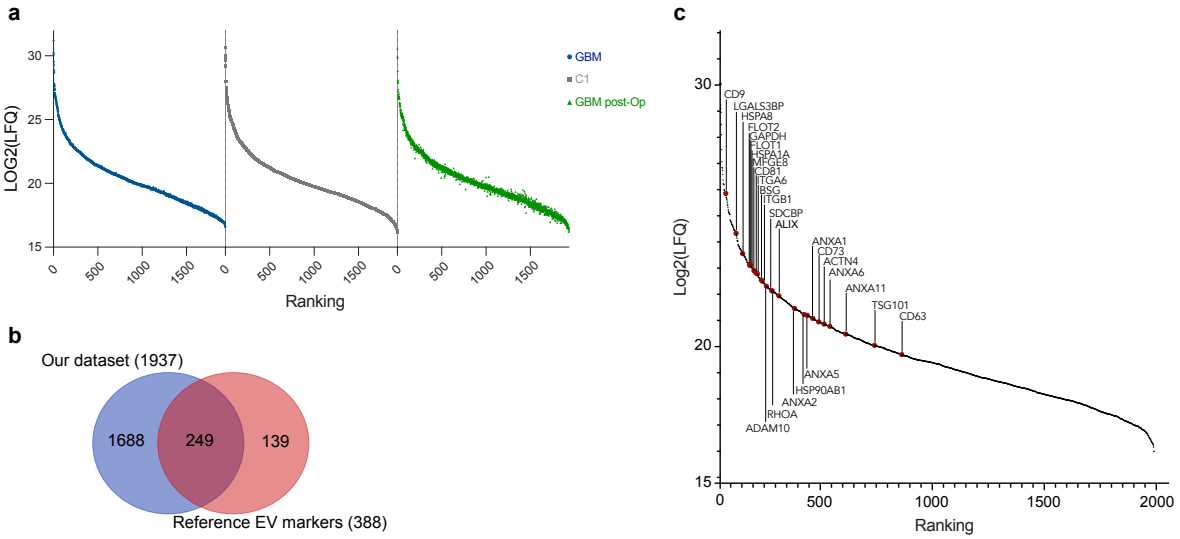

Figure 47. Analysis of the characteristics of the plasma EV proteome.

(a) Dynamic range plot of the expression of the 1937 proteins identified by mass spectrometry in plasma-EVs from pre-operative GBM patients (n=23), healthy subjects (n=31) and post-operative GBM patients (n=21). (b) Venn diagram showing the intersection of the list of reference EV-markers and the 1937 proteins identified in plasma EVs by mass spectrometry. (c) Ranking of selected reference EV markers among all EV proteins identified in GBM plasma samples.

We further characterized the features of our proteomic dataset via GO analysis. BP terms of platelet degranulation and aggregation, secretion, exocytosis, transport and regulation of the immune response were mostly represented in this dataset (**Figure 48**), mirroring the observations of the pilot experiment (**Figure 45**). Similarly, the top enriched cellular highlighted the abundance of extracellular vesicles, exosomes, surface adhesion and junction proteins (**Figure 48**).

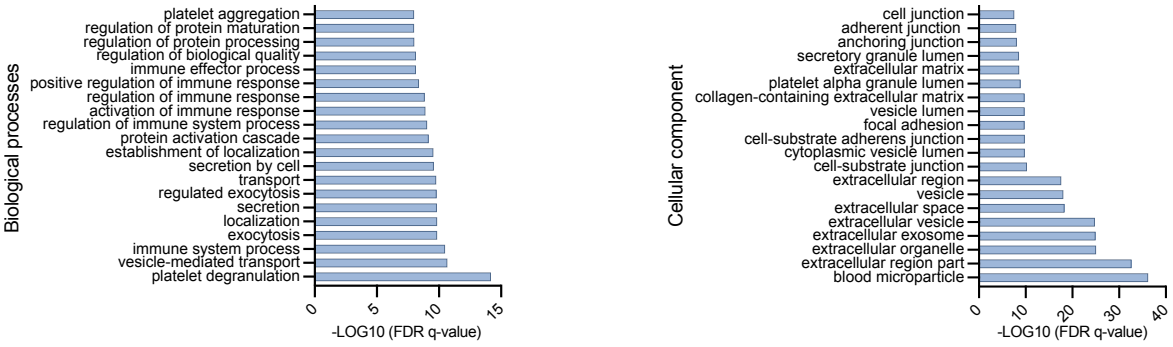

Figure 48. Gene ontology (GO) analysis of the 1937 identified proteins.

Bar plots showing the top 20 biological processes and cellular components enriched by GO analysis in the 1937 proteins identified in plasma-EVs.

Unsupervised hierarchical clustering separated all three groups, with the exception of three GBM preOp and two healthy samples that clustered with the healthy samples (**Figure 49a**).

Principal component analysis (PCA) confirmed that GBM preOp, healthy and GBM postOp samples can be distinguished by their EV protein content (**Figure 49b**).

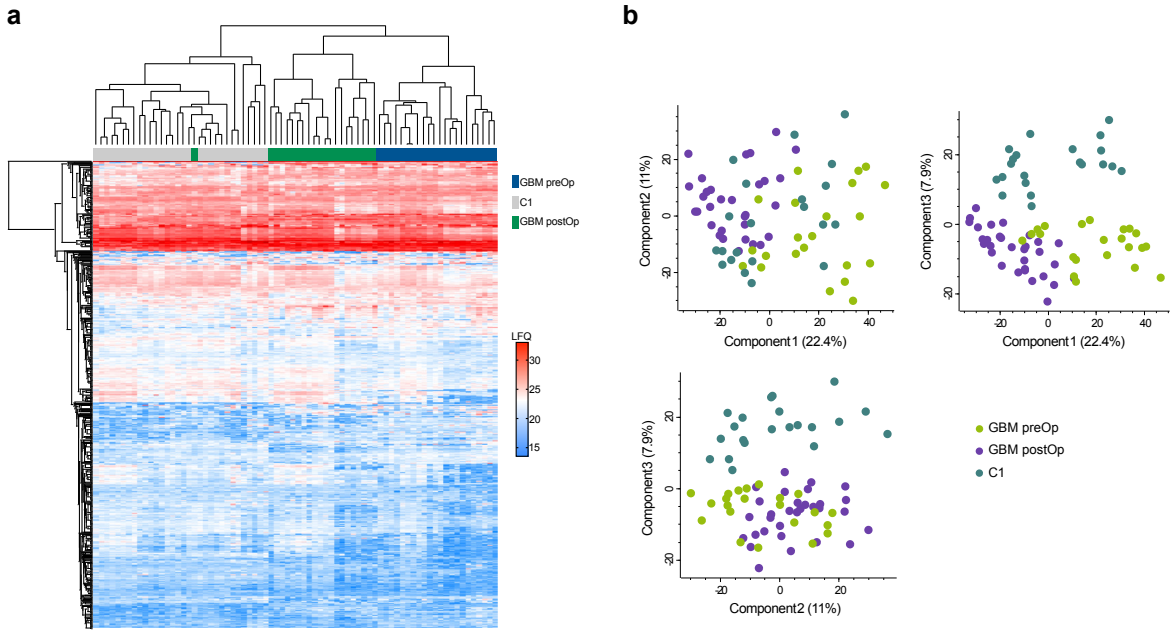

Figure 49. Clustering analysis of plasma EV samples based on EV protein expression.
(a, b) Unsupervised hierarchical clustering (a) and principal component analysis (PCA) (b) of GBM pre-operative (n=23), healthy (n=31) and GBM post-operative (n=21) plasma EV samples. The clustering was performed on 1166 proteins which were significantly different among the three groups by one-way Anova (FDR < 0,05), using Pearson correlation distance and average linkage.

We performed differential expression analysis between GBM preOp and healthy samples and identified 139 and 272 proteins respectively up- and downregulated in GBM preOp EVs (**Figure 50**).

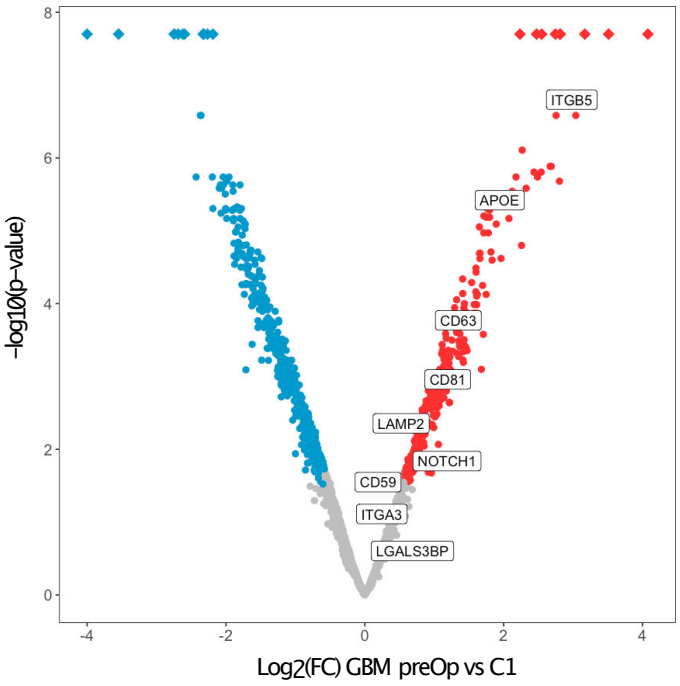

Figure 50. Differential expression analysis of the GBM and healthy EV proteomes.
Volcano plot showing differentially expressed proteins in GBM vs healthy EVs.

In GBM preOp EVs, BP terms of keratinization, lipoprotein particle organization, protein-lipid complex organization and lipid transport were enriched, while processes associated with fatty acid metabolism, redox reactions, and cellular respiration were downregulated (**Figure 51a**). The most significantly upregulated cellular components in GBM preOp EVs included proteins of the extracellular space, membrane proteins, and lipoproteins. Conversely, consistent with the BP ontologies, protein components of mitochondria and the respiratory chain were downregulated (**Figure 51b**).

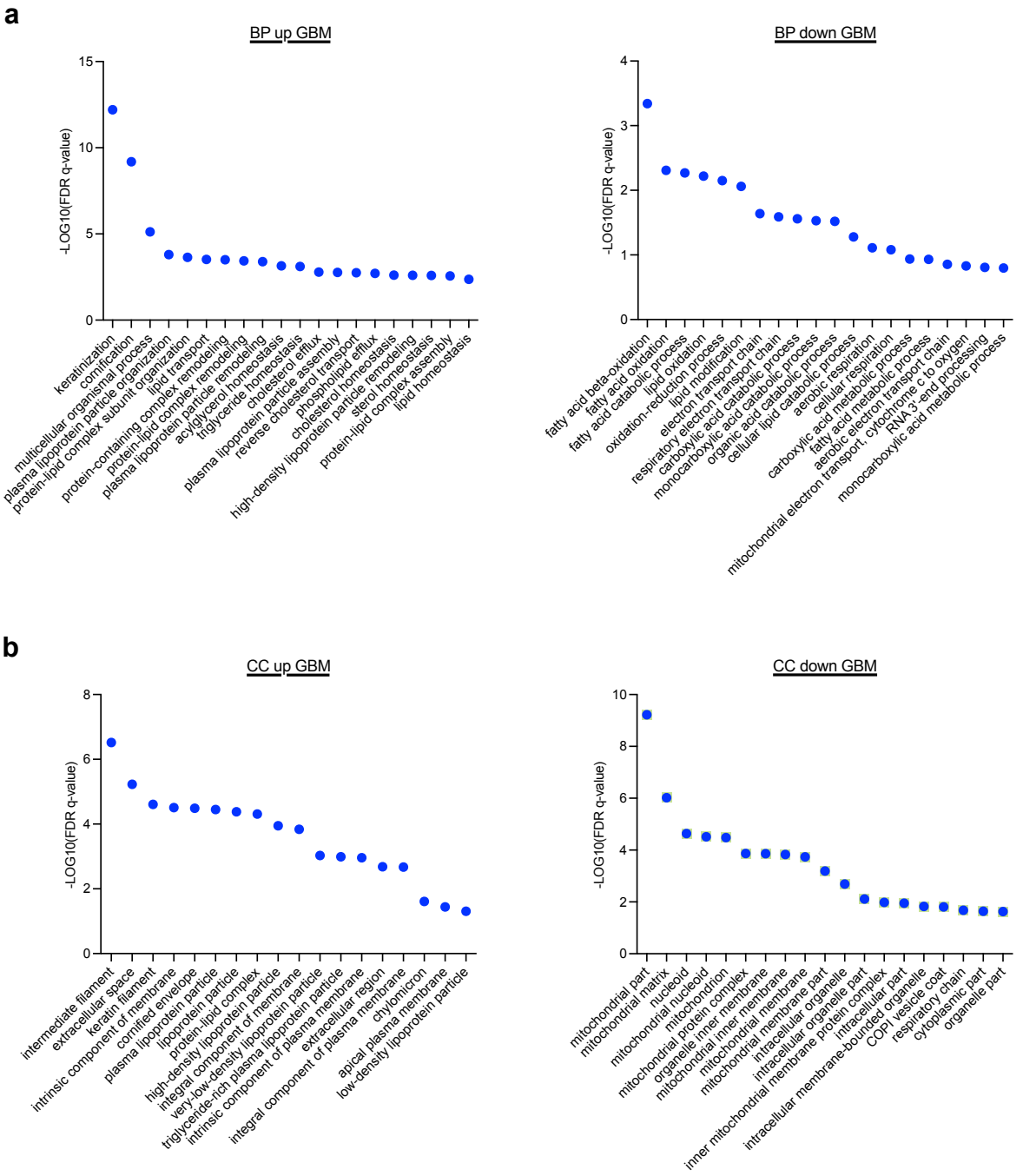

Figure 51. Gene ontology (GO) analysis of plasma EV proteins deregulated between GBM and healthy samples. (a, b) Dot plots showing the top biological processes (a) and cellular components (b) up- and downregulated in GBM pre-operative plasma EVs with respect to healthy controls.

Next, we compared the proteome of GBM preOp and postOp EVs and identified a total of 271 deregulated proteins (**Figure 52**).

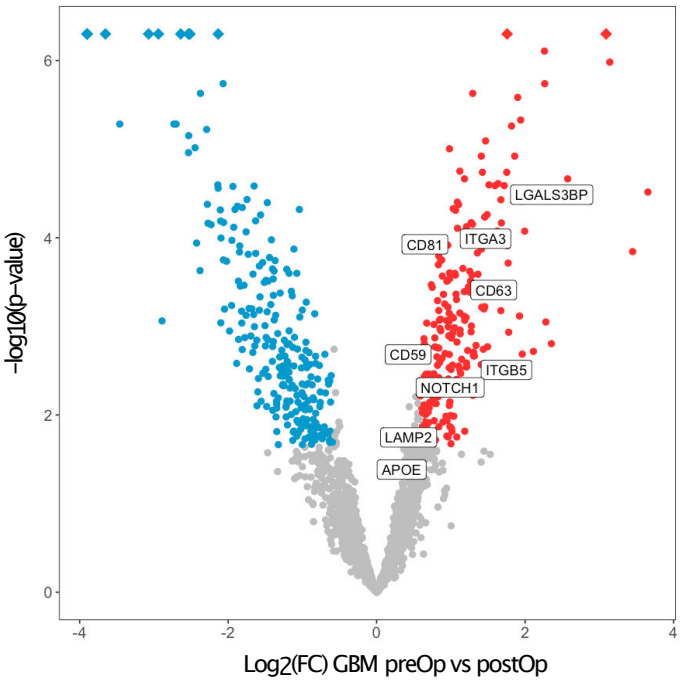

Figure 52. Differential expression analysis of the GBM pre- and post-operative EV proteomes.
Volcano plot showing differentially expressed proteins in GBM pre-operative (GBM preOp) vs GBM post-operative (GBM postOp) EVs.

GBM preOp EVs were enriched in BP terms of cholesterol efflux and regulation of cholesterol transport, production of molecular mediators of the immune response and remodeling of high-density lipoproteins. On the other hand, BP of the respiratory electron transport chain, cellular respiration, redox processes and fatty acid processing were downregulated (**Figure 53a**). In terms of cellular components, immunoglobulin complexes, plasma membrane and extracellular proteins, and lipoproteins were augmented in GBM pre-operative samples, while mitochondrial proteins and components of the respiratory chain complex were down-modulated (**Figure 53b**).

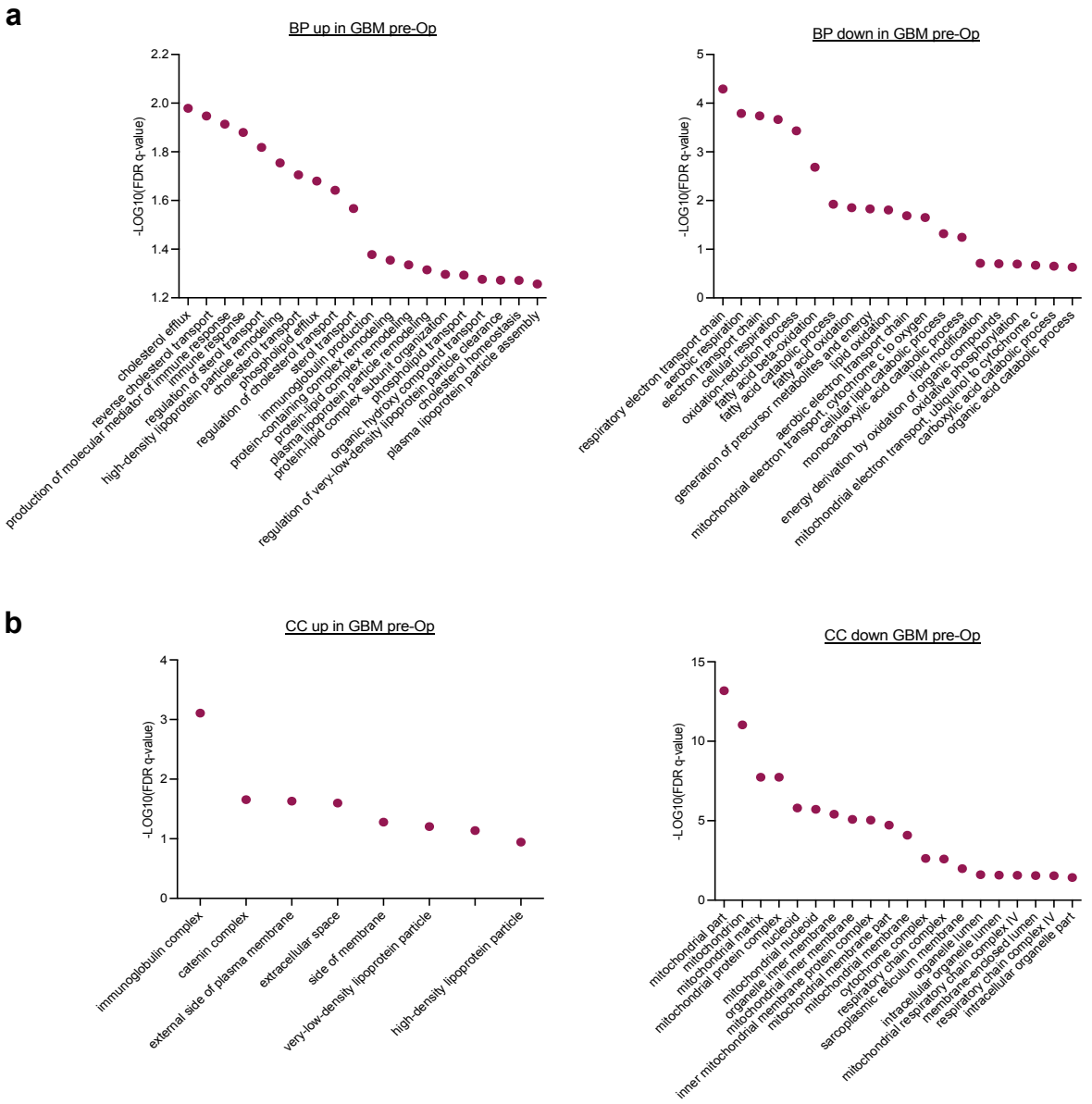

Figure 53. Gene ontology (GO) analysis of plasma EV proteins deregulated between GBM pre-operative and post-operative samples.

(a, b) Dot plots showing the top biological processes (a) and cellular components (b) up- and downregulated in GBM pre-operative vs GBM post-operative plasma EVs.

4.17 Weighted gene co-expression network analysis (WGCNA) reveals protein sets enriched in EV markers that provide further insights into GBM pathogenesis

In the last years, several papers demonstrated that blood-derived EVs present a protein corona that is constituted by soluble plasma proteins, mainly albumin and apolipoproteins[240]. While corona proteins have been shown to stabilize EVs in plasma[188], their abundance poses a significant challenge in proteomic studies, limiting the identification of disease biomarkers and relevant deregulated biological processes[241]. By co-expression network analysis we were able to cluster soluble plasma proteins ("contaminants") separately from "EV proteins"[242],

and identify nine modules of co-expressed proteins and enriched either in contaminants or EV proteins (**Figure 54**). Contaminants were found mainly in three of the nine clusters (black, pink and yellow), while EV proteins were enriched in six of the nine modules (blue, brown, green, red, turquoise, yellow) (**Figure 54**).

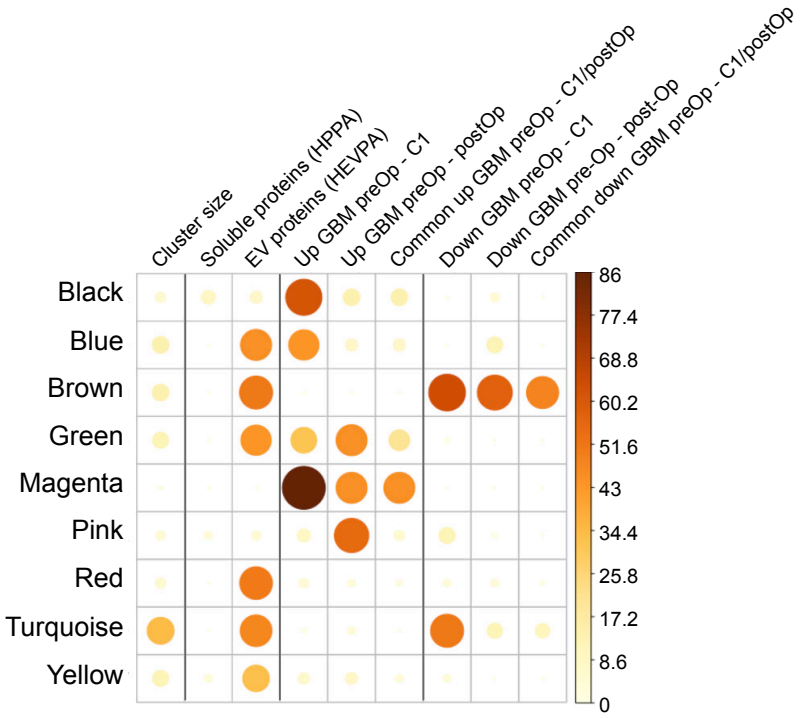

Figure 54. WGCNA analysis of plasma EV proteins.

Bubble plot showing the size of the nine modules identified by WGCNA, along with the enrichment of "contaminants" and "EV proteins" in each cluster. The dimension of the bubbles in the 'Size' column is proportional to the the fraction of the 1937 identified proteins present in each module, and matches the color scale. In the other columns, the bubbles size and color indicate the percentage of proteins of each module that are found within each group. "Contaminants" include the proteins of the Human Plasma Peptide Atlas (HPPA), while "EV proteins" were extrapolated from the Human Extracellular Vesicles Peptide Atlas (HEVPA)[242]. The bubble plot also shows the number of proteins enriched or down-modulated in GBM pre-operative (GBM preOp) EVs vs healthy (C1) and GBM post-operative (GBM postOp) EVs.

Proteins within the black cluster were mostly upregulated in GBM preOp vs healthy (C1) EVs. BP terms of activation and regulation of the complement and coagulation cascade, platelets degranulation and activation were enriched in this module (**Figure 55a**). Similar pathways were enriched in the pink cluster, which contained few contaminants and EV markers, and mostly proteins upregulated in GBM preOp EVs with respect to GBM postOp samples (**Figure 55f**).

In clusters enriched in EV markers and proteins upregulated in GBM preOp EVs, enriched BP included neutrophil degranulation, immune system, vesicles, focal adhesion (blue)

(**Figure 55b**), cell adhesion, and endosome development (green) (**Figure 55d**). Additionally, proteins in the green cluster were involved T-cell signaling, regulation of T-cell activation, Th1 and Th2 cell differentiation and TCR signaling. The magenta cluster was rich of keratins, that were upregulated in GBM preOp with respect to healthy EVs (**Figure 55e**).

In line with the GO analysis performed above, genes associated to oxidative phosphorylation, TCA cycle, metabolism, interaction of ER and mitochondria, fatty acid metabolism and mTORC1 signaling were down-modulated in GBM preOp EVs, and clustered in the brown module (**Figure 55c**). The red, turquoise and yellow clusters were also enriched in EV markers. While proteins annotated as 'red' or 'yellow' didn't contain many deregulated proteins, more than 30% of the 'turquoise' proteins were downregulated in GBM preOp EVs. Enriched BP in this module recalled mTORC1 signaling and development of the nervous system, alongside cell-substrate junction, focal adhesion, innate immune system and platelet aggregation (**Figure 55h**).

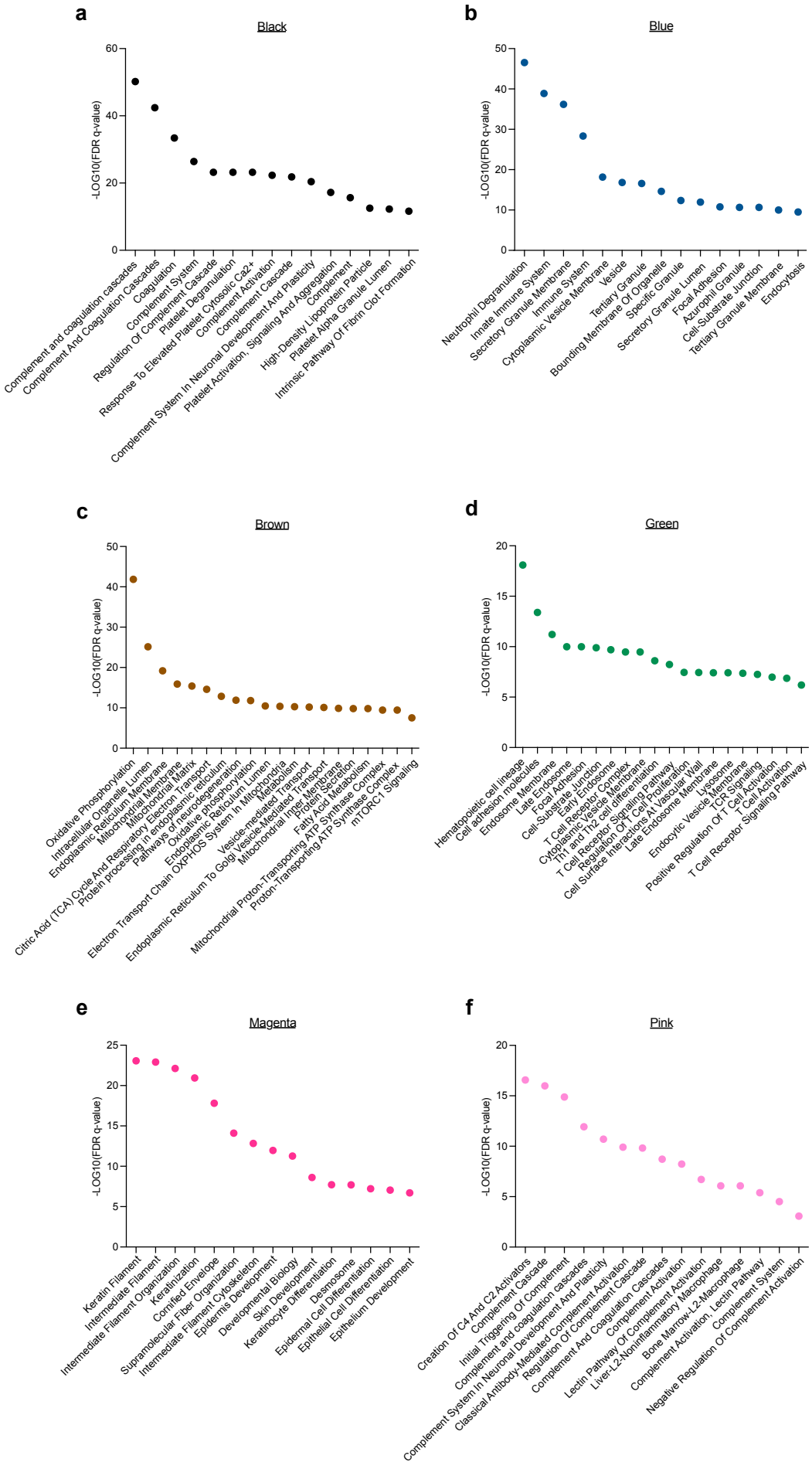
a
Black
-LOG10(FDR q-value)
Complement and coagulation cascades
Complement And Coagulation Cascades
Coagulation
Complement System
Regulation Of Complement Cascade
Platelet Degranulation
Response To Elevated Platelet Cytosolic Ca2+
Complement Activation
Complement Cascade
Complement System In Neuronal Development And Plasticity
Platelet Activation, Signaling And Aggregation
Complement
High-Density Lipoprotein Particle
Platelet Alpha Granule Lumen
Intrinsic Pathway Of Fibrin Clot Formation
b
Blue
-LOG10(FDR q-value)
Neutrophil Degranulation
Innate Immune System
Secretory Granule Membrane
Immune System
Cytoplasmic Vesicle Membrane
Vesicle
Tertiary Granule
Bounding Membrane Of Organelle
Specific Granule
Secretory Granule Lumen
Focal Adhesion
Azurophil Granule
Cell-Substrate Junction
Tertiary Granule Membrane
Endocytosis
c
Brown
-LOG10(FDR q-value)
Oxidative Phosphorylation
Intracellular Organelle Lumen
Endoplasmic Reticulum Membrane
Mitochondrial Membrane
Mitochondrial Matrix
Citric Acid (TCA) Cycle And Respiratory Electron Transport
Protein processing in endoplasmic reticulum
Pathways of neurodegeneration
Oxidative phosphorylation
Endoplasmic Reticulum Lumen
Mitochondria
Electron Transport Chain OXPHOS System In Mitochondria
Metabolism
Endoplasmic Reticulum To Golgi Vesicle-Mediated Transport
Vesicle-mediated Transport
Mitochondrial Inner Membrane
Protein Secretion
Mitochondrial Proton-Transporting ATP Synthase Complex
Fatty Acid Metabolism
Proton-Transporting ATP Synthase Complex
mTORC1 Signaling
d
Green
-LOG10(FDR q-value)
Hematopoietic cell lineage
Cell adhesion molecules
Endosome Membrane
Late Endosome
Focal Adhesion
Cell-Substrate Junction
Early Endosome
T Cell Receptor Complex
Cytoplasmic Vesicle Membrane
Th1 and Th2 cell differentiation
T Cell Receptor Signaling Pathway
Regulation Of T Cell Proliferation
Cell Surface Interactions At Vascular Wall
Late Endosome Membrane
Lysosome
Endocytic Vesicle Membrane
TCR Signaling
Positive Regulation Of T Cell Activation
T Cell Activation
T Cell Receptor Signaling Pathway
e
Magenta
-LOG10(FDR q-value)
Keratin Filament
Intermediate Filament
Intermediate Filament Organization
Keratinization
Cornified Envelope
Supramolecular Fiber Organization
Intermediate Filament Cytoskeleton
Epidermis Development
Developmental Biology
Skin Development
Keratinocyte Differentiation
Desmosome
Epidermal Cell Differentiation
Epithelial Cell Differentiation
Epithelium Development
f
Pink
-LOG10(FDR q-value)
Creation Of C4 And C2 Activators
Complement Cascade
Initial Triggering Of Complement
Complement and coagulation cascades
Complement System In Neuronal Development And Plasticity
Classical Antibody-Mediated Complement Activation
Regulation Of Complement Cascade
Complement And Coagulation Cascades
Complement Activation
Lectin Pathway Of Complement Activation
Liver-L2-Noninflammatory Macrophage
Bone Marrow-L2-Macrophage
Complement Activation, Lectin Pathway
Complement System
Negative Regulation Of Complement Activation

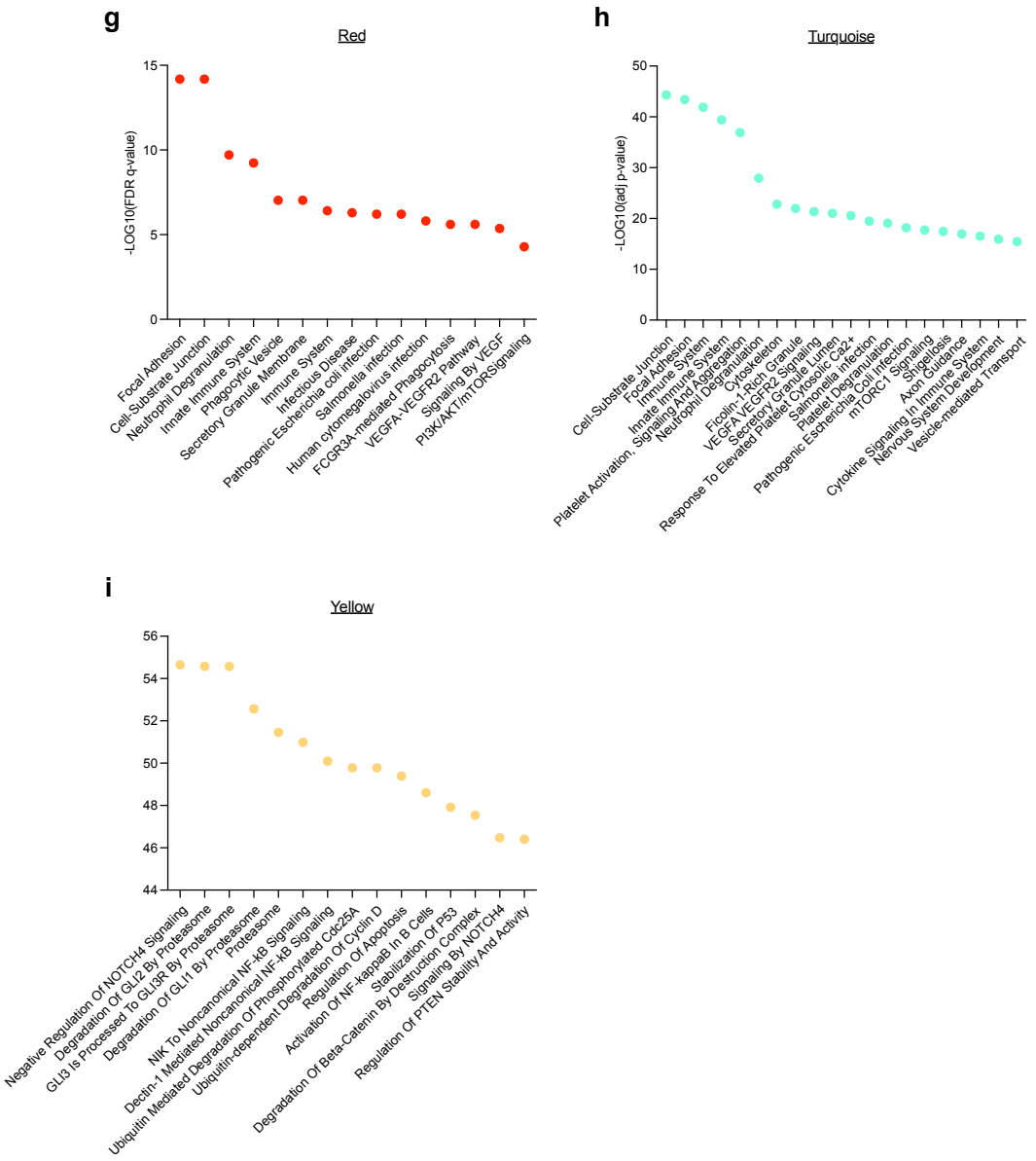

Figure 55. Gene ontology (GO) analysis of EV proteins clustering by WGCNA.

(a-i) Dot plots showing the top biological processes enriched in each cluster identified by the co-expression analysis of EV proteins.

4.18 GBM EVs are enriched in proteins implicated in GBM tumorigenesis

The clustering analysis allowed to identify modules of proteins upregulated in GBM preOp samples, that are more likely associated with the EV, rather than with the soluble compartment of plasma. In order to identify candidate GBM biomarkers, we focused our attention on the proteins of the blue and green clusters that were enriched in GBM preOp EVs. Few proteins stood out as they were also among the reference EV markers listed above (**Table 8**), including the lysosome-associated membrane protein 2 (LAMP2), cluster of differentiation (CD) 59, CD63, CD81, integrin beta 5 (ITGB5) and APOE (**Figure 50**,

Figure 52). Bulk RNAseq data from the GEPIA repository (http://gepia.cancer-pku.cn/) confirmed the overexpression of these targets in GBM vs normal tissue (**Figure 56**).

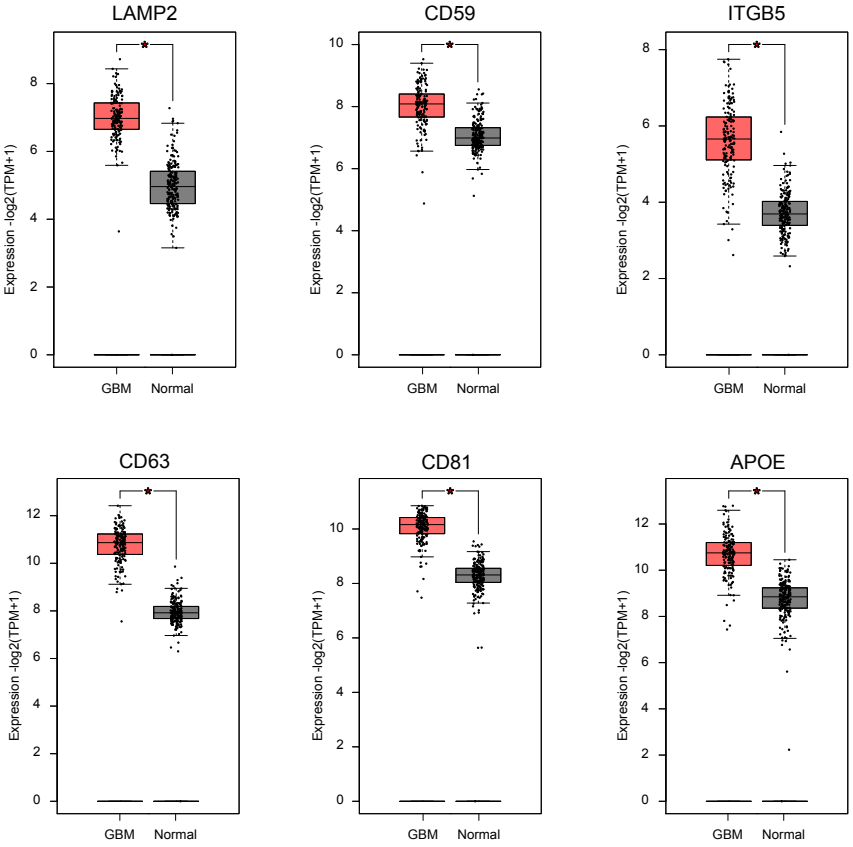

Figure 56. Average level of candidate biomarkers in in GBM and normal tissue based on GEPIA database.
Boxplot of the transcript levels of expression of candidate GBM-EV biomarkers selected from our proteomic analysis. Dots represent different GBM (n=163) and normal (n=207) tissue samples.

The involvement of these proteins in tumorigenesis has been described in literature. For instance, the constitutive activation of LAMP2, also known as CD107b, promotes cancer cell survival via chaperone-mediated autophagy (CMA) in breast cancer[243], and its overexpression acts as prognostic biomarker as well as marker of immune infiltration in various human cancers[243]. In glioma stem cells, LAMP2 levels correlate with the expression of stem cell markers (i.e. SOX2 and SOX9), and scRNAseq and proteomic analysis revealed the higher expression of LAMP2 in GBM tumor center with respect to matched peri-tumoral edema zone and low-grade glioma samples, suggesting the activation of LAMP2-associated programs that promote cancer progression[244,245].

Also ITGB5, a surface protein involved in cell adhesion and cell-surface signaling, has potential implications in GBM development. ITGB5 has a major role in Type3 epithelial-to-mesenchymal transition (EMT) which is associated with poor prognosis, immune escape and

invasiveness in GBM[246]. Indeed, despite GBM cells originate from astrocytes and not from an epithelial lineage, EMT-like processes are active in GBM cells[247], and contribute to their migratory/infiltrating potential[248].

CD59, a well characterized complement regulator, is highly expressed in glioma tissues and cell lines, and to a lower degree in normal astrocytes[249]. CD59 acts as an immune system component associated with GBM microenvironment, and is expressed on GBM cells and not on tumor-associated macrophages (TAMs)[250]. GBM cells that express CD59 are resistant to complement-mediated lysis[251]. Indeed, among complement regulators, CD59 was considered the key complement regulator of GBM cells[251].

We found few studies that state an association between the expression of the tetraspanins CD63 and CD81 and GBM development and/or progression. One review on the role of EVs in GBM, highlighted that high expression of EV markers, including both CD63 and CD81, is associated with poor survival in glioma patients[252]. CD63 expression investigated by IHC was significantly higher in glioblastoma with respect to other astrocytomas[253]. A recent study also demonstrated that CD63+ EVs in plasma from GBM patients are loaded with a tumor-associated variant of EGFR, and that their abundance is higher in GBM than in healthy plasma[254].

Despite not included in the reference EV markers list defined above (**Table 8**), we found interesting the upregulation of NOTCH1 - and its ligand jagged canonical Notch ligand 1 (JAG1) - in GBM EV samples, given its multifaceted role in cell proliferation, apoptosis, migration, self-renewal, and differentiation[255]. Several papers reported the activation of NOTCH signaling in the glioblastoma stem cells (GSCs) niche, where it suppresses differentiation and contribute to the maintenance of stem-like properties, supporting GBM tumorigenesis and resistance to conventional treatments[256,257]. GSCs expressing high levels of NOTCH displayed higher tumor initiation and self-renewal capacity, by increasing the expression of stem cell markers such as Oct4, Sox2, and CD44[256]. Finally, spatial proteomic analysis of GBM tissues detected high levels of expression of five proteins related to Notch signaling in clusters enriched in TCGA glioma gene signatures[257].

Of note, all these proteins were downregulated in matched GBM postOp samples (**Figure 57**). This makes them interesting candidate biomarkers to validate, with potential clinical utility for both GBM diagnosis and monitoring.

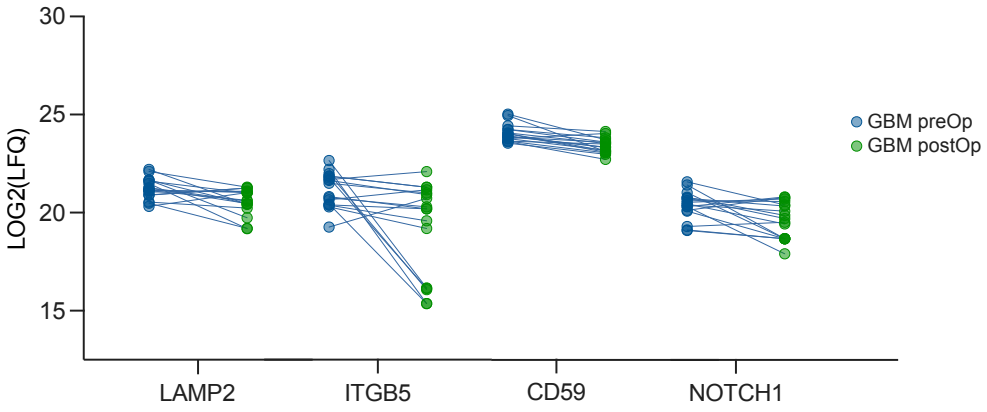

Figure 57. Expression levels of candidate GBM EV biomarkers in matched pre- and post-operative GBM plasma.
The expression of selected candidate GBM biomarkers dropped in 17 matched GBM pre- and post-operative plasma EV samples analyzed by mass spectrometry.

5. Discussion

The study of circulating biomarkers is fundamental for the management of brain malignancies such as GBM, whose anatomical location and heterogeneity hamper the longitudinal and comprehensive monitoring of tumor dynamics. Since EVs cross the blood brain barrier, carrying tumor-associated information, they are a promising tool for GBM care by liquid biopsy.

From a clinical perspective, we established a rapid, economic, and straightforward assay that allowed us to demonstrate the specific enrichment of plasma EVs in GBM. To our knowledge, this is an unprecedented result. Our method allows the efficient isolation of EVs from as low as 2mL of plasma using SEC, in a short time and with minimal costs per patient. Our data prove that TRPS provides precise and reproducible measurement of EV concentration and size, which is cardinal for their use as biomarkers. Indeed, we assessed TRPS reproducibility systematically, finding that EV measurements were largely consistent across replicates, even with different sample dilution. Importantly, variability in repeated measures was noted primarily when the particle rate fell outside the recommended range (i.e. 100 and 1500 particles/min) or neared the extremes. These findings reaffirm the necessity of evaluating the reliability of EV measurements to support their translation from bench to bedside.

We demonstrated that pre-operative GBM (GBM preOp) plasma contains, on average, ten times more EVs compared to healthy controls (C1) and patients with other CNS pathologies (C2). This highlights the potential of assessing EVs abundance as a companion biomarker for GBM detection, achieving a diagnostic specificity that MRI alone may not always provide. One reasonable hypothesis underlying the higher abundance of EVs in GBM plasma is the increased cell-to-vessels ratio in GBM with respect to the healthy brain and to other CNS pathologies[258]. The cerebral vasculature is already very dense *per se*, but in GBM the degree of vascularization is boosted by vasculogenesis and sprouting angiogenesis, as well as less canonical mechanisms including vessel co-option, vascular mimicry and transdifferentiation of GBM stem cells to give rise to tumor endothelium[258,259]. In fact, increased microvascular proliferation is a key feature of high grade gliomas[1,2]. It is also reported that GBM endothelial cells (EVs) show increased ability to develop an intensive vasculature (i.e. vessels are longer and more branched)[260] with respect to low-grade glioma (LGG) and meningiomas (MNG) ECs. Additionally, vessels created by GBM ECs are more

permeable, and the vasculature was overall more fenestrated[260]. As a consequence, the secretome of most cells of GBM tumor core and TME will have increased access to the bloodstream.

Within the C2 cohort, the subgroup of brain metastasis showed higher EVs abundance in comparison to the other brain tumors, but not to GBMs. Brain metastasis derive from diverse primary tumors and represent a systemic disease. Indeed, EVs were shown to take part in tumor progression via the establishment of pre-metastatic niches that favor the colonization of circulating tumor cells (CTCs) to specific organs, including the brain[261]. As a result, an increase in the levels of plasmatic EVs could be observed in patients with metastatic tumors. The significance of the differences in EV concentration among the C2 subgroups is limited by the low number of patients enrolled. We will enlarge the cohort of brain metastasis and other gliomas patients to validate the potential of plasma EVs concentration for the differential diagnosis of these CNS malignancies.

Upon tumor resection, EVs concentration drops significantly, reaching levels resembling those of healthy samples. These data confirm that the augmented abundance of EVs in GBM plasma is strongly dependent on tumor presence. We will assess if the abundance of GBM postOp EVs in plasma correlates with MRI data and is indicative of the extent of tumor resection. Further, the comparison with patients' clinical parameters (PFS, OS) will reveal if plasma EV concentration is also a reliable prognostic indicator.

Alongside EV concentration, we also measured the EV size and showed that GBM EVs are larger compared to both C1 and C2 samples. EVs > 150nm were the least abundant in all cohorts, but we found a relative enrichment of these medium-size EVs in GBM plasma. To our knowledge, these are unprecedented results. We speculate that tumor-associated EVs might be mostly in the size range of microvesicles (MVs), whose blebbing from the plasma membrane is a fast process[262]. Exosomes secretion, on the other hand, is multi-step and tightly regulated by the interplay of several enzymes and subcellular compartments[262]. Thus, fast proliferating cells (i.e. tumor cells) might prefer MVs secretion for intercellular communication within the tumor core and the TME. The isolation and characterization of small- and medium- GBM EVs will allow to understand if they have different implications in GBM pathology and if tumor-associated cells derive from specific biogenetic routes. Notably, we could distinguish brain metastasis EVs from GBM EVs based on their reduced size.

EV size drops after tumor resection in matched pre- and post-operative samples, mirroring tumor presence. Accordingly, the relative abundance of medium-size vesicles (i.e. EV diameter > 150nm) is higher in preOp GBM plasma, while EVs smaller than 100nm are

enriched in postOp GBM samples. These data demonstrate that also EV size distribution is a valuable companion biomarker of GBM presence.

We extended the measurement of EVs longitudinally in GBM plasma collected one month post-operative, at regular two months intervals after treatment and, when possible, until relapse. In the patients analyzed this far, EV fluctuations reflected disease progression as monitored by MRI: in detail, when MRI showed signs of relapse, EV concentration was increased with respect to the early post-operative timepoint. Actually, EV concentration at follow-up increased before clear signs of progression were detectable by MRI. We also measured high levels of EVs at relapse, and a drop after tumor removal, consistent with our observations at the baseline. These results suggest that routine screening of plasma vesiclemia[263] in GBM patients can serve as non-invasive monitoring tool of disease progression, and could complement MRI for the early detection of tumor progression and relapse. We will extend the longitudinal analysis to a larger cohort of patients and assess if measurements of EVs abundance correlate with treatment efficacy as well as disease progression, allowing prompt therapeutic intervention.

Of note, we also assessed the changes in EV size in longitudinal plasma samples but we did not observe a clear correlation with disease progression.

DNA can be found in circulation either free (cfDNA) or associated with proteins and membranous particles, including EVs[212]. We demonstrated that DNA is associated with EVs from GBM and healthy plasma, and that some EVs show a higher content of nucleic acids. Biologically, the variability in the amount of DNA associated with plasma EVs could be attributed to their heterogeneity in terms of cell of origin, biogenesis, function and ultimately, their cargo[264,265]. We assessed if plasma EV-DNA cargo is informative about the primary tumor. We found that EV-DNA is scarce and not enriched in EVs. Of note, DNA concentration remained undetectable by Qubit even when we scaled up the input volume of plasma from 2mL up to 6mL. We also compared different DNA isolation methods but none improve our results.

The targeted detection of parental mutations and copy number alterations in EV-DNA was inconclusive. These findings are in line with the current literature on circulating EV-DNA in other tumors[96,266], and devalue the use of EV-DNA as surrogate of tissue DNA for tumor profiling. Considering that the DNA cargo of cell-derived EVs recapitulates the genomic landscape of parental cells[212,267], it is likely that the utility of plasma EV-DNA as surrogate of tumor DNA has intrinsic challenges related to its dilution in physiological EV-bound and cell-free DNA. Similarly, plasma extracellular DNA (exDNA, including both EV-DNA and

cfDNA) did not mirror the genetic alterations present in the matched tumor tissue, despite the higher concentration with respect to EV-DNA alone.

We did not find significant differences in exDNA abundance between GBM and healthy samples. The variability in the outcome with respect to other studies might depend on the biofluid collection and DNA isolation procedures[268], on patient's physiology[269], as well as to the presence of the BBB, whose extent of disruption and permeability in different patients might affect the levels of cfDNA detectable in plasma. On the other hand, we measured a smaller fragment size of exDNA in GBM patients with respect to healthy controls, in agreement with previous observations[224,270], and witnessing the secretion of truncated DNA from apoptotic cells[271]. The size of our cohort will be increased, and longitudinal GBM samples will be included, to demonstrate the clinical impact of the analysis of exDNA fragment size.

The assessment of genomic alterations by shallow WGS revealed that exDNA recapitulates only a small subset of the alterations found in matched tumor tissue. Ongoing analysis of shared CNA regions will determine their relevance for GBM diagnosis. The low tumor fraction in exDNA indicates that, even with sNGS, the dilution of tumor DNA in plasma limits the retrieval of CNAs present in tissue samples. Additionally, the significant tumor heterogeneity in GBM may account for the discrepancies between alterations detected in tissue versus extracellular DNA. We plan to apply a guided molecular targeting approach, selecting genomic alterations with a high variant allele frequency (VAF) in the tumor tissue from each patient, and searching for these in exDNA via ddPCR and targeted sequencing. The utility of this analysis will be evaluated at follow-up.

Private alterations are often identified in GBM tissue sampled from different tumor regions[224], highlighting the extensive intratumor heterogeneity. In this context, we will further investigate the private mutations identified in exDNA, hypothesizing that we may uncover genetic alterations overlooked in tumor biopsies due to sampling bias. If so, the analysis of exDNA could provide a non-invasive method for detecting tumor presence and potentially profiling GBM at the time of diagnosis.

EV proteins are abundant, and a rich source of disease biomarkers[233–237]. In a pilot experiment we showed the feasibility of analyzing the EV protein cargo by LC-MS/MS and the potential to identify DEPs among GBM and healthy plasma EVs. In a large cohort of GBM pre-operative, healthy and GBM post-operative samples, we detected a broad range of protein expression levels, in line with other proteomic studies of plasma EVs[237,272]. A majority of reference EV markers were present and abundant in our dataset, further

confirming the efficiency of SEC to enrich EVs from plasma. Few proteins (n=173) overlapped with the Human Plasma Peptide Atlas (HPPA) database[242], including albumin, apolipoproteins, serpins and complement proteins. While they constitute a small fraction of our EV proteomic datasets, they are overall more abundant than EV-markers.

The functional annotation of identified proteins highlighted the enrichment of biological processes related to platelets activation, neutrophils degranulation and immune system activation. Indeed, platelets and immune cells are the major contributors of circulating EVs[185,273,274], and the GO analysis highlights that most EVs in our samples derive from non-tumor cells and likely from cells outside the CNS.

The unsupervised clustering of all deregulated proteins highlighted similar protein expression across samples, suggesting that the separation of GBM, healthy and GBM postOp cohorts based on the plasma EV proteome relies on the differential expression of few proteins, among which we ought to identify candidate GBM biomarkers. Indeed, a GBM-specific signature of 139 proteins emerged from the differential expression analysis of the GBM and healthy EV proteomes. Notably, some proteins included in this signature were downregulated in GBM post-operative plasma. This EV protein signature will be monitored longitudinally to confirm its clinical significance for GBM detection and to track disease progression.

While SEC outperforms other EV isolation methods to purify EVs from plasma contaminants, it does not completely remove soluble proteins or the protein corona surrounding EVs[275]. Proteins such as immunoglobulins[240] and apolipoproteins[276] adhere to the EV surface, co-elute with EVs and appear in proteomic datasets. The abundance of these proteins in EV preparations complicates the identification of disease biomarkers, which are often expressed at lower levels[272]. To address this, we applied weighted co-expression network analysis to identify clusters of proteins with minimal content of “contaminants”. Indeed, “contaminants” and intrinsic “EV proteins” segregated into distinct modules. In contaminants-rich clusters, proteins upregulated in pre-operative GBM samples were enriched in pathways related to the complement and coagulation cascades, consistent with previous findings from our lab[100]. The high levels of complement proteins suggest a hypercoagulable state in GBM patients, aligning with evidence of thrombosis and coagulation disorders commonly observed in GBM[277]. Moreover, there is evidence that GBM cells promote the expression of complement proteins by the TME, co-opting them to support growth and maintain stemness features[278,279].

Within clusters with fewer contaminants and higher levels of true EV proteins, we identified biological processes likely linked to GBM that did not emerge in the initial, unbiased GO

analysis. In particular, pathways of T-cell signaling, regulation of T-cell activation, Th1 and Th2 cell differentiation and TCR signaling were enriched in GBM preOp EVs. It is now established that infiltrating T-cells are abundant in the GBM tumour microenvironment (TME) and play key roles in immunity and disease progression[280,281]. The enrichment of specific immune markers in pre-operative GBM samples highlights the potential of plasma EV proteomics to provide insights into active immune responses within the TME.

Furthermore, the protein cargo analysis of GBM-derived EVs reveals metabolic dysregulations, a hallmark of GBM[282]. In GBM, genetic alterations affecting TCA cycle and oxidative phosphorylation (OXPHOS) enzymes lead to the disruption of oncogenic pathways, making metabolic reprogramming frequent and essential for sustained cancer cell proliferation[283].

We identified potential GBM biomarkers within clusters enriched in EV markers and proteins that are upregulated in pre-operative GBM EVs. Our primary focus was on proteins previously linked to GBM tumorigenesis and whose levels decrease following tumor resection. Further validation of these proteins through targeted approaches, coupled with the evaluation of their expression in longitudinal plasma EV samples and in relation with patients' clinical parameters (PFS, OS), will help confirm their biomarker role. Ultimately, our major goal is the identification of a panel of reliable biomarkers to enrich GBM-associated EVs. By this strategy, we could improve the analysis of EV-DNA, damping the effect of the dilution of tumor-derived material in plasma on the efficiency of retrieving parental genetic alterations. This additional layer of data will support the implementation of liquid biopsies in clinical practice, enabling early GBM detection and effective monitoring of disease progression.

Annex

In the final three months of my PhD, I visited Professor Samir El Andaloussi's lab at Karolinska Institutet in Stockholm to learn and apply single-EV imaging flow cytometry (IFCM) for validating the selected candidate biomarkers. Although the results are still preliminary, they are promising, and I will briefly present them in this annex.

To verify that IFCM can reliably detect single EVs, we stained serial dilutions of SEC-isolated GBM EVs with a cocktail of FITC-conjugated antibodies targeting the tetraspanins CD9, CD63 and CD81 (PAN-TS). FITC+ events were gated based on the background detected in unstained EVs. Optimized IFCM settings[187] enabled us to distinguish smaller, SSClow/FITC+ events (EVs ranging from 70 nm to 350 nm) and larger, SSCint/FITC+ events (EVs between 400 nm and 1 µm).. The number of FITC+ events was proportional to the input quantity of EVs. The number of SSCint/FITC+ events was lower with respect to SSClow/FITC+ at all concentrations. This aligns with the prevalence of EVs in the 50 nm to 350 nm range observed during SEC EV characterization.

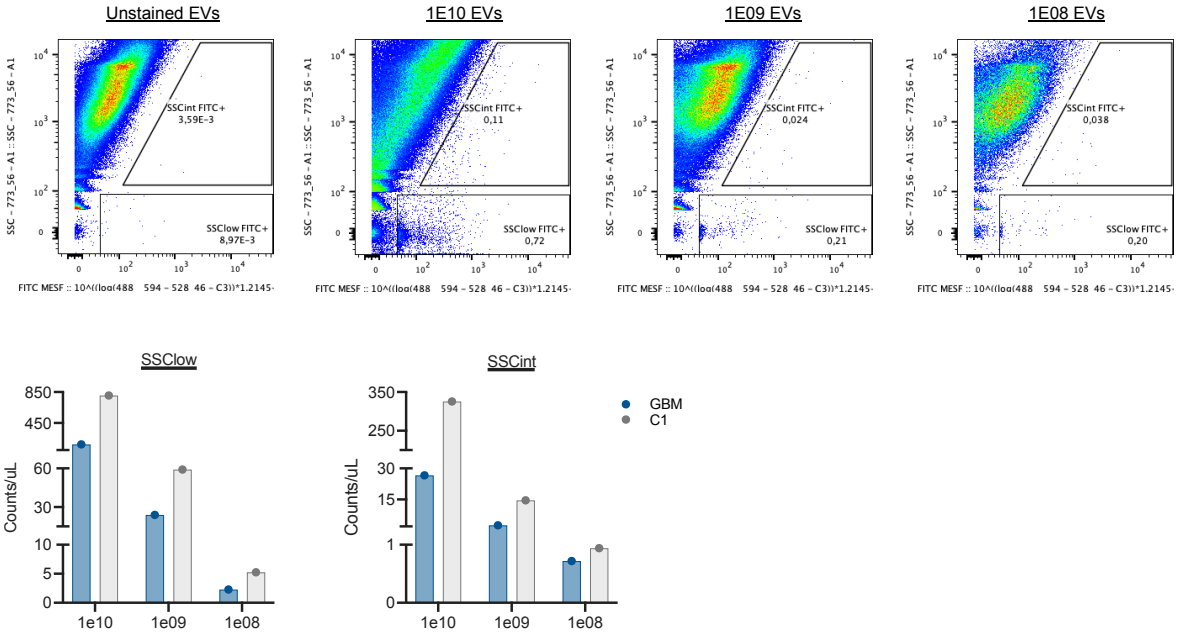

Given the feasibility of analyzing SEC EVs by IFCM, we began the validation by staining EVs from GBM and healthy control samples with a mix of FITC-conjugated antibodies targeting CD63 and CD81. In this pilot experiment, we pooled equal numbers of EVs from five GBM and five healthy subjects. IFCM analysis confirmed higher CD63/CD81 expression in GBM EVs across both SSClow and SSCint size ranges.

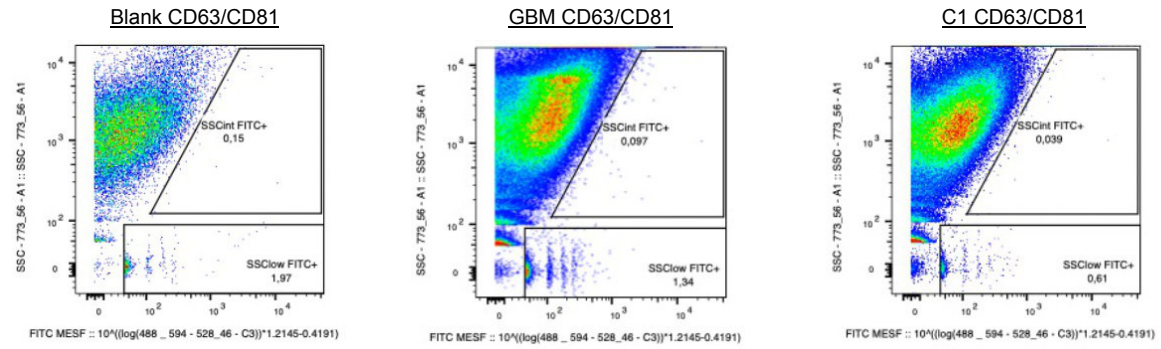

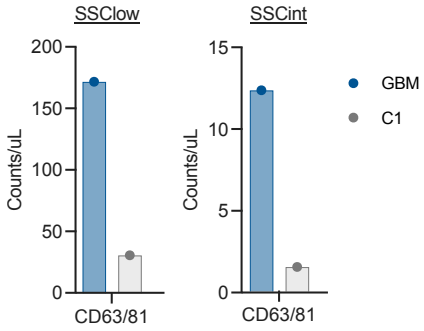

Next, we stained EVs from five GBM patients and four healthy subjects with antibodies against CD49c, CD107b and ITGB5. For all three targets, we counted more SSClow fluorescent events in GBM samples compared to healthy controls. The number of fluorescent events within the SSCint gate was always below the background. Additionally, we verified the higher expression of CD63/CD81 in GBM EVs.

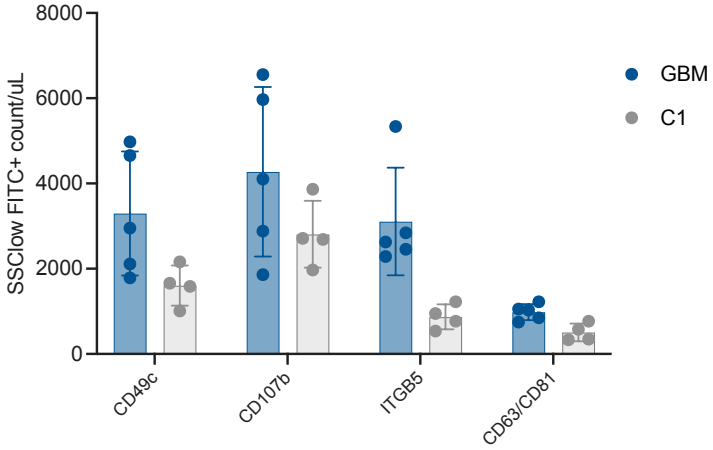

We tested the expression of CD59 and NOTCH1 too. However, a high antibody background signal for CD59 interfered with the detection of CD59+ EVs, and further antibody testing is ongoing. For NOTCH1, despite minimal background, we detected no fluorescent events in either GBM or C1 EVs. Indeed, as NOTCH1 is not annotated as an EV marker, and both plasma and EV proteomic studies suggest that NOTCH1 is more likely a secreted protein, our findings are consistent with these observations.

We are currently validating these preliminary results on a larger cohort of GBM patients and healthy subjects, and plan to include post-operative GBM samples to further corroborate the proteomic data.

Bibliography

1. Louis, D. N. *et al.* The 2021 WHO classification of tumors of the central nervous system: A summary. *Neuro Oncol* 23, 1231–1251 (2021).
2. Redlich, J.-P. *et al.* Applications of artificial intelligence in the analysis of histopathology images of gliomas: a review. *npj Imaging* 2, (2024).
3. Ostrom, Q. T., Cioffi, G., Waite, K., Kruchko, C. & Barnholtz-Sloan, J. S. CBTRUS Statistical Report: Primary Brain and Other Central Nervous System Tumors Diagnosed in the United States in 2014-2018. *Neuro Oncol* 23, III1–III105 (2021).
4. Smith, C. J. *et al.* Risk factors for glioblastoma are shared by other brain tumor types. *Human and Experimental Toxicology* vol. 43 Preprint at https://doi.org/10.1177/09603271241241796 (2024).
5. Gunasegaran, B., Ashley, C. L., Marsh-Wakefield, F., Guillemin, G. J. & Heng, B. Viruses in glioblastoma: an update on evidence and clinical trials. *BJC Reports* 2, (2024).
6. Gilard, V. *et al.* Diagnosis and management of glioblastoma: A comprehensive perspective. *Journal of Personalized Medicine* vol. 11 Preprint at https://doi.org/10.3390/jpm11040258 (2021).
7. Yuile, P., Dent, O., Cook, R., Biggs, M. & Little, N. Survival of glioblastoma patients related to presenting symptoms, brain site and treatment variables. *Journal of Clinical Neuroscience* 13, 747–751 (2006).
8. Comba, A. *et al.* Uncovering Spatiotemporal Heterogeneity of High-Grade Gliomas: From Disease Biology to Therapeutic Implications. *Frontiers in Oncology* vol. 11 Preprint at https://doi.org/10.3389/fonc.2021.703764 (2021).
9. Ohgaki, H. & Kleihues, P. The definition of primary and secondary glioblastoma. *Clinical Cancer Research* vol. 19 764–772 Preprint at https://doi.org/10.1158/1078-0432.CCR-12-3002 (2013).
10. Ohgaki, H. & Kleihues, P. Genetic pathways to primary and secondary glioblastoma. *American Journal of Pathology* vol. 170 1445–1453 Preprint at https://doi.org/10.2353/ajpath.2007.070011 (2007).
11. Liu, A., Hou, C., Chen, H., Zong, X. & Zong, P. Genetics and epigenetics of glioblastoma: Applications and Overall Incidence of IDH1 Mutation. *Front Oncol* 6, (2016).

12. Das, S. & Marsden, P. A. Angiogenesis in Glioblastoma. *New England Journal of Medicine* 369, 1561–1563 (2013).
13. Munir, S., Khan, S. A., Hanif, H. & Khan, M. Diagnostic accuracy of magnetic resonance imaging in detection of intra-axial gliomas. *Pak J Med Sci* 37, 1–6 (2021).
14. Bonm, A. V., Ritterbusch, R., Throckmorton, P. & Graber, J. J. Clinical Imaging for Diagnostic Challenges in the Management of Gliomas: A Review. *Journal of Neuroimaging* vol. 30 139–145 Preprint at https://doi.org/10.1111/jon.12687 (2020).
15. Young, J. S., Al-Adli, N., Scotford, K., Cha, S. & Berger, M. S. Pseudoprogression versus true progression in glioblastoma: what neurosurgeons need to know. *J Neurosurg* 139, 748–759 (2023).
16. Reithmeier, T. *et al.* Intraindividual comparison of histopathological diagnosis obtained by stereotactic serial biopsy to open surgical resection specimen in patients with intracranial tumours. *Clin Neurol Neurosurg* 115, 1955–1960 (2013).
17. Pathology, R. S. *Limitations of Stereotactic Biopsy in the Initial Management of Gliomas 1,2*. *Neuro-Oncology* vol. 3 https://academic.oup.com/neuro-oncology/article/3/3/193/1163793.
18. Stupp, R. *et al. Radiotherapy plus Concomitant and Adjuvant Temozolomide for Glioblastoma*. www.nejm.org.
19. Neftel, C. *et al.* An Integrative Model of Cellular States, Plasticity, and Genetics for Glioblastoma. *Cell* 178, 835-849.e21 (2019).
20. Wang, J. *et al.* Clonal evolution of glioblastoma under therapy. *Nat Genet* 48, 768–776 (2016).
21. Bao, S. *et al.* Glioma stem cells promote radioresistance by preferential activation of the DNA damage response. *Nature* 444, 756–760 (2006).
22. Poon, M. T. C., Sudlow, C. L. M., Figueroa, J. D. & Brennan, P. M. Longer-term (≥ 2 years) survival in patients with glioblastoma in population-based studies pre- and post-2005: a systematic review and meta-analysis. *Sci Rep* 10, (2020).
23. Brennan, C. W. *et al.* The somatic genomic landscape of glioblastoma. *Cell* 155, 462 (2013).
24. Lassman, A. B. *et al.* Depatuxizumab mafodotin in EGFR-amplified newly diagnosed glioblastoma: A phase III randomized clinical trial. *Neuro Oncol* 25, 339–350 (2023).
25. Gallia, G. L. *et al.* PIK3CA gene mutations in pediatric and adult glioblastoma multiforme. *Molecular Cancer Research* 4, 709–714 (2006).
26. Wen, P. Y. *et al.* PHASE II TRIAL OF THE PHOSPHATIDYINOSITOL-3 KINASE (PI3K) INHIBITOR BUPARLISIB (BKM120) IN RECURRENT

GLIOBLASTOMA CONDUCTED BY THE IVY FOUNDATION EARLY PHASE CLINICAL TRIALS CONSORTIUM. *Neuro Oncol* 16, iii47–iii47 (2014).

27. Maira, S. M. *et al.* Identification and characterization of NVP-BEZ235, a new orally available dual phosphatidylinositol 3-kinase/mammalian target of rapamycin inhibitor with potent in vivo antitumor activity. *Mol Cancer Ther* 7, 1851–1863 (2008).
28. Bhat, K. P. L. *et al.* Mesenchymal Differentiation Mediated by NF-κB Promotes Radiation Resistance in Glioblastoma. *Cancer Cell* 24, 331–346 (2013).
29. Avci, N. G. *et al.* NF-κB inhibitor with Temozolomide results in significant apoptosis in glioblastoma via the NF-κB(p65) and actin cytoskeleton regulatory pathways. *Sci Rep* 10, (2020).
30. Xu, R. *et al.* Molecular and clinical effects of notch inhibition in glioma patients: A phase 0/I trial. *Clinical Cancer Research* 22, 4786–4796 (2016).
31. Reardon, D. A. *et al.* Effect of Nivolumab vs Bevacizumab in Patients with Recurrent Glioblastoma: The CheckMate 143 Phase 3 Randomized Clinical Trial. *JAMA Oncol* 6, 1003–1010 (2020).
32. Rios, S. A. *et al.* Emerging Therapies for Glioblastoma. *Cancers* vol. 16 Preprint at https://doi.org/10.3390/cancers16081485 (2024).
33. Todo, T. *et al.* Intratumoral oncolytic herpes virus G47Δ for residual or recurrent glioblastoma: a phase 2 trial. *Nat Med* 28, 1630–1639 (2022).
34. Markert, J. *et al. Conditionally Replicating Herpes Simplex Virus Mutant, G207 for the Treatment of Malignant Glioma: Results of a Phase I Trial*. *Gene Therapy* vol. 7 www.nature.com/gt (2000).
35. Hamad, A., Yusubalieva, G. M., Baklaushev, V. P., Chumakov, P. M. & Lipatova, A. V. Recent Developments in Glioblastoma Therapy: Oncolytic Viruses and Emerging Future Strategies. *Viruses* vol. 15 Preprint at https://doi.org/10.3390/v15020547 (2023).
36. Kessler, A. F. *et al.* Effects of tumor treating fields (TTFields) on glioblastoma cells are augmented by mitotic checkpoint inhibition. *Cell Death Discov* 4, (2018).
37. Olatunji, G. *et al.* Efficacy of tumour-treating fields therapy in recurrent glioblastoma: A narrative review of current evidence. *Medicine (United States)* 102, (2023).
38. Rominiyi, O. *et al.* Tumour treating fields therapy for glioblastoma: current advances and future directions. *British Journal of Cancer* vol. 124 697–709 Preprint at https://doi.org/10.1038/s41416-020-01136-5 (2021).

39. Moser, J. C. *et al.* The Mechanisms of Action of Tumor Treating Fields. *Cancer Research* vol. 82 3650–3658 Preprint at https://doi.org/10.1158/0008-5472.CAN-22-0887 (2022).
40. Roque, D. *et al.* Nanoparticle-Based Treatment in Glioblastoma. *Journal of Personalized Medicine* vol. 13 Preprint at https://doi.org/10.3390/jpm13091328 (2023).
41. Koziara, J. M., Lockman, P. R., Allen, D. D. & Mumper, R. J. Paclitaxel nanoparticles for the potential treatment of brain tumors. *Journal of Controlled Release* 99, 259–269 (2004).
42. Allen, N. C., Chauhan, R., Bates, P. J. & O'Toole, M. G. Optimization of Tumor Targeting Gold Nanoparticles for Glioblastoma Applications. *Nanomaterials* 12, (2022).
43. Marrugo-Ramírez, J., Mir, M. & Samitier, J. Blood-based cancer biomarkers in liquid biopsy: A promising non-invasive alternative to tissue biopsy. *International Journal of Molecular Sciences* vol. 19 Preprint at https://doi.org/10.3390/ijms19102877 (2018).
44. Michela, B. Liquid biopsy: A family of possible diagnostic tools. *Diagnostics* vol. 11 Preprint at https://doi.org/10.3390/diagnostics11081391 (2021).
45. Kilgour, E., Rothwell, D. G., Brady, G. & Dive, C. Liquid Biopsy-Based Biomarkers of Treatment Response and Resistance. *Cancer Cell* vol. 37 485–495 Preprint at https://doi.org/10.1016/j.ccell.2020.03.012 (2020).
46. Fabisiewicz, A. & Grzybowska, E. CTC clusters in cancer progression and metastasis. *Medical Oncology* vol. 34 Preprint at https://doi.org/10.1007/s12032-016-0875-0 (2017).
47. Alix-Panabières, C. & Pantel, K. Liquid biopsy: From discovery to clinical application. *Cancer Discov* 11, 858–873 (2021).
48. Ju, S. *et al.* Detection of circulating tumor cells: opportunities and challenges. *Biomarker Research* vol. 10 Preprint at https://doi.org/10.1186/s40364-022-00403-2 (2022).
49. McDonald, B., Barth, K. & Schmidt, M. H. H. The origin of brain malignancies at the blood–brain barrier. *Cellular and Molecular Life Sciences* vol. 80 Preprint at https://doi.org/10.1007/s00018-023-04934-1 (2023).
50. Westphal, M. *et al.* Circulating tumor cells and extracellular vesicles as liquid biopsy markers in neuro-oncology: prospects and limitations. *Neurooncol Adv* 4, II45–II52 (2022).

51. Nguyen, T. N. A., Huang, P. S., Chu, P. Y., Hsieh, C. H. & Wu, M. H. Recent Progress in Enhanced Cancer Diagnosis, Prognosis, and Monitoring Using a Combined Analysis of the Number of Circulating Tumor Cells (CTCs) and Other Clinical Parameters. *Cancers* vol. 15 Preprint at https://doi.org/10.3390/cancers15225372 (2023).
52. Trapp, E. *et al.* Presence of circulating tumor cells in high-risk early breast cancer during follow-up and prognosis. *J Natl Cancer Inst* 111, 380–387 (2019).
53. Smerage, J. B. *et al.* Circulating tumor cells and response to chemotherapy in metastatic breast cancer: SWOG S0500. *Journal of Clinical Oncology* 32, 3483–3489 (2014).
54. Hayes, D. F. *et al.* Circulating tumor cells at each follow-up time point during therapy of metastatic breast cancer patients predict progression-free and overall survival. *Clin Cancer Res* 12, 4218–4224 (2006).
55. Magbanua, M. J. M. *et al.* Clinical Significance of Circulating Tumor Cells in Hormone Receptor–positive Metastatic Breast Cancer Patients who Received Letrozole with or without Bevacizumab. *Clinical Cancer Research* 26, 4911–4920 (2020).
56. *Effect of CTCs and INHBA Level on the Effect and Prognosis of Different Treatment Methods for Patients with Early Breast Cancer*.
57. Abdalla, T. S. A. *et al.* Prognostic value of preoperative circulating tumor cells counts in patients with UICC stage I-IV colorectal cancer. *PLoS One* 16, (2021).
58. De Bono, J. S. *et al.* Circulating tumor cells predict survival benefit from treatment in metastatic castration-resistant prostate cancer. *Clinical Cancer Research* 14, 6302–6309 (2008).
59. Gallo, M. *et al.* Clinical utility of circulating tumor cells in patients with non-small-cell lung cancer. *Translational Lung Cancer Research* vol. 6 486–498 Preprint at https://doi.org/10.21037/tlcr.2017.05.07 (2017).
60. Vivek Raut, N. *et al. Circulating Tumor Cells as a Biomarker for Monitoring: Disease Progression, Treatment Response, and Minimal Residual Disease*. (2022).
61. Marcinak, C. T., Murtaza, M. & Wilke, L. G. Genomic Profiling and Liquid Biopsies for Breast Cancer. *Surgical Clinics of North America* vol. 103 49–61 Preprint at https://doi.org/10.1016/j.suc.2022.08.003 (2023).
62. Cescon, D. W., Bratman, S. V., Chan, S. M. & Siu, L. L. Circulating tumor DNA and liquid biopsy in oncology. *Nature cancer* vol. 1 276–290 Preprint at https://doi.org/10.1038/s43018-020-0043-5 (2020).

63. Underhill, H. R. *et al.* Fragment Length of Circulating Tumor DNA. *PLoS Genet* 12, (2016).
64. Qi, T. *et al.* Cell-Free DNA Fragmentomics: The Novel Promising Biomarker. *International Journal of Molecular Sciences* vol. 24 Preprint at https://doi.org/10.3390/ijms24021503 (2023).
65. Visser, E. *et al.* Up-front mutation detection in circulating tumor DNA by droplet digital PCR has added diagnostic value in lung cancer. *Transl Oncol* 27, (2023).
66. Zaikova, E. *et al.* Circulating tumour mutation detection in triple-negative breast cancer as an adjunct to tissue response assessment. *NPJ Breast Cancer* 10, (2024).
67. Hallermayr, A. *et al.* Somatic copy number alteration and fragmentation analysis in circulating tumor DNA for cancer screening and treatment monitoring in colorectal cancer patients. *J Hematol Oncol* 15, (2022).
68. Nguyen, M. T. N. *et al.* Circulating tumor DNA-based copy-number profiles enable monitoring treatment effects during therapy in high-grade serous carcinoma. *Biomedicine and Pharmacotherapy* 168, (2023).
69. Sharbatoghli, M. *et al.* Copy Number Variation of Circulating Tumor DNA (ctDNA) Detected Using NIPT in Neoadjuvant Chemotherapy-Treated Ovarian Cancer Patients. *Front Genet* 13, (2022).
70. Hai, L., Li, L., Liu, Z., Tong, Z. & Sun, Y. Whole-genome circulating tumor DNA methylation landscape reveals sensitive biomarkers of breast cancer. *MedComm (Beijing)* 3, (2022).
71. Kwon, H. J. *et al.* Advances in methylation analysis of liquid biopsy in early cancer detection of colorectal and lung cancer. *Sci Rep* 13, (2023).
72. Burgener, J. M. *et al.* Tumor-Naïve multimodal profiling of circulating tumor DNA in head and neck squamous cell carcinoma. *Clinical Cancer Research* 27, 4230–4244 (2021).
73. Zhang, Y. *et al.* Pan-cancer circulating tumor DNA detection in over 10,000 Chinese patients. *Nat Commun* 12, (2021).
74. Strijker, M. *et al.* Circulating tumor DNA quantity is related to tumor volume and both predict survival in metastatic pancreatic ductal adenocarcinoma. *Int J Cancer* 146, 1445–1456 (2020).
75. Openshaw, M. R. *et al.* Longitudinal monitoring of circulating tumour DNA improves prognostication and relapse detection in gastroesophageal adenocarcinoma. *Br J Cancer* 123, 1271–1279 (2020).

76. Reichert, Z. R. *et al.* Prognostic value of plasma circulating tumor DNA fraction across four common cancer types: a real-world outcomes study. *Annals of Oncology* 34, 111–120 (2023).
77. Jones, J. J. *et al.* Plasma ctDNA liquid biopsy of IDH1, TERTp, and EGFRvIII mutations in glioma. *Neurooncol Adv* 6, (2024).
78. Han, D. S. C. & Lo, Y. M. D. The Nexus of cfDNA and Nuclease Biology. *Trends in Genetics* vol. 37 758–770 Preprint at https://doi.org/10.1016/j.tig.2021.04.005 (2021).
79. Dziadziuszko, R. *et al.* Circulating Cell-free DNA as a Prognostic Biomarker in Patients with Advanced ALKþ Non–small Cell Lung Cancer in the Global Phase III ALEX Trial. *Clinical Cancer Research* 28, 1800–1808 (2022).
80. Tissot, C. *et al.* Circulating free DNA concentration is an independent prognostic biomarker in lung cancer. *Eur Respir J* 46, 1773–1780 (2015).
81. Avanzini, S. *et al. A Mathematical Model of CtDNA Shedding Predicts Tumor Detection Size*. *Sci. Adv* vol. 6 (2020).
82. Tran, H. T. *et al.* Circulating tumor DNA and radiological tumor volume identify patients at risk for relapse with resected, early-stage non-small-cell lung cancer. *Annals of Oncology* 35, 183–189 (2024).
83. Goto, T. *et al. Distribution of Circulating Tumor DNA in Lung Cancer: Analysis of the Primary Lung and Bone Marrow along with the Pulmonary Venous and Peripheral Blood*. www.impactjournals.com/oncotarget.
84. Xu, F. *et al.* Detection of Circulating Tumor DNA Methylation in Diagnosis of Colorectal Cancer. *Clin Transl Gastroenterol* 12, E00386 (2021).
85. Myint, N. N. M. *et al.* Circulating tumor DNA in patients with colorectal adenomas: assessment of detectability and genetic heterogeneity. *Cell Death Dis* 9, (2018).
86. Guo, K. *et al.* Detection of epidermal growth factor receptor (EGFR) mutations from preoperative circulating tumor DNA (ctDNA) as a prognostic predictor for stage I–III non-small cell lung cancer (NSCLC) patients with baseline tissue EGFR mutations. *Transl Lung Cancer Res* 10, 3213–3225 (2021).
87. Pinheiro, M. *et al.* KRAS and NRAS mutational analysis in plasma ctDNA from patients with metastatic colorectal cancer by real-time PCR and digital PCR. *Int J Colorectal Dis* 37, 895–905 (2022).
88. Mas, L. *et al.* Braf mutation status in circulating tumor dna from patients with metastatic colorectal cancer: Extended mutation analysis from the ageo rasanc study. *Cancers (Basel)* 11, (2019).

89. Loupakis, F. *et al.* KRAS codon 61, 146 and BRAF mutations predict resistance to cetuximab plus irinotecan in KRAS codon 12 and 13 wild-type metastatic colorectal cancer. *Br J Cancer* 101, 715–721 (2009).
90. Sobczuk, P. *et al.* The Use of ctDNA for BRAF Mutation Testing in Routine Clinical Practice in Patients with Advanced Melanoma. *Cancers (Basel)* 14, (2022).
91. Castellani, G. *et al.* BRAF Mutations in Melanoma: Biological Aspects, Therapeutic Implications, and Circulating Biomarkers. *Cancers* vol. 15 Preprint at https://doi.org/10.3390/cancers15164026 (2023).
92. Emelyanova, M. A. *et al.* Microarray-based analysis of the BRAF V600 mutations in circulating tumor DNA in melanoma patients. *Cancer Genet* 250–251, 25–35 (2021).
93. Yáñez-Mó, M. *et al.* Biological properties of extracellular vesicles and their physiological functions. *Journal of Extracellular Vesicles* vol. 4 1–60 Preprint at https://doi.org/10.3402/jev.v4.27066 (2015).
94. Simeone, P. *et al.* Extracellular vesicles as signaling mediators and disease biomarkers across biological barriers. *International Journal of Molecular Sciences* vol. 21 Preprint at https://doi.org/10.3390/ijms21072514 (2020).
95. Hagey, D. W. *et al.* Extracellular vesicles are the primary source of blood-borne tumour-derived mutant KRAS DNA early in pancreatic cancer. *J Extracell Vesicles* 10, (2021).
96. Tkach, M. *et al.* Circulating extracellular vesicles provide valuable protein, but not DNA, biomarkers in metastatic breast cancer. *Journal of Extracellular Biology* 1, (2022).
97. Strimbu, K. & Tavel, J. A. What are biomarkers? *Current Opinion in HIV and AIDS* vol. 5 463–466 Preprint at https://doi.org/10.1097/COH.0b013e32833ed177 (2010).
98. Kalra, H. *et al.* Comparative proteomics evaluation of plasma exosome isolation techniques and assessment of the stability of exosomes in normal human blood plasma. *Proteomics* 13, 3354–3364 (2013).
99. Görgens, A. *et al.* Identification of storage conditions stabilizing extracellular vesicles preparations. *J Extracell Vesicles* 11, (2022).
100. Osti, D. *et al.* Clinical significance of extracellular vesicles in plasma from glioblastoma patients. *Clinical Cancer Research* 25, 266–276 (2019).
101. Zonneveld, M. I. *et al.* Recovery of extracellular vesicles from human breast milk is influenced by sample collection and vesicle isolation procedures. *J Extracell Vesicles* 3, (2014).

102. Teixeira-Marques, A. *et al.* Improved recovery of urinary small extracellular vesicles by differential ultracentrifugation. *Sci Rep* 14, (2024).
103. Alić, V. K. *et al.* Extracellular Vesicles from Human Cerebrospinal Fluid Are Effectively Separated by Sepharose CL-6B—Comparison of Four Gravity-Flow Size Exclusion Chromatography Methods. *Biomedicines* 10, (2022).
104. Kumar, M. A. *et al.* Extracellular vesicles as tools and targets in therapy for diseases. *Signal Transduction and Targeted Therapy* vol. 9 Preprint at https://doi.org/10.1038/s41392-024-01735-1 (2024).
105. Buzas, E. I. The roles of extracellular vesicles in the immune system. *Nature Reviews Immunology* Preprint at https://doi.org/10.1038/s41577-022-00763-8 (2022).
106. Kaur, G. & Lakkaraju, A. Early endosome morphology in health and disease. in *Advances in Experimental Medicine and Biology* vol. 1074 335–343 (Springer New York LLC, 2018).
107. Van Niel, G., D'Angelo, G. & Raposo, G. Shedding light on the cell biology of extracellular vesicles. *Nature Reviews Molecular Cell Biology* vol. 19 213–228 Preprint at https://doi.org/10.1038/nrm.2017.125 (2018).
108. Adell, M. A. Y. *et al.* Coordinated binding of Vps4 to ESCRT-III drives membrane neck constriction during MVB vesicle formation. *Journal of Cell Biology* 205, 33–49 (2014).
109. Juan, T. & Fürthauer, M. Biogenesis and function of ESCRT-dependent extracellular vesicles. *Seminars in Cell and Developmental Biology* vol. 74 66–77 Preprint at https://doi.org/10.1016/j.semcdb.2017.08.022 (2018).
110. Willms, E. *et al.* Cells release subpopulations of exosomes with distinct molecular and biological properties. *Sci Rep* 6, (2016).
111. Frankel, E. B. & Audhya, A. ESCRT-dependent cargo sorting at multivesicular endosomes. *Seminars in Cell and Developmental Biology* vol. 74 4–10 Preprint at https://doi.org/10.1016/j.semcdb.2017.08.020 (2018).
112. Wenzel, E. M. *et al.* Concerted ESCRT and clathrin recruitment waves define the timing and morphology of intraluminal vesicle formation. *Nat Commun* 9, (2018).
113. Alsleben, S. & Kölling, R. Vps68 cooperates with ESCRT-III in intraluminal vesicle formation. *J Cell Sci* 135, (2022).
114. Baietti, M. F. *et al.* Syndecan-syntenin-ALIX regulates the biogenesis of exosomes. *Nat Cell Biol* 14, 677–685 (2012).
115. Wei, D. *et al.* RAB31 marks and controls an ESCRT-independent exosome pathway. *Cell Res* 31, 157–177 (2021).

116. Kumar, A. & Kumar, S. Inhibition of extracellular vesicle pathway using neutral sphingomyelinase inhibitors as a neuroprotective treatment for brain injury. *Neural Regeneration Research* vol. 16 2349–2352 Preprint at https://doi.org/10.4103/1673-5374.313014 (2021).
117. Sapon, K., Manka, R., Janas, T. & Janas, T. The role of lipid rafts in vesicle formation. *Journal of Cell Science* vol. 136 Preprint at https://doi.org/10.1242/jcs.260887 (2023).
118. van Niel, G. *et al.* The Tetraspanin CD63 Regulates ESCRT-Independent and -Dependent Endosomal Sorting during Melanogenesis. *Dev Cell* 21, 708–721 (2011).
119. Suárez, H. *et al.* CD9 inhibition reveals a functional connection of extracellular vesicle secretion with mitophagy in melanoma cells. *J Extracell Vesicles* 10, (2021).
120. Toribio, V. & Yáñez-Mó, M. Tetraspanins interweave EV secretion, endosomal network dynamics and cellular metabolism. *Eur J Cell Biol* 101, (2022).
121. Cai, H., Reinisch, K. & Ferro-Novick, S. Coats, Tethers, Rabs, and SNAREs Work Together to Mediate the Intracellular Destination of a Transport Vesicle. *Developmental Cell* vol. 12 671–682 Preprint at https://doi.org/10.1016/j.devcel.2007.04.005 (2007).
122. Bi, J. *et al.* Oncogene Amplification in Growth Factor Signaling Pathways Renders Cancers Dependent on Membrane Lipid Remodeling. *Cell Metab* 30, 525-538.e8 (2019).
123. Wang, T. *et al.* Hypoxia-inducible factors and RAB22A mediate formation of microvesicles that stimulate breast cancer invasion and metastasis. *Proc Natl Acad Sci U S A* 111, (2014).
124. Taylor, J., Azimi, I., Monteith, G. & Bebawy, M. Ca2+ mediates extracellular vesicle biogenesis through alternate pathways in malignancy. *J Extracell Vesicles* 9, (2020).
125. Bian, X. *et al.* Microvesicles and chemokines in tumor microenvironment: Mediators of intercellular communications in tumor progression. *Molecular Cancer* vol. 18 Preprint at https://doi.org/10.1186/s12943-019-0973-7 (2019).
126. Al-Nedawi, K. *et al.* Intercellular transfer of the oncogenic receptor EGFRvIII by microvesicles derived from tumour cells. *Nat Cell Biol* 10, 619–624 (2008).
127. Kreger, B. T., Dougherty, A. L., Greene, K. S., Cerione, R. A. & Antonyak, M. A. Microvesicle cargo and function changes upon induction of cellular transformation. *Journal of Biological Chemistry* 291, 19774–19785 (2016).
128. Minciacchi, V. R., Freeman, M. R. & Di Vizio, D. Extracellular Vesicles in Cancer: Exosomes, Microvesicles and the Emerging Role of Large Oncosomes. *Seminars in*

Cell and Developmental Biology vol. 40 41–51 Preprint at https://doi.org/10.1016/j.semcdb.2015.02.010 (2015).

129. Lynch, C., Panagopoulou, M. & Gregory, C. D. Extracellular vesicles arising from apoptotic cells in tumors: Roles in cancer pathogenesis and potential clinical applications. *Frontiers in Immunology* vol. 8 Preprint at https://doi.org/10.3389/fimmu.2017.01174 (2017).
130. Minciacchi, V. R. *et al. Large Oncosomes Contain Distinct Protein Cargo and Represent a Separate Functional Class of Tumor-Derived Extracellular Vesicles*. www.impactjournals.com/oncotarget/ (2015).
131. Ciardiello, C. *et al.* Large oncosomes overexpressing integrin alpha-V promote prostate cancer adhesion and invasion via AKT activation. *Journal of Experimental and Clinical Cancer Research* 38, (2019).
132. Minciacchi, V. R. *et al.* MYC mediates large oncosome-induced fibroblast reprogramming in prostate cancer. *Cancer Res* 77, 2306–2317 (2017).
133. Poon, I. K. H., Lucas, C. D., Rossi, A. G. & Ravichandran, K. S. Apoptotic cell clearance: Basic biology and therapeutic potential. *Nature Reviews Immunology* vol. 14 166–180 Preprint at https://doi.org/10.1038/nri3607 (2014).
134. Coleman, M. L. *et al. Membrane Blebbing during Apoptosis Results from Caspase-Mediated Activation of ROCK I*. *NATURE CELL BIOLOGY* vol. 3 http://cellbio.nature.com (2001).
135. Sebbagh, M. *et al. Caspase-3-Mediated Cleavage of ROCK I Induces MLC Phosphorylation and Apoptotic Membrane Blebbing*. *NATURE CELL BIOLOGY* vol. 3 http://cellbio.nature.com346 (2001).
136. Poon, I. K. H., Lucas, C. D., Rossi, A. G. & Ravichandran, K. S. Apoptotic cell clearance: Basic biology and therapeutic potential. *Nature Reviews Immunology* vol. 14 166–180 Preprint at https://doi.org/10.1038/nri3607 (2014).
137. Liu, J. *et al.* Apoptotic bodies derived from mesenchymal stem cells promote cutaneous wound healing via regulating the functions of macrophages. *Stem Cell Res Ther* 11, (2020).
138. Hus, I. *et al.* Allogeneic dendritic cells pulsed with tumor lysates or apoptotic bodies as immunotherapy for patients with early-stage B-cell chronic lymphocytic leukemia. *Leukemia* 19, 1621–1627 (2005).
139. Liu, D. *et al.* Circulating apoptotic bodies maintain mesenchymal stem cell homeostasis and ameliorate osteopenia via transferring multiple cellular factors. *Cell Res* 28, 918–933 (2018).

140. Park, J. O. *et al.* Identification and characterization of proteins isolated from microvesicles derived from human lung cancer pleural effusions. *Proteomics* 13, 2125–2134 (2013).
141. Pang, Y. *et al.* Personalized detection of circling exosomal PD-L1 based on Fe3O4@TiO2 isolation and SERS immunoassay. *Biosens Bioelectron* 148, (2020).
142. Han, L., Shi, W. J., Xie, Y. Bin & Zhang, Z. G. Diagnostic value of four serum exosome microRNAs panel for the detection of colorectal cancer. *World J Gastrointest Oncol* 13, 970–979 (2021).
143. Wei, P. *et al.* Plasma extracellular vesicles detected by Single Molecule array technology as a liquid biopsy for colorectal cancer. *J Extracell Vesicles* 9, (2020).
144. Rahman, S., Garrel, S., Gerber, M., Maitra, R. & Goel, S. Therapeutic targets of kras in colorectal cancer. *Cancers* vol. 13 Preprint at https://doi.org/10.3390/cancers13246233 (2021).
145. Li, S. *et al.* Exosomal ephrinA2 derived from serum as a potential biomarker for prostate cancer. *J Cancer* 9, 2659–2665 (2018).
146. Zhou, Y. G. *et al.* Interrogating Circulating Microsomes and Exosomes Using Metal Nanoparticles. *Small* 12, 727–732 (2016).
147. Joshi, G. K. *et al.* Label-Free Nanoplasmonic-Based Short Noncoding RNA Sensing at Attomolar Concentrations Allows for Quantitative and Highly Specific Assay of MicroRNA-10b in Biological Fluids and Circulating Exosomes. *ACS Nano* 9, 11075–11089 (2015).
148. Melo, S. A. *et al.* Glypican-1 identifies cancer exosomes and detects early pancreatic cancer. *Nature* 523, 177–182 (2015).
149. Margolis, E. *et al.* Predicting high-grade prostate cancer at initial biopsy: clinical performance of the ExoDx (EPI) Prostate Intelliscore test in three independent prospective studies. *Prostate Cancer Prostatic Dis* 25, 296–301 (2022).
150. Krug, A. K. *et al.* Improved EGFR mutation detection using combined exosomal RNA and circulating tumor DNA in NSCLC patient plasma. *Annals of Oncology* 29, 700–706 (2018).
151. Asai, H. *et al.* Depletion of microglia and inhibition of exosome synthesis halt tau propagation. *Nat Neurosci* 18, 1584–1593 (2015).
152. Singh, R. *et al.* Circulating small extracellular vesicles in Alzheimer's disease: a case–control study of neuro-inflammation and synaptic dysfunction. *BMC Med* 22, (2024).
153. Shi, M. *et al.* Plasma exosomal α-synuclein is likely CNS-derived and increased in Parkinson's disease. *Acta Neuropathol* 128, 639–650 (2014).

154. Ronvaux, L. *et al.* Liquid Biopsy in Glioblastoma. *Cancers* vol. 14 Preprint at https://doi.org/10.3390/cancers14143394 (2022).
155. Juratli, T. A. *et al.* TERT promoter mutation detection in cell-free tumor-derived DNA in patients with IDH wild-type glioblastomas: A pilot prospective study. *Clinical Cancer Research* 24, 5282–5291 (2018).
156. Wang, Q. *et al.* Concordance analysis of cerebrospinal fluid with the tumor tissue for integrated diagnosis in gliomas based on next-generation sequencing. *Pathology and Oncology Research* 29, (2023).
157. De Mattos-Arruda, L. *et al.* Cerebrospinal fluid-derived circulating tumour DNA better represents the genomic alterations of brain tumours than plasma. *Nat Commun* 6, (2015).
158. Miller, A. M. *et al.* Tracking tumour evolution in glioma through liquid biopsies of cerebrospinal fluid. *Nature* 565, 654–658 (2019).
159. Figueroa, J. M. *et al.* Detection of wild-Type EGFR amplification and EGFRvIII mutation in CSF-derived extracellular vesicles of glioblastoma patients. *Neuro Oncol* 19, 1494–1502 (2017).
160. Akers, J. C. *et al. A Cerebrospinal Fluid MicroRNA Signature as Biomarker for Glioblastoma*. vol. 8 www.impactjournals.com/oncotarget (2017).
161. Akers, J. C. *et al.* miR-21 in the Extracellular Vesicles (EVs) of Cerebrospinal Fluid (CSF): A Platform for Glioblastoma Biomarker Development. *PLoS One* 8, (2013).
162. Schmid, D. *et al.* Diagnostic biomarkers from proteomic characterization of cerebrospinal fluid in patients with brain malignancies. *J Neurochem* 158, 522–538 (2021).
163. García-Romero, N. *et al. DNA Sequences within Glioma-Derived Extracellular Vesicles Can Cross the Intact Blood-Brain Barrier and Be Detected in Peripheral Blood of Patients*. *Oncotarget* vol. 8 www.impactjournals.com/oncotarget/ (2017).
164. Fiandaca, M. S. *et al.* Identification of preclinical Alzheimer's disease by a profile of pathogenic proteins in neurally derived blood exosomes: A case-control study. *Alzheimer's and Dementia* 11, 600-607.e1 (2015).
165. Cheng, L. *et al.* Small RNA fingerprinting of Alzheimer's disease frontal cortex extracellular vesiclesand their comparison with peripheral extracellular vesicles. *J Extracell Vesicles* 9, (2020).
166. Buzás, E. I., Tóth, E., Sódar, B. W. & Szabó-Taylor, K. Molecular interactions at the surface of extracellular vesicles. *Seminars in Immunopathology* vol. 40 453–464 Preprint at https://doi.org/10.1007/s00281-018-0682-0 (2018).

167. Ricklefs, F. L. *et al.* Circulating extracellular vesicles as biomarker for diagnosis, prognosis, and monitoring in glioblastoma patients. *Neuro Oncol* 26, 1280–1291 (2024).
168. Rosas-Alonso, R. *et al.* Evaluation of the clinical use of MGMT methylation in extracellular vesicle-based liquid biopsy as a tool for glioblastoma patient management. *Sci Rep* 14, (2024).
169. Maniya, N. H. *et al.* An anion exchange membrane sensor detects EGFR and its activity state in plasma CD63 extracellular vesicles from patients with glioblastoma. *Commun Biol* 7, (2024).
170. Westphal, M. & Lamszus, K. Circulating biomarkers for gliomas. *Nature Reviews Neurology* vol. 11 556–566 Preprint at https://doi.org/10.1038/nrneurol.2015.171 (2015).
171. Cilibrasi, C. *et al.* Definition of an Inflammatory Biomarker Signature in Plasma-Derived Extracellular Vesicles of Glioblastoma Patients. *Biomedicines* 10, (2022).
172. Royo, F., Théry, C., Falcón-Pérez, J. M., Nieuwland, R. & Witwer, K. W. Methods for Separation and Characterization of Extracellular Vesicles: Results of a Worldwide Survey Performed by the ISEV Rigor and Standardization Subcommittee. *Cells* 9, (2020).
173. Liangsupree, T., Multia, E. & Riekkola, M. L. Modern isolation and separation techniques for extracellular vesicles. *J Chromatogr A* 1636, (2021).
174. Kowal, J. *et al.* Proteomic comparison defines novel markers to characterize heterogeneous populations of extracellular vesicle subtypes. *Proc Natl Acad Sci U S A* 113, E968–E977 (2016).
175. Sharma, S., LeClaire, M., Wohlschlegel, J. & Gimzewski, J. Impact of isolation methods on the biophysical heterogeneity of single extracellular vesicles. *Sci Rep* 10, (2020).
176. Monguió-Tortajada, M., Gálvez-Montón, C., Bayes-Genis, A., Roura, S. & Borràs, F. E. Extracellular vesicle isolation methods: rising impact of size-exclusion chromatography. *Cellular and Molecular Life Sciences* vol. 76 2369–2382 Preprint at https://doi.org/10.1007/s00018-019-03071-y (2019).
177. Welsh, J. A. *et al.* Minimal information for studies of extracellular vesicles (MISEV2023): From basic to advanced approaches. *J Extracell Vesicles* 13, (2024).
178. Deutsch, E. W. *et al.* Advances and Utility of the Human Plasma Proteome. *Journal of Proteome Research* vol. 20 5241–5263 Preprint at https://doi.org/10.1021/acs.jproteome.1c00657 (2021).

179. Vogel, R. *et al.* Measuring particle concentration of multimodal synthetic reference materials and extracellular vesicles with orthogonal techniques: Who is up to the challenge? *J Extracell Vesicles* 10, (2021).
180. Desgeorges, A. *et al.* Differential fluorescence nanoparticle tracking analysis for enumeration of the extracellular vesicle content in mixed particulate solutions. *Methods* 177, 67–73 (2020).
181. Midekessa, G. *et al.* Zeta Potential of Extracellular Vesicles: Toward Understanding the Attributes that Determine Colloidal Stability. *ACS Omega* 5, 16701–16710 (2020).
182. Mathieu, M., Martin-Jaular, L., Lavieu, G. & Théry, C. Specificities of secretion and uptake of exosomes and other extracellular vesicles for cell-to-cell communication. *Nature Cell Biology* vol. 21 9–17 Preprint at https://doi.org/10.1038/s41556-018-0250-9 (2019).
183. Joo, K. M. *et al.* Patient-Specific Orthotopic Glioblastoma Xenograft Models Recapitulate the Histopathology and Biology of Human Glioblastomas In Situ. *Cell Rep* 3, 260–273 (2013).
184. Luen Tang Editor, B. *Membrane Traa Cking Second Edition Methods in Molecular Biology 1270*. http://www.springer.com/series/7651.
185. Wiklander, O. P. B. *et al.* Systematic methodological evaluation of a multiplex bead-based flow cytometry assay for detection of extracellular vesicle surface signatures. *Front Immunol* 9, (2018).
186. Welsh, J. A. *et al.* MPAPASS software enables stitched multiplex, multidimensional EV repertoire analysis and a standard framework for reporting bead-based assays. *Cell Reports Methods* 2, (2022).
187. Görgens, A. *et al.* Optimisation of imaging flow cytometry for the analysis of single extracellular vesicles by using fluorescence-tagged vesicles as biological reference material. *J Extracell Vesicles* 8, (2019).
188. Görgens, A. *et al.* Identification of storage conditions stabilizing extracellular vesicles preparations. *J Extracell Vesicles* 11, (2022).
189. Pelicci, S., Furia, L., Pelicci, P. G. & Faretta, M. Correlative Multi-Modal Microscopy: A Novel Pipeline for Optimizing Fluorescence Microscopy Resolutions in Biological Applications. *Cells* 12, (2023).
190. Furia, L., Pelicci, P. G. & Faretta, M. A computational platform for robotized fluorescence microscopy (I): High-content image-based cell-cycle analysis. *Cytometry Part A* 83 A, 333–343 (2013).

191. Furia, L. *et al.* Automated multimodal fluorescence microscopy for hyperplex spatial-proteomics: Coupling microfluidic-based immunofluorescence to high resolution, high sensitivity, three-dimensional analysis of histological slides. *Front Oncol* 12, (2022).
192. Pelicci, S., Furia, L., Pelicci, P. G. & Faretta, M. From Cell Populations to Molecular Complexes: Multiplexed Multimodal Microscopy to Explore p53-53BP1 Molecular Interaction. *Int J Mol Sci* 25, (2024).
193. Danecek, P. *et al.* Twelve years of SAMtools and BCFtools. *Gigascience* 10, (2021).
194. Pedersen, B. S. & Quinlan, A. R. Mosdepth: Quick coverage calculation for genomes and exomes. *Bioinformatics* 34, 867–868 (2018).
195. Adalsteinsson, V. A. *et al.* Scalable whole-exome sequencing of cell-free DNA reveals high concordance with metastatic tumors. *Nat Commun* 8, (2017).
196. Meier, F., Geyer, P. E., Virreira Winter, S., Cox, J. & Mann, M. BoxCar acquisition method enables single-shot proteomics at a depth of 10,000 proteins in 100 minutes. *Nat Methods* 15, 440–448 (2018).
197. Hendriks, I. A., Akimov, V., Blagoev, B. & Nielsen, M. L. MaxQuant.Live Enables Enhanced Selectivity and Identification of Peptides Modified by Endogenous SUMO and Ubiquitin. *J Proteome Res* 20, 2042–2055 (2021).
198. Wichmann, C. *et al.* MaxQuant.live enables global targeting of more than 25,000 peptides. *Molecular and Cellular Proteomics* 18, 982–994 (2019).
199. Chambers, M. C. *et al.* A cross-platform toolkit for mass spectrometry and proteomics. *Nature Biotechnology* vol. 30 918–920 Preprint at https://doi.org/10.1038/nbt.2377 (2012).
200. Demichev, V., Messner, C. B., Vernardis, S. I., Lilley, K. S. & Ralser, M. DIA-NN: neural networks and interference correction enable deep proteome coverage in high throughput. *Nat Methods* 17, 41–44 (2020).
201. Tyanova, S. *et al.* The Perseus computational platform for comprehensive analysis of (prote)omics data. *Nature Methods* vol. 13 731–740 Preprint at https://doi.org/10.1038/nmeth.3901 (2016).
202. Suomi, T., Seyednasrollah, F., Jaakkola, M. K., Faux, T. & Elo, L. L. ROTS: An R package for reproducibility-optimized statistical testing. *PLoS Comput Biol* 13, (2017).
203. Eden, E., Navon, R., Steinfeld, I., Lipson, D. & Yakhini, Z. GOrilla: A tool for discovery and visualization of enriched GO terms in ranked gene lists. *BMC Bioinformatics* 10, (2009).

204. Langfelder, P. & Horvath, S. WGCNA: An R package for weighted correlation network analysis. *BMC Bioinformatics* 9, (2008).
205. Zhen, K. *et al.* Comparison of Different Isolation Methods for Plasma-Derived Extracellular Vesicles in Patients with Hyperlipidemia. (2022) doi:10.3390/life.
206. Szilágyi, M. *et al.* Circulating cell-free nucleic acids: Main characteristics and clinical application. *International Journal of Molecular Sciences* vol. 21 1–20 Preprint at https://doi.org/10.3390/ijms21186827 (2020).
207. Reymond, S., Gruaz, L. & Sanchez, J. C. Depletion of abundant plasma proteins for extracellular vesicle proteome characterization: benefits and pitfalls. *Anal Bioanal Chem* 415, 3177–3187 (2023).
208. Théry, C. *et al.* Minimal information for studies of extracellular vesicles 2018 (MISEV2018): a position statement of the International Society for Extracellular Vesicles and update of the MISEV2014 guidelines. *J Extracell Vesicles* 7, (2018).
209. Vogel, R. *et al.* A standardized method to determine the concentration of extracellular vesicles using tunable resistive pulse sensing. *J Extracell Vesicles* 5, (2016).
210. van der Pol, E. *et al.* Standardization of extracellular vesicle measurements by flow cytometry through vesicle diameter approximation. *Journal of Thrombosis and Haemostasis* 16, 1236–1245 (2018).
211. Ricklefs, F. L. *et al.* Circulating extracellular vesicles as biomarker for diagnosis, prognosis, and monitoring in glioblastoma patients. *Neuro Oncol* (2024) doi:10.1093/neuonc/noae068.
212. Maire, C. L. *et al.* Genome-wide methylation profiling of glioblastoma cell-derived extracellular vesicle DNA allows tumor classification. *Neuro Oncol* 23, 1087–1099 (2021).
213. Barros, B. D. de F. *et al.* Mutation detection in tumor-derived cell free DNA anticipates progression in a patient with metastatic colorectal cancer. *Front Oncol* 8, (2018).
214. Pereira, B. *et al.* Cell-free DNA captures tumor heterogeneity and driver alterations in rapid autopsies with pre-treated metastatic cancer. *Nat Commun* 12, (2021).
215. Bettegowda, C. *et al.* Detection of circulating tumor DNA in early- and late-stage human malignancies. *Sci Transl Med* 6, (2014).
216. Zill, O. A. *et al.* The landscape of actionable genomic alterations in cell-free circulating tumor DNA from 21,807 advanced cancer patients. *Clinical Cancer Research* 24, 3528–3538 (2018).

217. Huang, Y. F. *et al.* Genetic mutation patterns among glioblastoma patients in the Taiwanese population – insights from a single institution retrospective study. *Cancer Gene Ther* 31, 894–903 (2024).
218. Vitale, S. R. *et al.* Detection of tumor-derived extracellular vesicles in plasma from patients with solid cancer. *BMC Cancer* 21, (2021).
219. Barlin, M. *et al.* Proteins in Tumor-Derived Plasma Extracellular Vesicles Indicate Tumor Origin. *Molecular and Cellular Proteomics* 22, (2023).
220. Van Meir, E. G. *et al. Analysis of the P53 Gene and Its Expression in Human Glioblastoma Cells1*. *CANCER* vol. 54 http://aacrjournals.org/cancerres/article-pdf/54/3/649/2455914/cr0540030649.pdf (1994).
221. Mugoni, V. *et al.* Integrating extracellular vesicle and circulating cell-free DNA analysis using a single plasma aliquot improves the detection of HER2 positivity in breast cancer patients. *Journal of Extracellular Biology* 2, (2023).
222. Bagley, S. J. *et al.* Clinical utility of plasma cell-free DNA in adult patients with newly diagnosed glioblastoma: A pilot prospective study. *Clinical Cancer Research* 26, 397–407 (2020).
223. Fontanilles, M. *et al.* Cell-free DNA and circulating TERT promoter mutation for disease monitoring in newly-diagnosed glioblastoma. *Acta Neuropathol Commun* 8, (2020).
224. Mouliere, F. *et al.* Fragmentation patterns and personalized sequencing of cell-free DNA in urine and plasma of glioma patients. *EMBO Mol Med* 13, (2021).
225. van der Pol, Y. & Mouliere, F. Toward the Early Detection of Cancer by Decoding the Epigenetic and Environmental Fingerprints of Cell-Free DNA. *Cancer Cell* vol. 36 350–368 Preprint at https://doi.org/10.1016/j.ccell.2019.09.003 (2019).
226. Nakagawa, H. & Fujita, M. Whole genome sequencing analysis for cancer genomics and precision medicine. *Cancer Science* vol. 109 513–522 Preprint at https://doi.org/10.1111/cas.13505 (2018).
227. *Detection of Circulating Tumor DNA in Patients With Leiomyosarcoma With Progressive Disease*. (2018).
228. Escudero, L. *et al.* Circulating tumour DNA from the cerebrospinal fluid allows the characterisation and monitoring of medulloblastoma. *Nat Commun* 11, (2020).
229. Nair, N. Ulhas. *et al.* Chromosome 7 gain compensates for chromosome 10 loss in glioma. *Cancer Res* (2024) doi:10.1158/0008-5472.can-24-1366.
230. Stichel, D. *et al.* Distribution of EGFR amplification, combined chromosome 7 gain and chromosome 10 loss, and TERT promoter mutation in brain tumors and their

potential for the reclassification of IDHwt astrocytoma to glioblastoma. *Acta Neuropathol* 136, 793–803 (2018).

231. Funakoshi, Y. *et al.* Clinical significance of CDKN2A homozygous deletion in combination with methylated MGMT status for IDH-wildtype glioblastoma. *Cancer Med* 10, 3177–3187 (2021).
232. Welsh, J. A. *et al.* Minimal information for studies of extracellular vesicles (MISEV2023): From basic to advanced approaches. *J Extracell Vesicles* 13, (2024).
233. Pallet, N. *et al.* A comprehensive characterization of membrane vesicles released by autophagic human endothelial cells. *Proteomics* 13, 1108–1120 (2013).
234. Jeppesen, D. K. *et al.* Quantitative proteomics of fractionated membrane and lumen exosome proteins from isogenic metastatic and nonmetastatic bladder cancer cells reveal differential expression of EMT factors. *Proteomics* 14, 699–712 (2014).
235. Nielsen, J. E. *et al.* Shotgun-based proteomics of extracellular vesicles in Alzheimer's disease reveals biomarkers involved in immunological and coagulation pathways. *Sci Rep* 11, (2021).
236. Xie, F. *et al.* Breast cancer cell-derived extracellular vesicles promote CD8+ T cell exhaustion via TGF-β type II receptor signaling. *Nat Commun* 13, (2022).
237. McNamee, N., de la Fuente, L. R., Santos-Martinez, M. J. & O'Driscoll, L. Proteomics profiling identifies extracellular vesicles' cargo associated with tumour cell induced platelet aggregation. *BMC Cancer* 22, (2022).
238. Kim, D. K. *et al.* EVpedia: An integrated database of high-throughput data for systemic analyses of extracellular vesicles. *J Extracell Vesicles* 2, (2013).
239. Keerthikumar, S. *et al.* ExoCarta: A Web-Based Compendium of Exosomal Cargo. *J Mol Biol* 428, 688–692 (2016).
240. Tóth, E. *et al.* Formation of a protein corona on the surface of extracellular vesicles in blood plasma. *J Extracell Vesicles* 10, (2021).
241. Skoczylas, Ł. *et al.* Immune capture and protein profiling of small extracellular vesicles from human plasma. *Proteomics* vol. 24 Preprint at https://doi.org/10.1002/pmic.202300180 (2024).
242. Deutsch, E. W. *et al.* Advances and Utility of the Human Plasma Proteome. *Journal of Proteome Research* vol. 20 5241–5263 Preprint at https://doi.org/10.1021/acs.jproteome.1c00657 (2021).
243. Saha, T. LAMP2A overexpression in breast tumors promotes cancer cell survival via chaperone-mediated autophagy. *Autophagy* 8, 1643–1656 (2012).

244. Gusev, Y. *et al.* Data descriptor: The REMBRANDT study, a large collection of genomic data from brain cancer patients. *Sci Data* 5, (2018).
245. Auzmendi-Iriarte, J. *et al.* Chaperone-Mediated Autophagy Controls Proteomic and Transcriptomic Pathways to Maintain Glioma Stem Cell Activity. *Cancer Res* 82, 1283–1297 (2022).
246. Rabah, N., Ait Mohand, F. E. & Kravchenko-Balasha, N. Understanding Glioblastoma Signaling, Heterogeneity, Invasiveness, and Drug Delivery Barriers. *International Journal of Molecular Sciences* vol. 24 Preprint at https://doi.org/10.3390/ijms241814256 (2023).
247. Iser, I. C., Lenz, G. & Wink, M. R. EMT-like process in glioblastomas and reactive astrocytes. *Neurochemistry International* vol. 122 139–143 Preprint at https://doi.org/10.1016/j.neuint.2018.11.016 (2019).
248. Rabah, N., Ait Mohand, F. E. & Kravchenko-Balasha, N. Understanding Glioblastoma Signaling, Heterogeneity, Invasiveness, and Drug Delivery Barriers. *International Journal of Molecular Sciences* vol. 24 Preprint at https://doi.org/10.3390/ijms241814256 (2023).
249. Maenpaa, A., Junnikkala, S., Hakulinen, J., Timonen, T. & Merit, S. *Expression of Complement Membrane Regulators Membrane Cofactor Protein (CD46), Decay Accelerating Factor (CD55), and Protectin (CD59) in Human Malignant Gliomas*. *Anzeican journal of Pathology* vol. 148 (1996).
250. DeCordova, S. *et al.* Molecular Heterogeneity and Immunosuppressive Microenvironment in Glioblastoma. *Frontiers in Immunology* vol. 11 Preprint at https://doi.org/10.3389/fimmu.2020.01402 (2020).
251. Junnikkala, S. *et al.* Exceptional Resistance of Human H2 Glioblastoma Cells to Complement-Mediated Killing by Expression and Utilization of Factor H and Factor H-Like Protein 1. *The Journal of Immunology* 164, 6075–6081 (2000).
252. Whitehead, C. A. *et al.* Extracellular vesicles and their role in glioblastoma. *Critical Reviews in Clinical Laboratory Sciences* vol. 57 227–252 Preprint at https://doi.org/10.1080/10408363.2019.1700208 (2020).
253. Aaberg-Jessen, C. *et al.* Co-expression of TIMP-1 and its cell surface binding partner CD63 in glioblastomas. *BMC Cancer* 18, (2018).
254. Maniya, N. H. *et al.* An anion exchange membrane sensor detects EGFR and its activity state in plasma CD63 extracellular vesicles from patients with glioblastoma. *Commun Biol* 7, (2024).

255. Bazzoni, R. & Bentivegna, A. Role of Notch Signaling Pathway in Glioblastoma Pathogenesis. *Cancers* vol. 11 Preprint at https://doi.org/10.3390/cancers11030292 (2019).
256. Hai, L. *et al.* Notch1 is a prognostic factor that is distinctly activated in the classical and proneural subtype of glioblastoma and that promotes glioma cell survival via the NF-κB(p65) pathway article. *Cell Death Dis* 9, (2018).
257. Duhamel, M. *et al.* Spatial analysis of the glioblastoma proteome reveals specific molecular signatures and markers of survival. *Nat Commun* 13, (2022).
258. Rosińska, S. & Gavard, J. Tumor vessels fuel the fire in glioblastoma. *International Journal of Molecular Sciences* vol. 22 Preprint at https://doi.org/10.3390/ijms22126514 (2021).
259. Wang, R. *et al.* Glioblastoma stem-like cells give rise to tumour endothelium. *Nature* 468, 829–835 (2010).
260. Guarnaccia, L. *et al.* Angiogenesis in human brain tumors: Screening of drug response through a patient-specific cell platform for personalized therapy. *Sci Rep* 8, (2018).
261. Rodrigues, G. *et al.* Tumour exosomal CEMIP protein promotes cancer cell colonization in brain metastasis. *Nat Cell Biol* 21, 1403–1412 (2019).
262. Ståhl, A. lie, Johansson, K., Mossberg, M., Kahn, R. & Karpman, D. Exosomes and microvesicles in normal physiology, pathophysiology, and renal diseases. *Pediatric Nephrology* vol. 34 11–30 Preprint at https://doi.org/10.1007/s00467-017-3816-z (2019).
263. Sabbagh, Q., Andre-Gregoire, G., Guevel, L. & Gavard, J. Vesiclemia: counting on extracellular vesicles for glioblastoma patients. *Oncogene* vol. 39 6043–6052 Preprint at https://doi.org/10.1038/s41388-020-01420-x (2020).
264. Arraud, N. *et al.* Extracellular vesicles from blood plasma: Determination of their morphology, size, phenotype and concentration. *Journal of Thrombosis and Haemostasis* 12, 614–627 (2014).
265. Lässer, C., Jang, S. C. & Lötvall, J. Subpopulations of extracellular vesicles and their therapeutic potential. *Molecular Aspects of Medicine* vol. 60 1–14 Preprint at https://doi.org/10.1016/j.mam.2018.02.002 (2018).
266. Moldovan, N. *et al.* Circulating extracellular vesicles in lung cancer patients are not enriched in tumor-derived DNA fragments as revealed by whole genome sequencing. doi:10.1101/2022.07.22.501161.

267. García-Romero, N. *et al. DNA Sequences within Glioma-Derived Extracellular Vesicles Can Cross the Intact Blood-Brain Barrier and Be Detected in Peripheral Blood of Patients*. *Oncotarget* vol. 8 www.impactjournals.com/oncotarget/ (2017).
268. Bosschieter, J. *et al.* A protocol for urine collection and storage prior to DNA methylation analysis. *PLoS One* 13, (2018).
269. Teo, Y. V. *et al.* Cell-free DNA as a biomarker of aging. *Aging Cell* 18, (2019).
270. Casanova-Salas, I. *et al.* Circulating tumor extracellular vesicles to monitor metastatic prostate cancer genomics and transcriptomic evolution. *Cancer Cell* 42, 1301-1312.e7 (2024).
271. Jahr, S. *et al. DNA Fragments in the Blood Plasma of Cancer Patients: Quantitations and Evidence for Their Origin from Apoptotic and Necrotic Cells 1*. *CANCER RESEARCH* vol. 61 http://aacrjournals.org/cancerres/article-pdf/61/4/1659/3252577/ch040101659p.pdf (2001).
272. Vallejo, M. C. *et al.* A proteomic meta-analysis refinement of plasma extracellular vesicles. *Sci Data* 10, (2023).
273. Koliha, N. *et al.* Melanoma affects the composition of blood cell-derived extracellular vesicles. *Front Immunol* 7, (2016).
274. Auber, M. & Svenningsen, P. An estimate of extracellular vesicle secretion rates of human blood cells. *Journal of Extracellular Biology* 1, (2022).
275. György, B. *et al.* Effect of the 35 nm and 70 nm Size Exclusion Chromatography (SEC) Column and Plasma Storage Time on Separated Extracellular Vesicles. *Curr Issues Mol Biol* 46, 4337–4357 (2024).
276. Sódar, B. W. *et al.* Low-density lipoprotein mimics blood plasma-derived exosomes and microvesicles during isolation and detection. *Sci Rep* 6, (2016).
277. Yerrabothala, S. *et al.* Systemic coagulation is activated in patients with meningioma and glioblastoma. *J Neurooncol* 155, 173–180 (2021).
278. Lim, E. J. *et al.* Crosstalk between GBM cells and mesenchymal stemlike cells promotes the invasiveness of GBM through the C5a/p38/ZEB1 axis. *Neuro Oncol* 22, 1452–1462 (2020).
279. Broekman, M. L. *et al.* Multidimensional communication in the microenvirons of glioblastoma. *Nat Rev Neurol* 14, 482–495 (2018).
280. Mitsdoerffer, M. *et al.* The glioblastoma multiforme tumor site promotes the commitment of tumor-infiltrating lymphocytes to the T H 17 lineage in humans. (2022) doi:10.1073/pnas.

281. Ravi, V. M. *et al.* T-cell dysfunction in the glioblastoma microenvironment is mediated by myeloid cells releasing interleukin-10. *Nat Commun* 13, (2022).
282. Trejo-Solís, C. *et al.* Metabolic dysregulation of tricarboxylic acid cycle and oxidative phosphorylation in glioblastoma. *Reviews in the Neurosciences* Preprint at https://doi.org/10.1515/revneuro-2024-0054 (2024).
283. Gasmi, A. *et al.* Krebs cycle: activators, inhibitors and their roles in the modulation of carcinogenesis. *Archives of Toxicology* vol. 95 1161–1178 Preprint at https://doi.org/10.1007/s00204-021-02974-9 (2021).